

UNIVERSIDADE DE LISBOA
FACULDADE DE CIÊNCIAS
DEPARTAMENTO DE ENGENHARIA GEOGRÁFICA, GEOFÍSICA E ENERGIA



**Co-occurrence of marine and atmospheric heatwaves with
drought conditions and its association with fire activity in the
Mediterranean region**

Raquel Sofia Barbeiro dos Santos

Mestrado em Ciências Geofísicas

Dissertação orientada por:
Doutora Célia Marina Pedroso Gouveia
Doutora Ana Cristina Machado Russo

Acknowledgements

Firstly, I would like to thank my advisors, Prof. Célia Gouveia and Ana Russo for the crucial support throughout this journey. I am grateful not only for the extremely valuable assistance in producing this work, but also for always believing in my abilities, motivating me, providing advice, and offering the best tools and opportunities to start my career in the field.

To my colleagues from the university and from IPMA who have been part of this journey and encouraged me in numerous situations. I particularly thank my colleagues in room 3.5D for their help and for making this experience more enthusiastic.

I appreciate my closest friends for their presence. My feline friends, for their company. My family, especially my mother, father, brother, and maternal grandmother, who have always supported me and wished for my happiness throughout this process.

A special thanks to Diogo for being constantly by my side with love, care, support, and understanding, which were essential to overcome all the moments that were part of this path.

This work was supported by the European Union's Horizon 2020 research project FirEURisk (Grant Agreement no. 101003890), performed at the Portuguese Institute for Sea and Atmosphere (IPMA), and by the Portuguese Fundação para a Ciência e a Tecnologia (FCT) I.P./MCTES through national funds (PIDDAC) – UIDB/50019/2020- IDL, DHEFEUS - 2022.09185.PTDC. The subject matter of this thesis aligns with the objectives outlined in the DHEFEUS project.

Resumo

As alterações climáticas surgem como uma das maiores preocupações do século XXI. Nas últimas décadas, os eventos climáticos extremos têm-se tornado mais frequentes, longos e intensos, como resultado do efeito da mudança climática, muito potenciada pelo forçamento antropogénico. Um dos exemplos mais significativos relaciona-se com a ocorrência de ondas de calor, caracterizadas por episódios prolongados de temperaturas anormalmente quentes. Estes eventos podem ocorrer tanto na atmosfera como no oceano, com impactos severos nos respetivos ecossistemas, afetando a estrutura e distribuição de espécies, a produção de culturas agrícolas, a ocorrência de fogos rurais, comprometendo a saúde humana e consequentemente sendo responsável por um aumento das taxas de morbidade e mortalidade. Para além dos eventos de extremos de calor, a ocorrência de episódios de seca também se tem tornado mais frequente, podendo afetar áreas extensas por períodos muito longos. As consequências destes episódios podem ser devastadoras com efeitos na vegetação, agricultura, fogos rurais, reservas de água, entre outros, podendo comprometer o abastecimento de bens essenciais para a população, principalmente em regiões mais vulneráveis.

Nos últimos anos, a ocorrência de fogos rurais e as suas consequências no ambiente e em diversos sectores da sociedade tem despertado grande interesse na sociedade civil e na comunidade científica. Uma das particularidades deste tipo de eventos que tem vindo a ser evidenciada é a sua forte associação a episódios quentes e secos que, ocorrendo simultaneamente, amplificam o risco de incêndio. Nas últimas décadas, a região mediterrânea tem sido particularmente afetada por eventos climáticos extremos associados a incêndios devastadores, com impactos significantes na vida humana e ecossistemas. Esta situação poderá vir a ser exacerbada no futuro, já que se antecipa uma maior frequência de fogos associados a eventos quentes e secos, por força do agravamento do aquecimento global. Como tal, o estudo da ocorrência individual ou simultânea de extremos climáticos e o seu impacto na ocorrência de incêndios reveste-se de crucial importância.

Dada a sua importância e referidos impactos, os eventos extremos de origem natural têm vindo a ser amplamente estudados nos últimos anos. Nomeadamente, as ondas de calor marinhas e as suas características têm sido o foco principal de muitos estudos, devido à sua intensificação nas últimas décadas e os fortes impactos nos ecossistemas. No entanto, a maioria dos estudos exploram a sua ocorrência individual. Sabe-se, contudo, que existe uma possível relação entre as temperaturas do ar e do mar durante eventos de onda de calor, potencialmente associada a mecanismos de interação oceano-atmosfera. Este estudo pretende continuar a avaliação da relação entre eventos extremos climáticos, incorporando também o estudo de períodos anormalmente quentes no oceano e a sua co-ocorrência com os restantes. Deste modo, é explorada a ocorrência, tanto individual como simultânea, de fenómenos de onda de calor atmosférica e secas no Sul da Europa, e de ondas de calor marinhas adjacentes no mar Mediterrâneo e Oceano Atlântico Nordeste. A conexão entre os eventos mencionados e a ocorrência de fogos florestais na região mediterrânea é analisada para as escalas sazonal e anual, desde 2001 até 2022, em três sub-regiões diferentes do continente: i) uma centrada na Península Ibérica e abrangendo a região atlântica,

excluindo o Mar Mediterrâneo, ii) uma centrada na Península Ibérica e no sul da França, incluindo o Mar Mediterrâneo e excluindo o Oceano Atlântico, e iii) uma centrada a Sul e Sudeste do continente (Itália, Grécia), considerando o Mar Mediterrâneo.

Na identificação de episódios de ondas de calor atmosféricas e marinhas, foram utilizados, respetivamente, dados de temperatura do ar a 2 metros (T2m) e temperatura da superfície do mar (SST), ambas obtidas da reanálise ERA5 produzidas pelo *European Centre for Medium-Range Weather Forecast* (ECMWF) e disponibilizadas na plataforma *Climate Data Store (Copernicus)*.

Para a caracterização destes episódios, foram calculadas e analisadas, no domínio temporal e espacial, algumas propriedades importantes tais como a frequência, a duração, a intensidade e a intensidade cumulativa destes eventos. Para o caso dos eventos secos, foram extraídos dados de precipitação acumulada também com base na reanálise ERA5. A definição e estudo temporal e espacial destes fenómenos foram realizados com base no índice de seca *Standardized Precipitation-Evapotranspiration Index (SPEI)*.

A ocorrência de incêndios florestais foi identificada através da deteção de áreas ardidas com base no produto *MCD64A1 Version 6 Burned Area Product*, extraído do sensor MODIS. Neste estudo, apenas foi explorada a ocorrência de incêndios rurais em zonas essencialmente ocupadas por floresta e mato, desconsiderando os fogos associados a práticas de gestão nas regiões ocupadas por campos agrícolas.

Os resultados obtidos neste trabalho destacam a potencial associação entre os eventos extremos que ocorrem no mar e em terra. Nomeadamente, verifica-se um padrão consistente na oscilação das características das ondas de calor na atmosfera e no oceano ao longo do período de estudo, bem como uma proximidade espacial das mesmas em anos como 2003, 2010, 2012 e 2022. A correlação estatística positiva observada entre T2m e SST nas diferentes sub-regiões realça também a potencial associação entre ambas.

Ao analisar os padrões de temperatura em terra, no oceano e a precipitação acumulada durante os meses de verão extenso (Maio-Outubro), os resultados revelam que, apesar de alguma variação nas diferentes regiões analisadas, a maioria dos anos com ocorrências severas de incêndios estão associados a épocas de precipitação reduzida e/ou temperaturas do ar elevadas durante a época de fogos. As temperaturas da superfície do mar sugerem uma ligação à ocorrência destes fenómenos conhecidos por influenciar significativamente a propagação de incêndios florestais. Essa associação é evidente em anos marcados por grandes incêndios, nomeadamente em 2003, 2017 e 2022 na Península Ibérica e em 2012 e 2021 no Sudeste da Europa. O estudo das condições de onda de calor e seca foi realizado especificamente sobre os pixels ardidos nas diferentes regiões a uma escala anual, tendo sido concluído que os anos marcados por condições mais extremas de ondas de calor marinha coincidem, em parte, com a intensificação de ondas de calor atmosféricas e/ou condições de seca sobre as regiões afetadas por incêndios, e vice-versa.

As condições climáticas extremas, quer ocorram individualmente ou de forma conjunta, sobre as áreas afetadas por incêndios, foram analisadas mensalmente, ao longo de todo o período e nas diferentes sub-regiões. Os meses em que as áreas ardidas permaneceram abaixo do percentil 80 surgem fortemente associados a condições de ondas de calor marinhas. Para os meses em que as áreas ardidas ultrapassaram este percentil (grandes fogos), os eventos secos predominam. Revela-se ainda que os meses caracterizados por grandes incêndios estão predominantemente associados a condições climáticas extremas (ondas de calor atmosféricas, ondas de calor marinhas, condições secas) em todas as regiões analisadas. A ocorrência combinada destes eventos também se torna evidente, indicando que a existência simultânea de condições severamente quentes e secas poderá contribuir para a incidência de incêndios florestais mais severos. Esta análise evidencia a potencial relação entre a ocorrência de temperaturas elevadas da superfície do mar durante os meses que coincidem com eventos de incêndios florestais.

Ao examinar todo o período de estudo, verifica-se que, na Península Ibérica, as áreas ardidas durante

meses com maiores incêndios estão intimamente relacionadas com condições muito secas, enquanto na região a sudeste do continente, estes incêndios estão predominantemente associados a ondas de calor severas na atmosfera e mar adjacente em simultâneo.

Este estudo realça a relevância de considerar a componente ‘oceano’ no estudo de eventos climáticos compostos. Futuramente, a análise crítica dos mecanismos subjacentes a estas ocorrências simultâneas e das suas relações de dependência, tendo em considerando fatores atmosféricos e oceânicos, poderá proporcionar uma compreensão mais abrangente da sua interação e constituir uma ferramenta útil na gestão e mitigação de riscos meteorológicos. Esse tipo de abordagem é cada vez mais crucial no caso dos incêndios rurais, tanto na região mediterrânea como a nível global, que ameaçam a estabilidade dos ecossistemas e o bem-estar da sociedade, principalmente no contexto das alterações climáticas.

Palavras chave: Interação oceano-atmosfera, Eventos compostos, Extremos quentes e secos, Fogos florestais

Abstract

Climate change has become a major concern in the 21st century, leading to an increased frequency, duration, and intensity of extreme events. Namely, heatwaves and droughts have been growing in recent decades in the Mediterranean region, resulting in significant social and environmental repercussions. The impact of these extreme events can contribute to exacerbating rural fires.

This work explores the co-occurring interplay of different hazards in Mediterranean Europe, examining the occurrence of atmospheric heatwaves and drought conditions in southern Europe and marine heatwaves in the East Atlantic and the Mediterranean Sea. Additionally, recorded burned areas between 2001 and 2022 are investigated, exploring the prevalence of dry and hot conditions and their linkage to rural fires, on an individual and compound approach. The analysis will be performed over monthly, seasonal and annual scales, with a primary focus on the most extreme years, relying on reanalysis, satellite datasets and standard indicators.

A consistent pattern in the fluctuation of heatwave characteristics in both the atmosphere and ocean is observed throughout the study period, and a positive correlation between air and sea temperatures is found. Severe wildfires mostly associate with reduced precipitation and/or elevated air temperatures during the summer season, revealing a close relationship with heightened sea surface temperatures. Months marked by fire activity surpassing the 80th percentile threshold are predominantly associated with extreme climatic conditions, showcasing a substantial occurrence of compound events. Burned areas associated with extreme wildfires primarily relate to very dry conditions in the Iberian Peninsula. In eastern and southern Europe, extensive fires are mostly associated with compound hot conditions over land and adjacent oceans.

This study highlights the potential role played by both atmospheric and marine conditions when exploring compound extremes, which might be crucial to ensure effective preparedness and mitigate the risks of climatic disasters, particularly wildfires.

Keywords: Air-sea interaction, Compound events, Hot and dry extremes, Rural fires

Index

Acknowledgements	I
Resumo	III
Abstract	VII
List of Figures	XI
List of Tables	XV
1 Introduction	1
1.1 Heatwaves and droughts	1
1.2 Compound occurrence of hot and dry events and its impact on wildfire activity	3
1.3 Marine conditions and its interaction with other extremes	5
1.4 Thesis research goals	6
2 Data	7
2.1 ERA5 reanalysis data	7
2.2 Land cover remote sensing data	7
2.3 MODIS remote sensing data	8
3 Methodology	11
3.1 Study regions	11
3.2 Marine and atmospheric heatwaves	12
3.3 Drought conditions	13
3.4 Interannual evaluation and coincidence analysis	15
4 Results	17
4.1 Temporal evolution and spatial distribution of heatwave conditions	17
4.2 Temporal evolution and spatial distribution of drought conditions	24
4.3 Long-term changes in the correlation between temperature and precipitation in the extended summer	26
4.4 Fire activity and its relationship with temperature and precipitation patterns	28
4.4.1 Temporal analysis and spatial distribution of wildfires	28
4.4.2 Seasonal averages of precipitation, air temperature and sea temperature and its association with fire occurrence	30
4.5 Heatwave and drought conditions over burned regions on an annual scale	33

INDEX

4.6 Monthly heatwave and drought conditions over burned regions	34
4.7 Wildfire incidence under the occurrence of single and compound hazards for 2001-2022	38
5 Discussion and conclusions	41
References	47
Appendix	59

List of Figures

1.1	(Upper panel) Spatial patterns of daily maximum air temperature anomaly values at 2 meters above the surface ($^{\circ}\text{C}$), in the Mediterranean Sea and Northeast Atlantic; (Lower panel) Spatial patterns of sea surface temperature anomaly values ($^{\circ}\text{C}$), in southern Europe and North Africa, averaged for three different periods a,d) 1990-2000, b,e) 2001-2011 and c,f) 2012-2022. The reference period used was 1981-2010. Data was retrieved from ERA5 reanalysis dataset (Hersbach et al., 2023)	2
1.2	Spatial patterns of mean daily precipitation anomalies, in mm, averaged for three strongly dry years in European regions, a) 2003, b) 2015 and c) 2022. The reference period used was 1981-2010. Daily accumulated precipitation data was retrieved from ERA5 reanalysis dataset (Hersbach et al., 2023)	3
1.3	Annual average of burned areas, in hectares, in each country of European Union, considering data from 2006 to 2022. The data is extracted from The European Forest Fire Information System (EFFIS, 2023), available through its Current Statistics Portal.	4
3.1	Based on ESA CCI LC data, land cover classes are shown based on information for the year 2020. Three subregions were chosen: Region 1) centered on Iberia and southwestern France, considering the Atlantic region and excluding the Mediterranean Sea, Region 2) centered on Iberia and Mediterranean France and considering the Mediterranean Sea, Region 3) centered on Italy and the Peloponnese (Southeast of Europe) and considering the Mediterranean. Areas shown in gray are masked.	11
3.2	Schematic definition of heatwaves, according to Hobday et al. (2016)). The light orange curve represents the climatology and the dark orange curve the 90th percentile threshold. The black curve corresponds to daily temperatures and shaded areas to the occurrence of heatwave events.	12
3.3	Time series showing the 12-month SPEI for every month between 1979 and 2022, averaged over the whole region of study, where negative values correspond to drier conditions (filled up in red) and positive values correspond to wetter conditions (filled up in blue).	14
3.4	Schematic figure showing an exemplification of how SPEI and atmospheric ICI values are aggregated in each burned pixel, through the average of the 4 nearest points in ERA5's resolution. For each burned pixel, represented by the fire icon, the values of ICI and SPEI of the four nearest points are aggregated and averaged.	16

LIST OF FIGURES

4.1 Temporal evolution of heatwave properties between 1979 and 2022: (a) number of heatwaves, (b) mean duration of heatwaves (days), (c) mean intensity of heatwaves ($^{\circ}\text{C}$) and (d) ICI ($^{\circ}\text{C}\cdot\text{days}$). Blue curves represent MHWs, being area-averaged over the ocean pixels, while green curves denote AHWs, area-averaged over the land pixels. This analysis considers the full region of study. The dashed lines indicate significant linear trends, considering a 0.05 significance level.	18
4.2 Yearly number of heatwaves (AHWs in land and MHWs in the ocean) between 1979 and 2022. Areas shown in gray are masked.	19
4.3 Annual averages of heatwaves' mean duration (AHWs in land and MHWs in the ocean), in days, between 1979 and 2022. Areas shown in gray are masked.	21
4.4 Annual averages of heatwaves' mean intensities (AHWs in land and MHWs in the ocean), in $^{\circ}\text{C}$, between 1979 and 2022. Areas shown in gray are masked.	22
4.5 Atmospheric yearly ICI over land and the marine yearly ICI over the ocean, in $^{\circ}\text{C}\cdot\text{days}$, between 1979 and 2022. Areas shown in gray are masked.	23
4.6 Temporal evolution of drought conditions. In the upper panel are displayed the spatial-averaged values of the 12-month SPEI for December over land between 1979 and 2022, and the below panel shows the percentage of area under the occurrence of moderate droughts (yellow curve), severe droughts (green curve) and extreme droughts (black curve), using the definition by Agnew et al., (2000) and considering the December SPEI-12 values. This analysis considers the full region of study. Only land pixels were taken into account. The dashed lines indicate significant linear trends, considering a 0.05 significance level.	24
4.7 Values of the 12-month SPEI in December over the European land area, between 1979 and 2022.	25
4.8 Bivariate Gaussian probability distribution functions of extended summer mean temperatures (T2m and SST, $^{\circ}\text{C}$) and accumulated precipitation (mm) (central panel), and the univariate probability distribution functions of the corresponding average anomalies (lateral panels, in the units of the corresponding absolute values), for the period 1979-2000 in yellow, and 2001-2022 in green, over all the regions of interest. The dashed gray ellipses represent the 95% level of the Gaussian probability distributions.	27
4.9 Yearly normalized burned areas between 2001 and 2022 for region 1 (orange bars), region 2 (red bars), region 3 (blue bars) and for the overall study region (black curve). Normalized burned areas are obtained by dividing the BAs in hectares by the total land hectares in each of the regions.	29
4.10 Accumulated burned pixels for the period 2001-2022 considering the full land region and masking cropland areas.	29
4.11 Average values of daily accumulated precipitation and daily maximum temperatures (T2m and SST) for each year, calculated for the extended summer (scatter points), and summer accumulated burned area for each year (colors). The bivariate Gaussian probability distributions of all pairs of variables for the period 2001-2022 are represented by the gray ellipses (dashed gray ellipses represent the 95% level). Horizontal and vertical dashed lines correspond, respectively, to precipitation and temperature values averaged over all years of study.	31
4.12 As in Fig 4.9, but considering the extended summers.	32

LIST OF FIGURES

4.13 Spatial averages of the annual accumulated atmospheric ICI ($^{\circ}\text{C}\cdot\text{days}$) and SPEI-12 for December over burned pixels, regarding each of the study regions. In each region, the annual marine ICI ($^{\circ}\text{C}\cdot\text{days}$) is averaged over the corresponding marine areas and represented through the size of the scatter points, which represent different percentiles. The different scatter colours describe different years from 2001 to 2022. Horizontal and vertical dashed lines separate the 20% most extreme cases regarding the atmospheric ICI (A+) and SPEI-12 values (D+), obtained through the computation of the 80 th and 20 th percentile, respectively.	34
4.14 Monthly occurrences of single and compound hazards from 2001 to 2022. The 20% warmest and driest months were identified through the computation of the 80 th percentile of the monthly-averaged atmospheric and marine ICI and the 20 th percentile of the monthly-averaged SPEI-3 (colors), over burned pixels. "A+" and M+" denote a month with atmospheric and marine ICI equal to exceeding the 80 th percentile, respectively, and "D+" when the SPEI-3 value equals or falls below the 20 th percentile. Months marked with an "X" indicate those where the burned area equals or exceeds the 80 th percentile. Months that didn't record any burned pixels are filled in blank.	36
4.15 Single and compound climatic hazards and its association with wildfires. Percentage of months, shown in Fig. 4.14, that are associated to each of type of hazard or combined hazards, considering only months when any burned area was registered. The categorization is distinguished by the different regions of study and the predefined threshold for burned areas (80 th percentile).	38
4.16 Normalized burned areas, from 2001 to 2022, associated to each of type of hazard or combined hazards. The categorization is distinguished by the different regions of study and the predefined threshold for normalized burned areas: months burning less than the 80 th percentile threshold (left-side) and months burning above the 80 th percentile threshold (right-side). Normalized burned areas are obtained by dividing the BAs in hectares by the total burned pixels in each of the regions.	39
A1 Spatial-averaged values of the 12-month SPI for December over land, between 1979 and 2022. This analysis considers the full region of study.	59
A2 Spatial patterns of the 12-month SPI in December over the European land area, between 1979 and 2022.	60
A3 Yearly burned areas between 2001 and 2022, in hectares, for region 1 (orange bars), region 2 (red bars), region 3 (blue bars) and for the overall study region (black curve). Normalized burned areas are obtained by dividing the BAs in hectares by the total land hectares in each of the regions.	61
A4 As in Fig A3, but throughout the extended summer seasons.	61
A5 Monthly mean anomalies of accumulated precipitation for every month in 2003. The reference period used was 1979-2022. Daily accumulated precipitation data was retrieved from ERA5 reanalysis dataset (Hersbach et al., 2023)	62
A6 Monthly mean anomalies of maximum T2m for every month in 2007. The reference period used was 1979-2022. T2m data was retrieved from the ERA5 reanalysis dataset (Hersbach et al., 2023)	62
A7 As in Fig A5, but considering accumulated precipitation values.	63

List of Tables

4.1	Correlation coefficient values calculated for each pair of values analysed in Fig. 4.8., for the different periods and regions of study. The statistical significance was tested and revealed to be non-significant for all the coefficients in the case of SST - P, and significant for the rest.	28
A1	Land cover classes classification from the ESA CCI LC product. The colors represent the 6 primary categories aggregated in this work, based on IPCC land categories used for the change detection (Defourny et al., 2017).	64
A2	Thresholds values to identify the most extreme cases regarding monthly heatwave and dry conditions: the 80 th percentile of the monthly ICI is used to define the most severe months for atmospheric and marine hot conditions, and the 20 th percentile of the monthly SPEI-3 is utilized to find the driest months of the period.	65

List of acronyms, abbreviations and symbols

AppEARS	Application for Extracting and Exploring Analysis Ready Samples
AHW	Atmospheric Heatwave
AVHRR	Advanced Very-High-Resolution Radiometer
BA	Burned Area
°C	Celcius Degrees
CDS	Climate Data Store
C3S	Copernicus Climate Change Service
ECMWF	European Centre for Medium-Range Weather Forecasts
ESA CCI	European Space Agency Climate Change Initiative
GCOS	Global Climate Observing System
K	Kelvin Degrees
ICI	Intensity Composite Index
LC	Land Cover
LCCS	Land Cover Classification System
MERIS FR	Medium Resolution Imaging Spectrometer Full Resolution
MERIS RR	Medium Resolution Imaging Spectrometer Reduced Resolution
MHW	Marine Heatwave
MODIS	Moderate-Resolution Imaging Spectroradiometer
NASA	National Aeronautics and Space Administration
P	Total Precipitation
ET	Evapotranspiration
PROBA-V	PROBA-Vegetation mission
SPEI	Standardized Precipitation-Evapotranspiration Index
SPI	Standardized Precipitation Index
SPOT-VGT	SPOT-Vegetation Mission
SST	Sea Surface Temperature
S3 OLCI	The Ocean and Land Color Instrument aboard Sentinel-3
T2m	2-meter Air Temperature
UN FAO	United Nations Food and Agriculture Organization
WMO	World Meteorological Organization

Chapter 1

Introduction

1.1 Heatwaves and droughts

Climate change emerges as a prevailing social, economic, and environmental concern of the twenty-first century and has led to rising trends in temperatures and increasing occurrence of extreme weather events, exacerbated by anthropogenic activities (Lee et al., 2023).

Over the past decades, both air and sea temperatures have been increasing significantly (Fig. 1.1), leading to the rising frequency, duration, and intensity of heatwaves (Pörtner et al., 2022). These events, which are characterized by prolonged and consecutive periods of anomalously warm temperature values, occur both in the atmosphere – atmospheric heatwaves (AHWs) (Perkins-Kirkpatrick and Lewis, 2020), and in the ocean – marine heatwaves (MHWs) (Hobday et al., 2016; Oliver et al., 2018). AHWs can lead to significant repercussions on air quality, human health and potentially increase death rates (Theoharatos et al., 2010; Wu et al., 2019; McMichael and Lindgren, 2011; Robine et al., 2008), as well as exacerbate occurrence (Parente et al., 2018; Ruffault et al., 2020; García-Herrera et al., 2010). AHWs and MHWs can induce critical ecological disruptions, impacting the structure, function, and distribution of terrestrial and marine species, triggering their mortality (Simon et al., 2022; Oliver et al., 2019; Ruthrof et al., 2018). Crop productivity is also highly affected under extreme hot conditions, posing a substantial threat to agriculture and global food security (Lobell and Field, 2007; Beillouin et al., 2020; Brás et al., 2021).

Extensive literature analysed the drivers of AHW and MHW in order to better understand the phenomena. AHWs result from interactions among large- and small-scale processes occurring across diverse temporal scales, including persistent high-pressure systems (Tomczyk and Bednorz, 2016; García-Herrera et al., 2010), land-atmosphere interactions and moisture fluxes (e.g., Miralles et al. 2014; Fischer et al. 2007b,a), and seasonal climate variability (e.g., Li et al. 2020; Arblaster and Alexander 2012; Perkins 2015). Similarly to AHWs, MHWs also originate from regional processes interacting with large-scale modes of variability and teleconnections across various spatio-temporal scales. Local factors also play a crucial role in their occurrence, influencing changes in the heat budget of the upper-ocean mixed layer, related to factors such as heat transport, air-sea heat fluxes, and vertical mixing (Holbrook et al., 2020, 2019; Oliver et al., 2021; Barriopedro et al., 2023).

1. Introduction

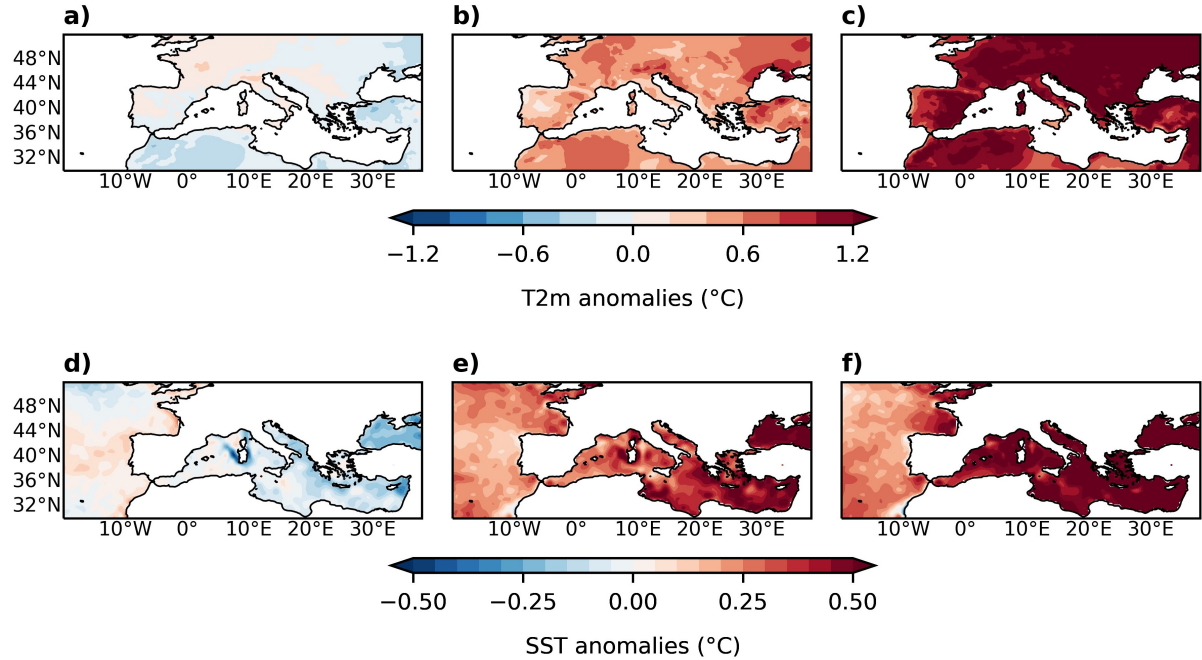


Figure 1.1: (Upper panel) Spatial patterns of daily maximum air temperature anomaly values at 2 meters above the surface (°C), in the Mediterranean Sea and Northeast Atlantic; (Lower panel) Spatial patterns of sea surface temperature anomaly values (°C), in southern Europe and North Africa, averaged for three different periods a,d) 1990-2000, b,e) 2001-2011 and c,f) 2012-2022. The reference period used was 1981-2010. Data was retrieved from ERA5 reanalysis dataset (Hersbach et al., 2023)

Along with these abnormally hot periods, climate change has also been manifesting through the persistent occurrence of droughts (Pörtner et al., 2022), marked by a considerable absence of precipitation or high evaporative demand at the land surface (Vicente-Serrano et al., 2020, 2014b). Droughts may persist for long periods and affect large areas. Europe has experienced some remarkably dry events through the last decade, including 2003 (Ciais et al., 2005; Fink et al., 2004), 2015 (Ionita et al., 2017; Laaha et al., 2017) and 2022 (Tripathy and Mishra, 2023; Faranda et al., 2023) (Fig. 1.2). Future climate projections indicate that extensive regions of Europe are expected to experience severe drought events in the future (Spinoni et al., 2018; Samaniego et al., 2018). These events can lead to substantial effects on human mortality (Salvador et al., 2022), vegetation dynamics (Gouveia et al., 2017), agricultural production (Madadgar et al., 2017; Páscoa et al., 2017; Ribeiro et al., 2020), fire occurrence (Turco et al., 2017; Libonati et al., 2022), water supply and quality (Stahl et al., 2016) and the reliability of hydroelectricity generation, reducing total power generation (Després et al., 2020). Rural areas facing substantial poverty rates and heavily dependent on agriculture are particularly vulnerable to the repercussions of droughts, consequently posing a significant risk to their food security (Rakotoarison et al., 2018; De Amorim et al., 2018).

1. Introduction

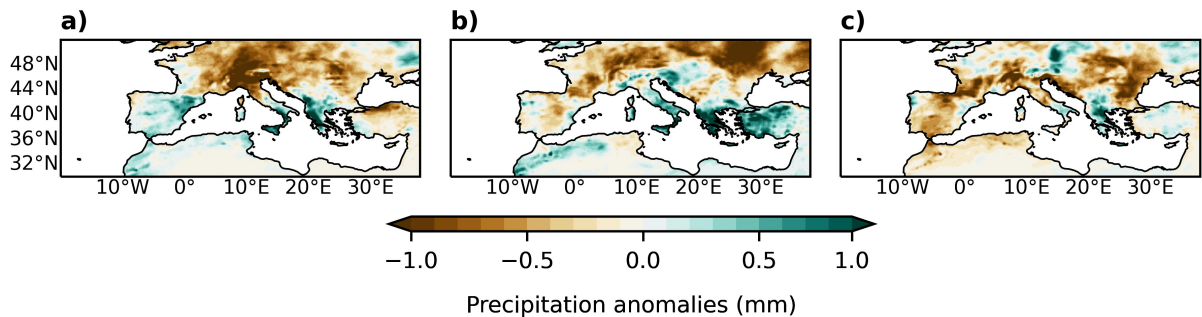


Figure 1.2: Spatial patterns of mean daily precipitation anomalies, in mm, averaged for three strongly dry years in European regions, a) 2003, b) 2015 and c) 2022. The reference period used was 1981-2010. Daily accumulated precipitation data was retrieved from ERA5 reanalysis dataset (Hersbach et al., 2023)

1.2 Compound occurrence of hot and dry events and its impact on wildfire activity

The combination of climate drivers and/or hazards - not necessarily extreme - leading to significant social or environmental impacts, constitutes a ‘compound event’ (Zscheischler et al., 2018). They can occur at the same time, in close succession, or concurrently in different regions, and the consequences often surpass the effects observed when each condition acts individually (Zampieri et al., 2017; Hao et al., 2022; Ribeiro et al., 2020; Gouveia et al., 2016; Ermitao et al., 2022; Ermitão et al., 2023). The simultaneous or lagged occurrence of meteorological hazards has been receiving increasing attention, with projections indicating a future intensification, posing immense challenges for adaptation strategies (Zscheischler and Seneviratne, 2017; Seneviratne et al., 2021; Hao et al., 2018; Bevacqua et al., 2021).

One significant impact concerning the compound effect of extreme hot and dry conditions relates to the occurrence of wildfires. Fire activity is largely driven by the simultaneous occurrence of three factors: available fuel, an ignition source (natural or human), and fire weather conditions that may favour fire ignition and propagation (Pausas and Ribeiro, 2013; Ramos et al., 2023; Jones et al., 2022). The synergy of increased temperatures, decreased soil moisture and low humidity levels, together with fuel accumulation and dryness, enhances the likelihood of fire ignition, potentially leading to the occurrence of catastrophic fires (Libonati et al., 2022; Pausas and Ribeiro, 2013; Jones et al., 2022; Ruffault et al., 2020; Ermitao et al., 2022; Gouveia et al., 2016; Ramos et al., 2023). Some of the effects of the occurrence of fire events relate to agriculture and vegetation losses, reduction of aquifer water quality and soil degradation (Rust et al., 2018; Pereira et al., 2018), but are not limited to. Another important consequence is an overall decrease of carbon stored on land, alongside the emissions of greenhouse gases, various trace gases and aerosols (Lasslop et al., 2019; Cascio, 2018). This has implications for air quality and consequently can have repercussions on human health due to exposure to wildfire smoke (Finlay et al., 2012; Cascio, 2018). A large rural fire can also cause substantial damage to the infrastructures and completely alter the economy of the region (Thomas et al., 2017). Besides these significant ecological and economic detriments, the occurrence of wildfires can also result in the loss of human lives, which can be either attributed to the exposure to toxic air pollutants or direct contact with the fire phenomenon (Ganteaume et al., 2021; Cascio, 2018).

Portugal, Greece, Cyprus, Croatia, Italy and Spain were among the most fire-affected countries of the European Union between 2006 and 2022 (Fig. 1.3, EFFIS 2023). All these countries are located

1. Introduction

in the Mediterranean basin which, during the last decades, has experienced strong land cover and land use changes that, together with some remarkable wildfires, have inflicted widespread destruction upon forests and human resources, resulting in a substantial number of casualties and injuries (Ganteaume et al., 2021; Turco et al., 2017, 2019; Gouveia et al., 2016; Ramos et al., 2023). The year 2017 was one of the most devastating on record, particularly in Portugal, which faced the compound effect of extreme hot and dry conditions during the fire season, witnessing an extremely high density of ignition and a burned area of about 500.000 hectares. The repercussions were severe and resulted in more than 120 fatalities (Turco et al., 2019). The compound nature of this particularly extreme event was described in Ramos et al. (2023), which made a thorough study on the determining conditions that led to these massive rural fires in Portugal, pointing to a conjugation of factors: i) a prolonged drought which led to preconditioned cumulative hydric stress of vegetation, ii) unusual meteorological conditions caused by the passage of hurricane Ophelia off the Coast of Portugal, and iii) negligent human-induced ignitions mostly associated with agricultural practices. In a similar way, the occurrence of exceptional heatwaves and a major drought in 2007 across Greece played a significant role in fuelling widespread fire events in the Peloponnese that were especially severe (Gouveia et al., 2016). Extreme climatic conditions were also observed in western Europe and Iberian Peninsula, in 2003 and 2005, which led to extreme and unexpected fire incidents (Trigo et al., 2006; García-Herrera et al., 2010; Gouveia et al., 2012). More recently, in the summer of 2023, Alexandroupolis, in Greece, experienced the largest single wildfire recorded in the European Union, with over 90.000 ha burned (Copernicus Emergency Management Service - Rapid Mapping, 2024).

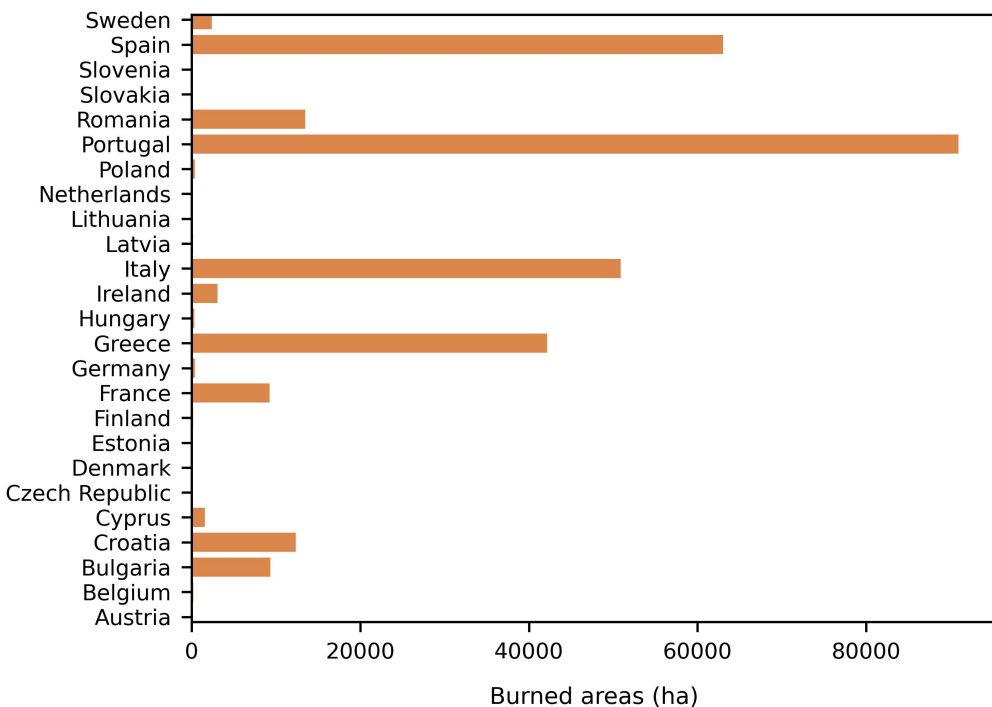


Figure 1.3: Annual average of burned areas, in hectares, in each country of European Union, considering data from 2006 to 2022. The data is extracted from The European Forest Fire Information System (EFFIS, 2023), available through its Current Statistics Portal.

Beyond the impactful incidence of wildfires, the Mediterranean basin should be highlighted due to its notable vulnerability and pronounced effects of climate change (Giorgi and Lionello, 2008; Tuel and Eltahir, 2020; Giorgi, 2006). This region is facing a growing threat of more frequent wildfires, the most extreme of which occur during compound drought and heatwave episodes. Under the most pessimistic

1. Introduction

scenario (RCP8.5), the frequency of wildfires driven by compound warm and dry conditions is expected to increase by 30% by the end of the century (2071-2100) (Ruffault et al., 2020). The compound nature of droughts and hot extremes has been associated with disastrous wildfires not only in the Mediterranean area. Their occurrence is not regionally limited and has been investigated across multiple regions such as Brazil (e.g., Libonati et al. 2022), Australia (e.g. Abram et al. 2021), California (e.g., Varga et al. 2022, North Africa (e.g., Belhadj-Khedher et al. 2020), Portugal (e.g., Turco et al. 2019; Ermitao et al. 2022) and other regions of Europe (e.g., Sutanto et al. 2020; Ruffault et al. 2020; Gouveia et al. 2016; García-Herrera et al. 2010).

1.3 Marine conditions and its interaction with other extremes

Although several attempts have been done linking the occurrence of AHW's and droughts to rural fires, the combined analysis of MHW's and AHW's and its linkage with the occurrence of other events remains less explored. It has been shown that, under the influence of human activity, not only AHWs but also MHWs are more likely to occur (Fischer and Knutti, 2015; Oliver et al., 2018), and future projections indicate that these events are expected to continue increasing as global warming proceeds (Amengual et al., 2014; Oliver et al., 2019; Plecha and Soares, 2020; Plecha et al., 2021).

A few studies have investigated a connection between sea surface temperatures and atmospheric temperatures during heatwaves, which may be attributed to shared primary drivers but may also arise from complex atmosphere-ocean interactions (Holbrook et al., 2020; Rodrigues et al., 2019). As example, during the exceptional 2003 European heatwave, the Mediterranean Sea surface temperatures (SSTs) were abnormally high (Simon et al., 2022, 2023a). Research has demonstrated that this abnormal warming of the ocean was primarily driven by atmospheric influences. AHWs over Europe resulted in increased rates of air-sea heat fluxes in the Mediterranean Sea which, together with reduced wind speeds, led to the warming of surface waters (Sparnocchia et al., 2006; Olita et al., 2007). Simon et al. (2022) also classified this event as significant according to the activity metric, leading to ecosystem mass mortality of marine species in the northwestern Mediterranean (Schiaparelli et al., 2007; Garrabou et al., 2009). On the other hand, certain studies highlight the significance of these high SST's in the persistence of the tropospheric anticyclone over the western Mediterranean, thereby intensifying the AHW (Feudale and Shukla, 2007; García-Herrera et al., 2010). The impact of these coincident heatwave episodes over land and ocean has been far-reaching, including widespread loss of human lives, as well as extensive destruction of marine and terrestrial ecosystems (Garrabou et al., 2009; García-Herrera et al., 2010).

In addition to the above-mentioned investigations, Hu (2021) revealed the existence of a significant coupling between coastal MHWs and increased air temperatures and humidity over the adjacent cities during the summer season, particularly pronounced at higher latitude regions. This study indicates that a significant portion, ranging from 60% to 80%, of summer heatwaves observed in mid-latitude coastal cities align with the occurrence of coastal MHWs globally. Aboelkhair et al. (2023) conducted a study examining the relationship between AHWs and MHWs in the eastern Mediterranean region for the period 1982-2021. Their findings indicated a high and significant correlation between AHWs and MHWs frequency. Furthermore, they concluded that more than half of the marine events observed occurred concurrently with atmospheric events. Pathmeswaran et al. (2022) focused on the relationship between AHW's and MHW's around coastal regions of Australia over the period 1982-2018, finding a significant increase in the number of terrestrial heatwave days when a co-occurring marine heatwave was present, impacting areas up to 150 kilometers inland. The authors underscore the role related to similar large-scale synoptic conditions in driving both AHW's and coastal MHW's. Record-breaking coupled MHW/AHW

1. Introduction

have also been investigated over the New Zealand region and Tasman Sea (Salinger et al., 2019, 2020, 2023). In these cases, the anomalously warm ocean temperatures were related to abnormally high air-sea heat fluxes into the ocean, where a strong and persistent high-pressure system reduced cloud cover and weakened the winds, thereby increasing shortwave radiation and causing substantial warming of the stratified surface layers of the Tasman Sea.

The role of atmospheric processes in driving the simultaneous occurrence of extreme events in the atmosphere and the ocean is also highlighted in Rodrigues et al. (2019). The authors showed that the mechanisms involving local changes in the air-ocean heat fluxes associated with atmospheric blocking, not only induce severe drought conditions, but also result in the development of MHW's in the adjacent ocean during the summer of 2013/14 in eastern South America. Over North America, Shi et al., (2021) further explore the occurrence of MHWs and dry events, quantifying the role of anthropogenic warming in increasing the co-occurrence of extreme warm northeast Pacific temperatures and dry California conditions.

1.4 Thesis research goals

The findings above-mentioned highlight the relevance of including both atmospheric and marine events when examining the spatiotemporal patterns and implications of heatwaves and droughts in a certain region. Even though the nexus between extreme events, namely between droughts-AHWs, drought-fires, AHWs-fires and AHWs-droughts-fires has been deeply explored in most of the European regions, the synergy between MHWs, AHWs and droughts and their impacts on fires still have not been critically examined over the Mediterranean Europe. Given the escalating frequency and magnitude of wildfires in southern and western Europe, the importance of compound events and the synergistic effects they have on exacerbating extreme fire outbreaks must continue to be carefully analysed. This study introduces MHW's to the compound research and evaluates its coincidence with other climatic episodes, considering its potential interconnections with other extreme events.

Thus, the primary objective of this study is to comprehensively examine the occurrence of heatwaves (both marine and atmospheric) and drought episodes and their single and compound association with the occurrence of extreme wildfires in the Mediterranean region over the past decades, conducting assessments over monthly, seasonal and annual scales, with a primary focus on the most extreme years. The analysis of atmospheric and marine heatwave indices, combined with the evaluation of drought indices and the identification of burned areas across southern Europe, will allow to further comprehend the potential relationship between these climatic extreme events. The innovative and crucial evaluation of the synergies between these contributing factors may improve the understanding of the mechanisms underlying fire behaviour, which is critical for developing preventive strategies and establishing resilience measures aimed at reducing the devastating effects of wildfires and therefore preserving ecological stability.

This work resulted in the production of a scientific paper, submitted to the Scientific Reports journal (Nature) in December 2023, as part of a Guest Edited Collection focused in the subject "Wildfires", currently undergoing peer review (c.f. Appendix) and was presented at several conferences, seminars and project meetings in 2023 (c.f. CV).

Chapter 2

Data

2.1 ERA5 reanalysis data

To proceed with the identification of AHWs, MHWs and droughts, data from the ERA 5th generation (ERA5) was retrieved. This dataset was produced by the European Centre for Medium-Range Weather Forecast (ECMWF) and offers several global atmospheric, ocean and land variables. The ECMWF is responsible for the production of numerical forecasts of the global climate through models that, in conjunction with data assimilation systems, enable the reanalysis of achieved observations, estimating a globally complete and consistent dataset. ERA5 is the latest ECMWF's reanalysis, which benefits from significant improvements when compared to the previously used ERA-Interim reanalysis (Hersbach et al., 2020). This dataset was developed under the Copernicus Climate Change Service (C3S) and is made accessible through the C3S Climate Data Store (CDS), which offers hourly and monthly data from 1940 onwards, either in single or pressure levels. The data is gridded to a regular $0.25^\circ \times 0.25^\circ$ horizontal resolution ($0.5^\circ \times 0.5^\circ$ for the case of ocean waves) Hersbach et al. (2023).

In the context of this work, ERA5 hourly data for the period spanning from 1979 to 2022 was retrieved for single levels and for different variables: 2-meter air temperature (T2m) to define AHWs, sea surface temperature (SST) to define MHW's, and total precipitation (P) to define droughts. T2m is the air temperature at a height of 2 meters above the Earth's surface, whether it's over land, sea, or inland waters. SST corresponds to the temperature of sea water near the surface. Both T2m and SST have units of Kelvin (K). P represents the cumulative amount of liquid and frozen water, encompassing both rain and snow, that falls to the Earth's surface. The measurement unit for P is depth in meters of water equivalent.

2.2 Land cover remote sensing data

Data from the European Space Agency Climate Change Initiative (ESA CCI) Land Cover (LC) project, which is made accessible through the C3S CDS (Copernicus Climate Change Service, 2019) was retrieved to account for different land covers. The LC project is part of the ESA CCI and aims to improve the algorithms used to generate a global land product, aligning with the requirements set by the Global Climate Observing System (GCOS) (European Space Agency (ESA) Climate Change Initiative, 2023).

The LC dataset was created from multiple observational products, which include the use of Medium Resolution Imaging Spectrometer (MERIS) both at Full Resolution (FR) and Reduced Resolution (RR) archive from 2003 through 2012, creating a baseline land cover map covering a 10-year period. This baseline map is further updated, combining data from the Advanced Very-High-Resolution Radiometer

2. Data

(AVHRR) time series from 1992 to 1999, SPOT-Vegetation (SPOT-VGT) time series from 1998 to 2012, PROBA-Vegetation (PROBA-V) from 2013 to 2019 and Sentinel-3 OLCI (S3 OLCI) for 2020. This processing chain involving data from different satellite missions is consistent over time and results in the generation of global annual LC maps that cover the period from 1992 to 2020, with a horizontal resolution of 300m (Defourny et al., 2017).

The LC data from the ESA CCI classification is divided into 22 global classes (level 1) and 37 regional classes (level 2) - where available, which have been defined using the United Nations Food and Agriculture Organization's (UN FAO) Land Cover Classification System (LCCS). In this work, LC classes were extracted for the years between 2001 and 2020 and grouped into six main categories: cropland, grassland, urban, forest, wetland, shrubland, water and others. Further details on the definition and arrangement of LC classes are provided in Table A1 of the Appendix.

2.3 MODIS remote sensing data

To detect occurrences of fire activity over the study period, burned area (BA) data was extracted from the MCD64A1 Version 6 Burned Area Product (Giglio et al., 2015). This data is acquired from NASA's Moderate-Resolution Imaging Spectroradiometer (MODIS) sensor aboard the Terra and Aqua satellite platforms.

The MCD64A1 burned-area algorithm aims to provide accurate mapping of burned areas using satellite data and statistical methods. Its approach employs 500-m MODIS daily surface reflectance imagery coupled with 1-km MODIS daily active fire observations. Valid daily reflectance values are extracted from MODIS short-wave infrared channels 5 and 7 and used to compute the daily burn-sensitive vegetation index, which successfully discriminates between burned and unburned pixels, due to its strong sensitivity to vegetation changes. Active-fire information is then considered to statistically distinguish areas in which changes are burned-related or non-burned related, using a dynamic threshold on the time series of composite imagery. The algorithm encodes the date of the burn in a single data layer by representing it as the julian day of the calendar year on which the burn occurred. A comprehensive explanation of this algorithm is further described in (Giglio et al., 2018). When compared to previous versions (e.g., Giglio et al. 2009, MDC64A1v006 exhibits enhanced tolerance to the presence of cloud and aerosol contamination. Furthermore, it detects smaller fires more precisely, provides reduced uncertainty in the estimation of the date of the burn, and a large reduction in the extent of unclassified grid cells (Giglio et al., 2018).

This dataset provides monthly values with a 500m spatial resolution, and contains five layers of information: Burned Date (julian day of burn for all pixels identified as burned, ranging from 1 to 366); Burned Date Uncertainty (estimated uncertainty in burn day); QA (quality assurance indicators); First Day (initial day when a potential burn event is detected based on changes in reflectance); Last Day (final day when a potential burn event is detected based on changes in reflectance).

In this work, monthly burned dates from MDC64A1v006 were extracted, from 2001 to 2022, since no data retrieved by this sensor is available prior to this period, and was accessed through the Application for Extracting and Exploring Analysis Ready Samples (AppEEARS Team, 2023). A simplified classification approach is used to categorize pixels into two distinct groups. All pixels that are identified as burned, regardless of the specific Julian day of the burn, are assigned a value of 1. Conversely, all other pixels, including those that are unburned, unmapped due to data limitations, and those over water, are assigned a value of 0.

The calculation of burned areas in hectares is performed using the Haversine formula, which is widely

2. Data

used to compute distances between two points on the surface of a sphere. Here, the Haversine formula is applied to calculate distances on Earth by considering the latitude and longitude coordinates of two points. Although the result is approximate as the formula assumes the Earth to be a perfect sphere, this is still a valuable tool to compute distances on the Earth's surface (Robusto, 1957).

It is important to highlight that this work is primarily concerned about rural fires that are mostly related to the occurrence of adverse climatic factors, namely heatwaves and droughts. The focus is not related to fires used in agricultural practices, which have different and non-climatic drivers (Bekar and Tavşanoğlu, 2017). LC yearly classification from the ESA CCI LC dataset is used to distinguish fires over forests and shrubland from seasonal fires to clean regions burned for agricultural practices over cropland areas. This data, which originally has a spatial resolution of 300m was resampled using the nearest neighbour and majority rule interpolation techniques to match the 500m resolution of the BA data. The land cover dataset only covers the period from 1992 until 2020. To address this limitation, the data from 2020 is used for the years 2021 and 2022, allowing the identification and exclusion of cropland areas from the study.

Chapter 3

Methodology

3.1 Study regions

The study area is defined by the area ranging from 30°N to 52°N and from 20°W to 38°E, mainly focused on three areas, as depicted in Fig 3.1. Fig. 3.1 also shows the land cover types within all the region of study, using data of 2020 from the ESA CCI LC project.

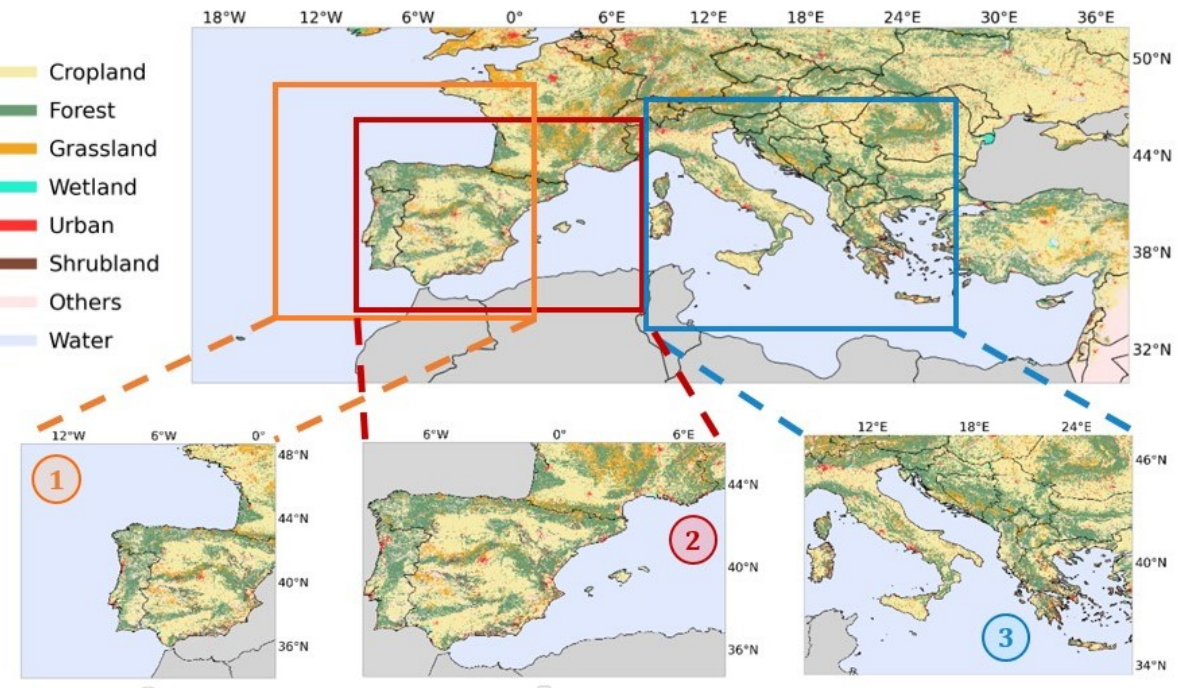


Figure 3.1: Based on ESA CCI LC data, land cover classes are shown based on information for the year 2020. Three subregions were chosen: Region 1) centered on Iberia and southwestern France, considering the Atlantic region and excluding the Mediterranean Sea, Region 2) centered on Iberia and Mediterranean France and considering the Mediterranean Sea, Region 3) centered on Italy and the Peloponnese (Southeast of Europe) and considering the Mediterranean. Areas shown in gray are masked.

3. Methodology

3.2 Marine and atmospheric heatwaves

One of the problems when analysing heatwaves statistically is related to the fact that a universal definition is non-existent. Previous studies have employed different definitions and indices to study the occurrence of heatwaves (Perkins, 2015; Perkins and Alexander, 2013). Therefore, the lack of a universally accepted definition has often resulted in ambiguity and inconsistency in the analysis. Hobday et al. (2016) proposed a flexible methodology to define MHWs, which has been widely used in numerous studies (Oliver et al., 2018; Plecha et al., 2021; Simon et al., 2022). This approach provides a consistent terminology, definition and metrics which enable meaningful comparisons between different heatwave events across different locations and time periods. Additionally, it offers a flexible classification customized for several practical applications. This definition was firstly developed for AHWs and then minor adjustments were introduced, so it could have a broader classification to account for the longer time scales of ocean variability compared to the atmosphere. In this study, this methodology is used to identify both AHWs and MHWs as periods with daily temperatures above the 90th percentile for at least five consecutive days. The climatological mean and the 90th percentile are calculated at each grid cell for each calendar day. The reference period over which the events are defined covers all years from 1979 to 2022, following the minimum recommendation of 30 years proposed by the WMO (World Meteorological Organization, 2018). If any interval of two days or less between heatwaves occurs, a continuous single event is considered. As ERA5 data offers an hourly resolution, the maximum daily temperatures were computed in order to identify the events, following the methodology adopted by Perkins and Alexander (2013) for AHW's. Here, this calculation is applied to both atmospheric and marine events to uphold consistency. A schematic definition of a heatwave is illustrated in Fig. 3.2.

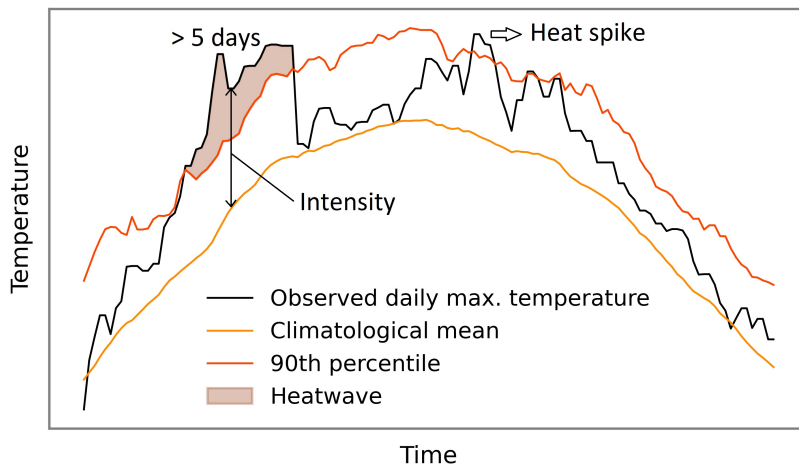


Figure 3.2: Schematic definition of heatwaves, according to Hobday et al. (2016)). The light orange curve represents the climatology and the dark orange curve the 90th percentile threshold. The black curve corresponds to daily temperatures and shaded areas to the occurrence of heatwave events.

In this study, AHW's are only analysed over land pixels, and the oceanic region will be solely characterized by MHW's. Once identified, heatwaves can be characterized by some properties (Golubeva et al., 2021):

- Duration of the event: period over which daily temperatures exceed the defined threshold;
- Intensity of the event: quantified by measuring the difference between the observed temperature and the corresponding climatological value. Within a certain event, the maximum intensity is the

3. Methodology

highest temperature deviation relative to the climatology, while the mean intensity represents the average temperature anomaly during the heatwave;

- Intensity Composite Index (ICI) serves as a composite measure that summarizes the heatwave properties mentioned above and is computed through the following formula:

$$ICI = \sum_{i=1}^n \sum_{d=1}^d \Delta T(i, d) \quad (3.1)$$

where $i = 1, \dots, n$ is the number of heatwave events, d is the duration of the i -th event, and $\Delta T(i, d)$ measures the intensity of the i -th event on its d -th day. This means that temperature anomalies are successively accumulated whenever a heatwave occurs over a specific period of time (units: $^{\circ}\text{C}\cdot\text{days}$). In this study, ICI is calculated monthly and yearly to capture heatwave conditions on both a monthly and annual scale. These properties were applied to both AHW's and MHW's.

3.3 Drought conditions

Drought events can be characterized through the computation of a panoply of indicators, being two of the most widely used multi-scale indices: the SPI (Standardized Precipitation Index) and SPEI (Standardized Precipitation-Evapotranspiration Index). SPI and SPEI allow for the identification of drought and wet events as well as the characterization of their duration, intensity, and magnitude, being used in multiple studies at global and regional scales (Vicente-Serrano et al., 2014b; Gouveia et al., 2017; Russo et al., 2017, 2019; Vogel et al., 2021). The SPI was proposed by McKee et al. (1993) as a drought monitoring index that relies solely on precipitation data and is widely used due to its simplicity. SPI has the advantage of being a multiscalar index, being comparable in time and space, allowing to monitor drought response with respect to different ecosystems. However, it is not able to account for the influence of temperature, which has been rising throughout the world in the last decades. On the other hand, SPEI, developed by Vicente-Serrano et al. (2010), not only considers precipitation but also evapotranspiration (ET) data in its computation, allowing for more effective detection of the effects of climate change on drought conditions while accounting for the influence of temperature variability and extremes. This is significant as it is well established that increased evapotranspiration levels can favour the development of more severe droughts, as a result of greater atmospheric evaporative demand stemming from temperature rise (Vicente-Serrano et al., 2014b). For this reason, the analyses in this study will rely on the SPEI method, although the SPI was also computed (c.f. Appendix, Figs. A1, A2).

The computation of SPEI was made using the period between 1979 and 2022 as the reference period, only considering the land pixels. Firstly, monthly accumulated precipitation was calculated, and evapotranspiration (ET) was also determined by applying the Hargreaves equation (Eq. 3.2), which relies on maximum and minimum temperature records (Hargreaves, 1994).

$$ET(\text{mm}/\text{day}) = 0.0023 \times RA \times (T^{\circ}\text{C} + 17.8) \times TD^{0.5} \quad (3.2)$$

where RA (mm/day) represents extraterrestrial radiation and depends on the day of the year, $TD = \text{Tmax} - \text{Tmin}$ ($^{\circ}\text{C}$), and $T^{\circ}\text{C}$ is $\frac{\text{Tmax} - \text{Tmin}}{2}$.

The difference between the precipitation and the ET provides a measure of water excess or deficit (Vicente-Serrano et al., 2010).

3. Methodology

$$D = P - ET \quad (3.3)$$

A log-logistic probability distribution was fitted to model the water deficit with a rectangular adjustment (Beguería et al., 2014; Vicente-Serrano et al., 2010). The probability distribution function of D according to this type of distribution is given by:

$$F(x) = \left[1 + \frac{\alpha}{(x - \gamma)} \right]^b \quad (3.4)$$

The parameters of the Log-logistic distribution α , β , and γ can be obtained following Singh et al. (1993) (see Vicente-Serrano et al. (2010) and Singh et al. (1993), for a clearer explanation).

The SPEI can be obtained as the standardized values of $F(x)$, following the classical approximation of (Abramowitz and Stegun, 1968) (Eq. 3.4). The result is a normal distribution with a mean of zero and a standard deviation of one, where positive values indicate wetter conditions and negative values imply drier conditions (Fig. 3.3). A SPEI of 0 indicates a value which corresponds to 50% of the cumulative probability of D , according to a log-logistic distribution.

$$SPEI = W - \frac{C_0 + C_1 W + C_2 W^2}{1 + d_1 W + d_2 W^2 + d_3 W^3} \quad (3.5)$$

The constants are $C_0 = 2.515517$, $C_1 = 0.802853$, $C_2 = 0.010328$, $d_1 = 1.432788$, $d_2 = 0.189269$, and $d_3 = 0.001308$. If $P \leq 0.5$, then $W = -2 \ln(P)$, where P is the probability of exceeding a determined D value, $P = 1 - F(x)$. If $P > 0.5$, then P is replaced by $1 - P$, and the sign of the resultant SPEI is reversed.

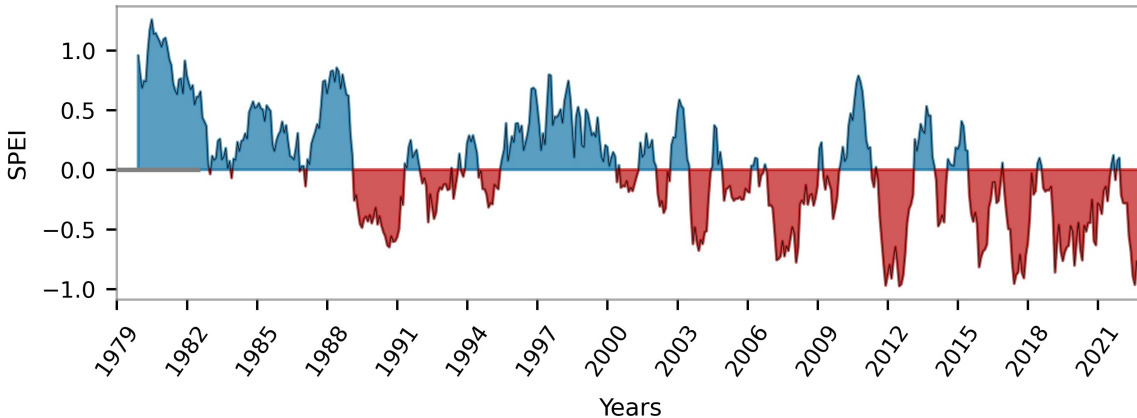


Figure 3.3: Time series showing the 12-month SPEI for every month between 1979 and 2022, averaged over the whole region of study, where negative values correspond to drier conditions (filled up in red) and positive values correspond to wetter conditions (filled up in blue).

The computation of the evapotranspiration and the drought index SPEI was performed using the SPEI R-package freely available (Beguería and Vicente-Serrano, 2023). The Hargreaves equation was used, as it has been suggested to be robust, particularly considering the limited data available for its computation (Páscoa et al., 2017; Vicente-Serrano et al., 2014a). The 12-month time scale is able to identify drought events on an annual perspective, reflecting hydrological drought conditions, whereas the 3-month SPEI reflects soil water conditions of short to medium duration and allows for seasonal drought recognition. In this study, SPEI was computed on a monthly basis at timescales of 3 and 12 months (respectively, SPEI-3 and SPEI-12 hereafter) to explore drought conditions on both a seasonal and annual scale.

3. Methodology

Areas affected by drought conditions can be identified based on probability classes. According to Agnew et al. (2000), moderate droughts correspond to a probability of occurrence of 0.201 (approximately the 20th percentile of the SPI series, -0.84), while severe and extreme droughts correspond to a probability of 0.10 (-1.28) and 0.05 (-1.65), respectively. These thresholds are often considered also in the case of SPEI (Páscoa et al., 2017; Vicente-Serrano et al., 2014b; Gouveia et al., 2017) and were adopted in this work.

3.4 Interannual evaluation and coincidence analysis

To investigate the interannual changes in heatwave conditions and explore the concurrent patterns in marine and atmospheric heatwave properties during the whole study period, yearly spatial averaging is performed for all of the heatwave properties, considering the full region of study, for the cases of AHW's and MHW's. Yearly spatial averages of SPEI-12 in December are also computed, as well as the annual percentage of pixels in moderate and severe levels of dryness, capturing the interannual drought conditions in the domain of study. The time evolution trends of heatwave properties and drought conditions are then tested for statistical significance using a Wald test (Ward and Ahlquist, 2018) with a t-distribution and a significance level of 0.05.

The statistical relationship between temperature and precipitation patterns was evaluated for two different periods: 1979-2000 and 2001-2022, through the computation of two probability density functions using bivariate Gaussian distributions, which are considered suitable to analyse seasonal values of precipitation and temperature (Bevacqua et al., 2022). The bivariate distributions were computed for different pairs of variables: T2m-P, SST-P and T2m-SST. For the cases of T2m and SST, daily maximum values were considered, whereas for P, daily accumulated values were taken into account. These pairs of variables were yearly averaged over the different regions of interest, considering only an extended summer season (May to October) when reduced precipitation and extremely high temperature values promote the ignition and rapid propagation of fires (Turco et al., 2017). The temporal correlation between each pair is calculated, and its statistical significance is assessed, testing at a significance level of 0.05. Univariate Gaussian distributions are also used to compute probability density functions of the average anomalies of each variable for the two periods, to analyse how T2m, SST and P average anomaly patterns individually changed in the different regions.

To evaluate the long-term relationship between areas affected by wildfires and the occurrence of hot and dry conditions, the spatial means of the annual atmospheric ICI and SPEI-12 in December were analysed over the burned pixels, spanning all regions under investigation, between 2001 and 2022. BA's data's resolution (500m) differs from the ICI and SPEI data's resolution (0.25°). Therefore, the computation of the values of ICI and SPEI for each burned pixel by averaging the values from its four nearest points in ERA5's resolution (Fig. 3.4). As marine ICI does not overlap geographically with the other variables, the ICI in the ocean was averaged yearly for the different marine areas of study to provide a clearer understanding of the phenomenon under investigation, assessing how it may be associated with the occurrence of the other events.

3. Methodology

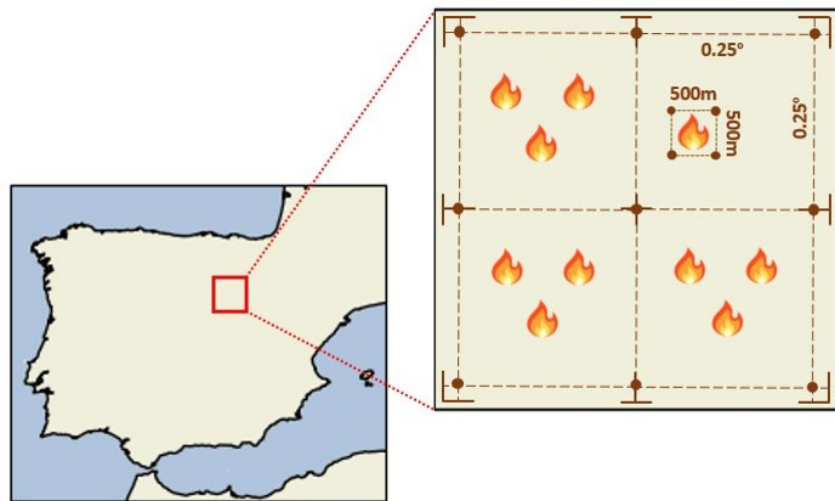


Figure 3.4: Schematic figure showing an exemplification of how SPEI and atmospheric ICI values are aggregated in each burned pixel, through the average of the 4 nearest points in ERA5's resolution. For each burned pixel, represented by the fire icon, the values of ICI and SPEI of the four nearest points are aggregated and averaged.

Adopting a similar methodology to understand the synergy between short-term extreme events and fire occurrence, the monthly-averaged atmospheric ICI and SPEI-3 over burned pixels and monthly-averaged marine ICI in the surrounding areas were calculated in each region for every month between 2001 and 2022. The 80th percentile of the monthly atmospheric and marine ICI and the 20th percentile of the monthly SPEI-3 were used to find the 20% warmest and driest months in the considered period, examined solely in the months where BA's were identified. The months characterized by such warm and dry conditions were explored, considering both individual and compound occurrences. Furthermore, in this evaluation, we distinguished between months when the overall burned area equalled or surpassed the 80th percentile and those that fell below this threshold. This differentiation provides valuable insights into the factors linked to the occurrence of notably extensive fires compared to those of lesser dimension.

In the last part of this work, monthly burned pixels occurring concurrently with each type of individual or compound hazards were aggregated, and their collective extent in hectares was calculated. Subsequently, an analysis was conducted to explore the prevalence of each event or compound events during the cumulative occurrences of less and more extensive fires spanning the years 2001 to 2022.

Chapter 4

Results

4.1 Temporal evolution and spatial distribution of heatwave conditions

The analysis of the temporal evolution of heatwave properties between 1979 and 2022, for both the atmosphere and the ocean, is presented in Fig. 4.1. Both marine and atmospheric yearly averages of ICI, number of events, mean duration and mean intensity of heatwaves show a statistically significant positive tendency. Variations in the yearly frequency of events are consistent when considering both curves (Fig. 4.1a), with a significant increase of 3.7 events in the atmosphere and 4.2 events in the sea over the entire period.

With the exception of the initial years, the mean duration of events is always higher in the ocean, which also shows a steeper upward trend (Fig. 4.1b). In AHWs, there is an annual increment of 0.08 days, while MHWs experience a yearly increase of 0.33 days. Mean durations in the ocean also show higher levels of variability in comparison with the atmosphere. The mean intensity of AHWs, however, reveals greater values and variability over the atmosphere, showing an increase of 3°C since 1979 until 2022 (Fig 4.1c). The interannual variability becomes less pronounced in the most recent decades, as for the case of the duration of the events (Fig. 4.1b). In the ocean, the average intensities exhibit reduced variability, showing an increase of 1°C over the whole period, which is less pronounced than in the atmosphere. The ICI of heatwaves (Fig. 4.1d) displays an upward trend considering both AHWs and MHWs due to its dependence on the other three heatwave properties. Higher values and a more accentuated trend are evidenced in the atmosphere, aligning with observations made for mean intensity (Fig 4.1c). Notably, the majority of years exhibit consistent behaviour when comparing the variations in the ICI values in the atmosphere and the ocean. In the latter half of the 1980s, specific years experienced significantly high ICI values, particularly in the atmosphere, due to heightened heatwave frequency (Fig. 4.1a) and mean intensity (Fig. 4.1c). However, in the most recent years, the situation has considerably intensified. This escalation is attributed to a combination of heightened intensity, frequency, and duration of events, surpassing previous levels, both regarding AHWs and MHWs.

4. Results

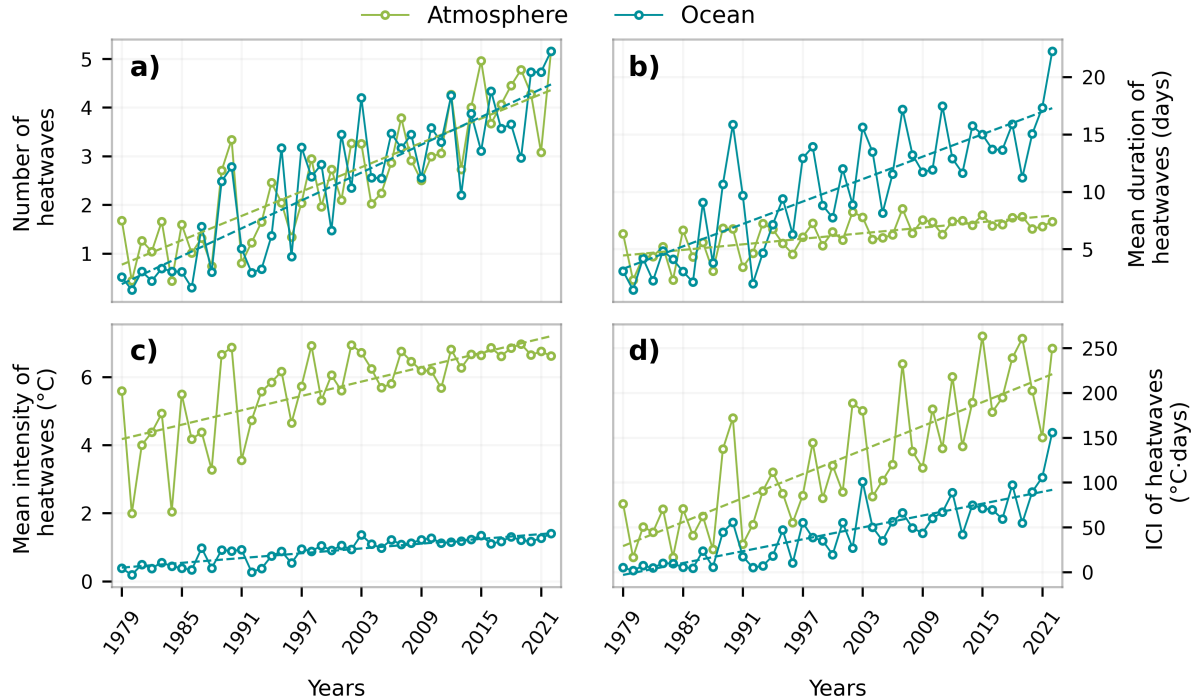


Figure 4.1: Temporal evolution of heatwave properties between 1979 and 2022: (a) number of heatwaves, (b) mean duration of heatwaves (days), (c) mean intensity of heatwaves ($^{\circ}\text{C}$) and (d) ICI ($^{\circ}\text{C}\cdot\text{days}$). Blue curves represent MHWs, being area-averaged over the ocean pixels, while green curves denote AHWs, area-averaged over the land pixels. This analysis considers the full region of study. The dashed lines indicate significant linear trends, considering a 0.05 significance level.

The spatial distribution of the heatwave characteristics above-mentioned is explored in the next step of this work, by primarily focusing on the most extreme years.

Fig. 4.2 shows the number of AHWs occurring over land and MHWs over the ocean across each pixel throughout the entire study period. The year 2022, which recorded the highest frequency of heatwave events, was particularly affected by AHWs in southern and southwestern Europe and by MHWs in the East Atlantic region. The years 2020 and 2021 also exhibited a noteworthy abundance of MHWs. Specifically, in 2021, the Mediterranean Sea experienced a pronounced impact, while in 2020, elevated values were distributed across the East Atlantic and Mediterranean Sea regions. In 2015, a substantial increase in the occurrence of AHWs was observed, particularly notable in southern Spain.

4. Results

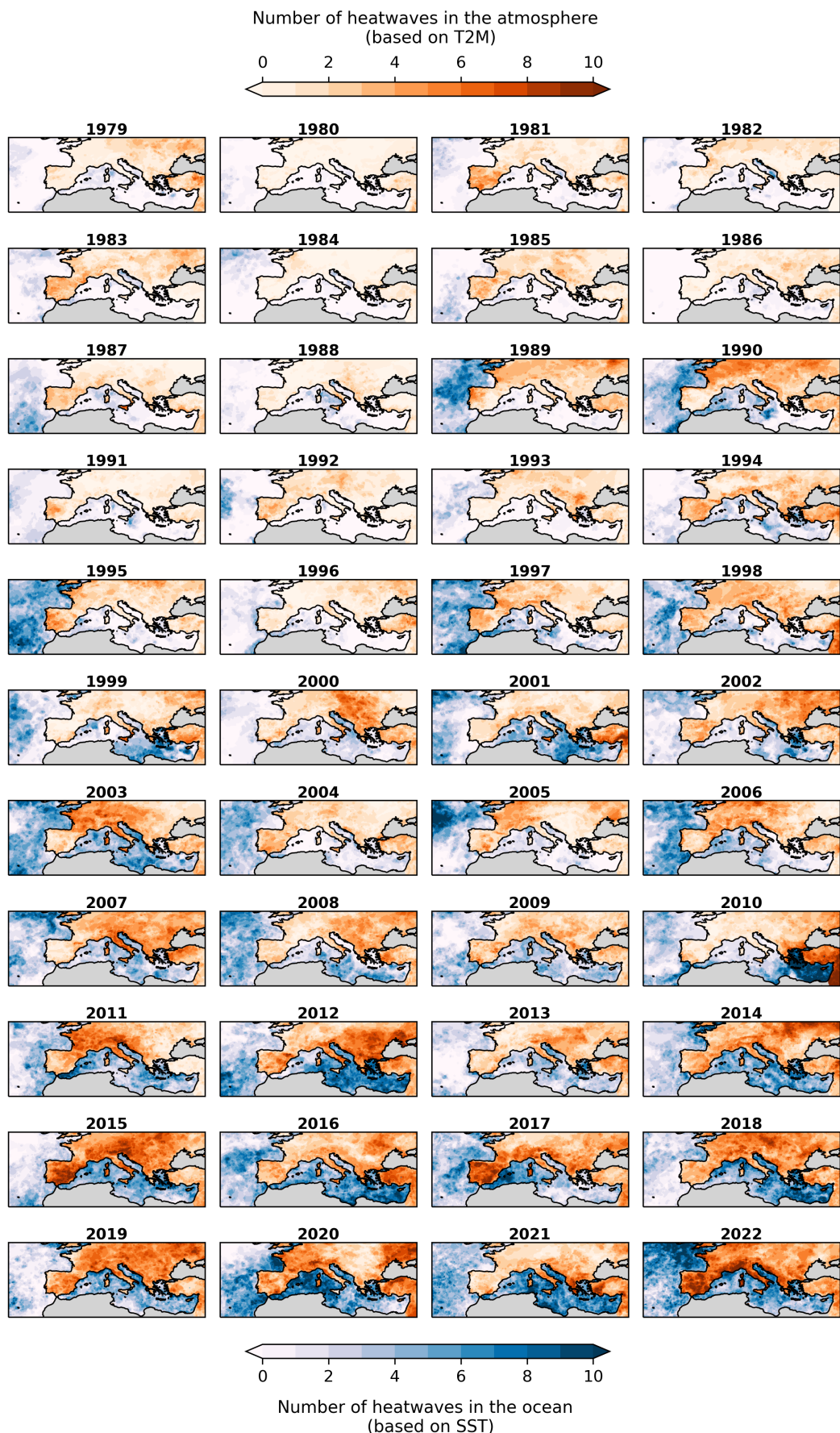


Figure 4.2: Yearly number of heatwaves (AHWs in land and MHWs in the ocean) between 1979 and 2022. Areas shown in gray are masked.

4. Results

The average mean duration of heatwaves, both in the atmosphere and in the ocean, for each year during the study period is illustrated in Fig. 4.3. Notably, certain years exhibit substantial spatial variability in the duration of MHWs (e.g., 1997, 2004, 2015). Over land, AHWs usually exhibit more evenly distributed values. Particularly, the year 2022 stands out with the highest mean duration of MHWs (Fig. 4.1b). It is evident that the more prolonged events predominantly occur in the western Mediterranean region. Notable instances of prolonged events include the years 2010, in Russia, and 2003 in the Iberian Peninsula and Mediterranean Sea. The year 2007 can also be highlighted for its prolonged events, particularly in eastern Europe and the Mediterranean Sea.

Figure 4.4 depicts the distribution of the annual mean intensity values across the entire domain and for all years. In marine regions, the Mediterranean region frequently exhibits higher intensities compared to the Atlantic Ocean. This is evident in specific years, such as 2003, 2012, 2015, and 2022. Over land, intense heatwave events can be highlighted, particularly in Central Europe, for instance, in 1989, 1990, 1998, 2003, 2007, 2019 and 2021.

Fig. 4.5, consolidating information from the indicators depicted in Figures 4.2, 4.3, and 4.4 into a composite index (ICI), offers a more comprehensive visualization of the annual heatwave conditions both in land and in the ocean. Over land, the year 2015, the most severe of all (Fig. 4.1d) was particularly intense in parts of central Europe and the southeastern Iberian Peninsula. Occurrences of other extreme situations included particularly central and eastern Europe, in 2019, western Europe, in 2022, central Europe, in 2003, Iberian Peninsula, in 2017, and Russia, in 2010. When considering marine regions, the Mediterranean Sea contributed to the highest ICI values (Fig 4.1d) in 2003, 2018, and 2022. It becomes evident, as is the case of mean intensities, that the Mediterranean Sea usually shows to have more extreme levels of ICI than the Atlantic Ocean.

Fig 4.5 also provides clear spatial contrasts, allowing not only a comprehensive exploration of the annual heatwave conditions over land and ocean but also a more detailed insight into the proximity of concurrent atmospheric and marine conditions. For instance, several years display simultaneous extreme annual ICI values over both sea and land in relatively proximate regions. This phenomenon occurred in 1997 in Portugal and the adjacent Atlantic Ocean coast. In 2003, heightened ICI values were observed not only over central Europe but also across the Mediterranean Sea. Further cases of co-occurring events were seen in 2010 and 2012 in eastern Europe and the eastern Mediterranean Sea. The most recent case occurred in 2022, when western Europe and the western Mediterranean were notably affected by severe heatwave conditions over both land and sea.

4. Results

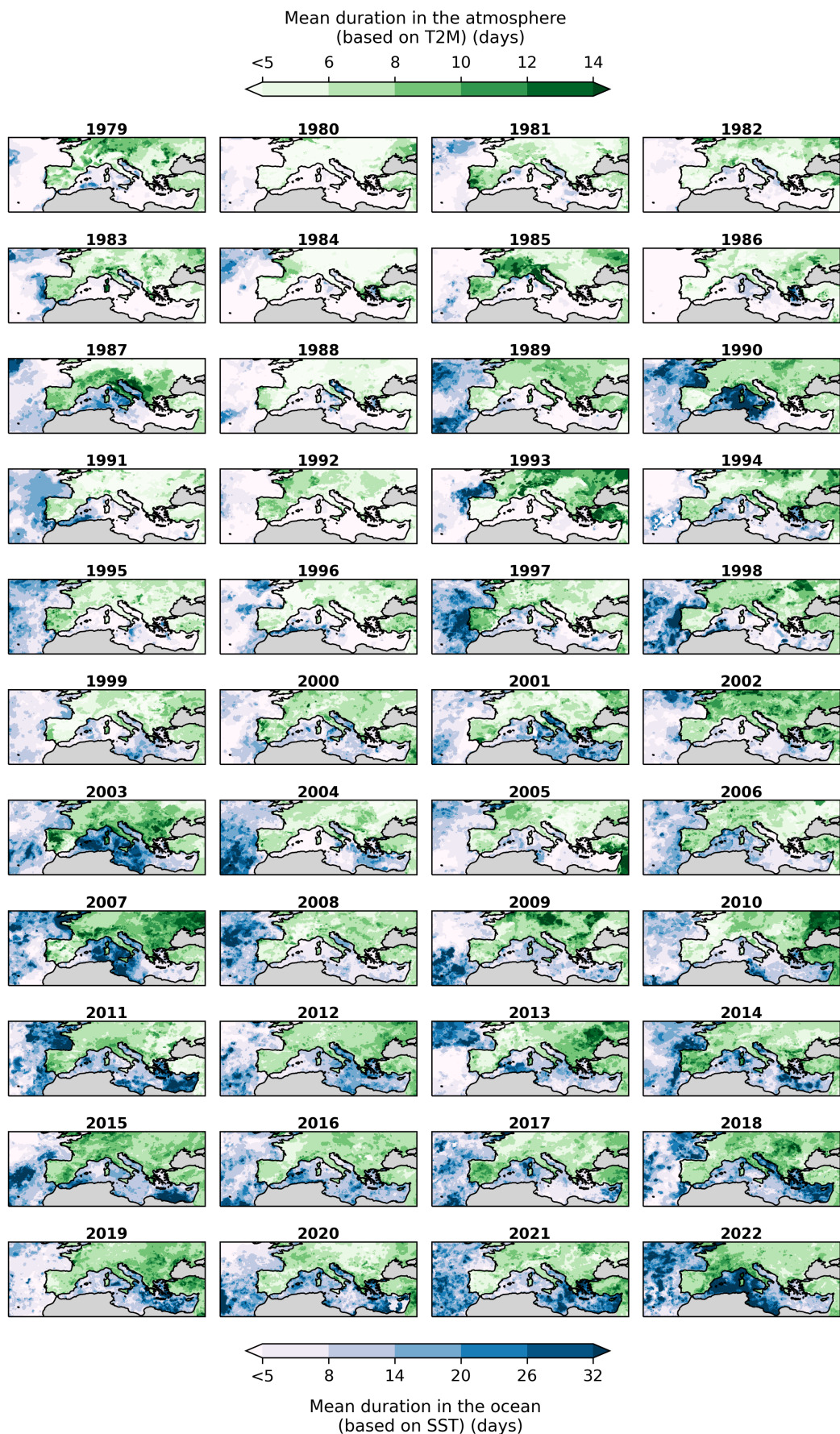


Figure 4.3: Annual averages of heatwaves' mean duration (AHWs in land and MHWs in the ocean), in days, between 1979 and 2022. Areas shown in gray are masked.

4. Results

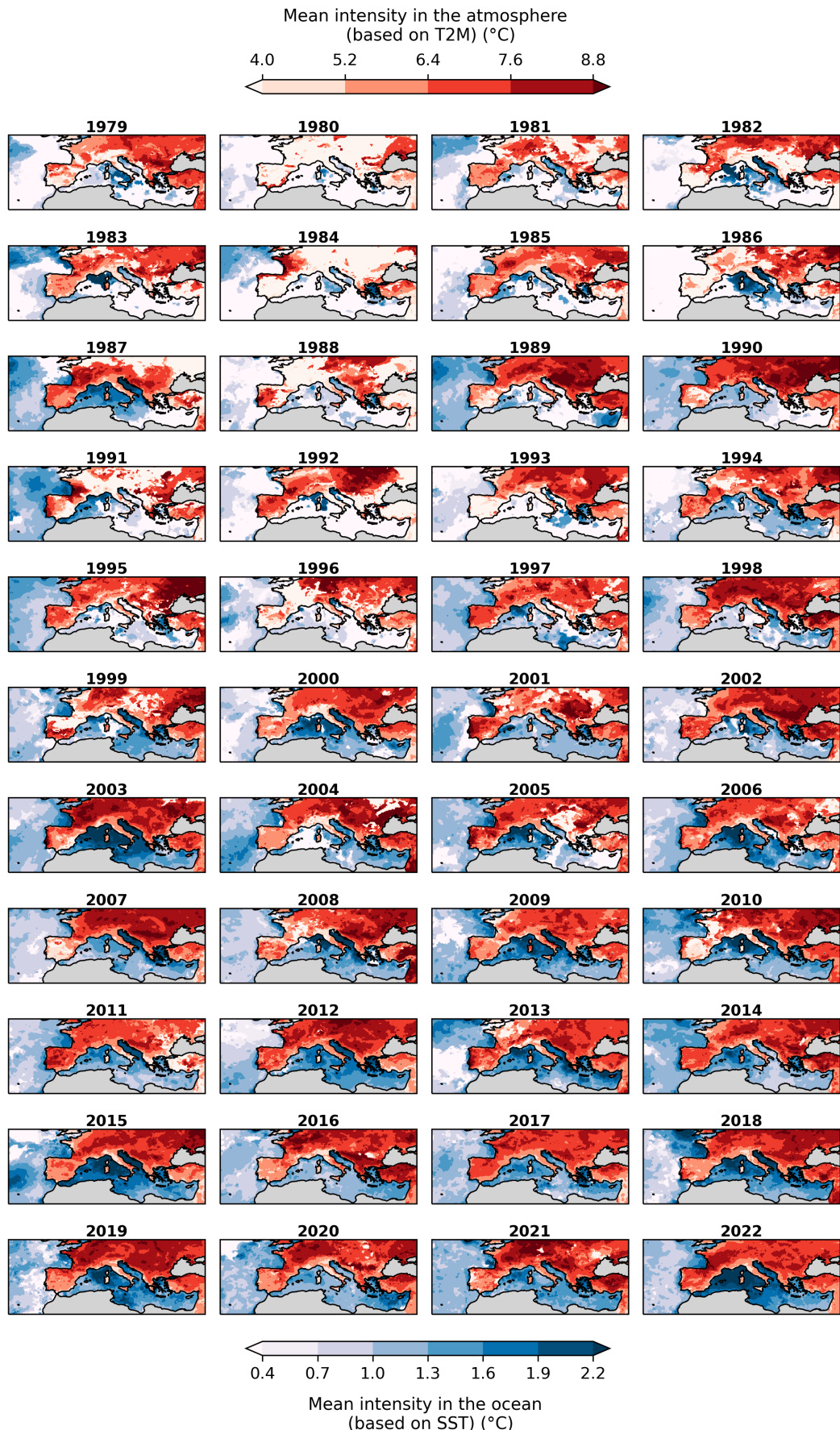


Figure 4.4: Annual averages of heatwaves' mean intensities (AHWs in land and MHWs in the ocean), in °C, between 1979 and 2022. Areas shown in gray are masked.

4. Results



Figure 4.5: Atmospheric yearly ICI over land and the marine yearly ICI over the ocean, in $^{\circ}\text{C}\cdot\text{days}$, between 1979 and 2022. Areas shown in gray are masked.

4. Results

4.2 Temporal evolution and spatial distribution of drought conditions

This subsection focuses on the evaluation of the evolution of drought conditions over the years, with a particular emphasis on the most extreme years, and the spatial distribution of drought affected areas. Although this evaluation relies on the analysis of SPEI, the time and spatial analysis of the SPI were also computed and revealed similar results (c.f. Appendix, Figs. A1, A2). The temporal evolution of drought conditions after computing the spatial averages of SPEI-12 for December is shown in Fig. 4.6 (upper panel). The percentage of area under moderate, severe and extreme dry conditions is displayed in the lower panel. In the current century, there is a higher prevalence of years characterized by dry conditions, with only 36% of years exhibiting positive SPEI levels. Among these years, 2010 stands out as the most humid one, while 2011, 2015 and 2022 reveal to be the driest ones. In contrast, the 20th century witnessed 73% of years with positive SPEI levels. The most significant exceptions are the years 1989 and 1990, which were notably hot, as revealed by heatwave properties (Fig. 4.1), and also strongly affected by drought conditions (Fig. 4.6). Moderate droughts exhibit greater frequency and have experienced a more significant increase over the years compared to severe and extreme droughts. Positive and statistically significant trends are evident in the below panel for all types of droughts, indicating a clear increase from 1979 to 2022, at a rate of 0.54% of area per year for moderate droughts, 0.35% per year for severe droughts, and 0.17% per year for extreme droughts. The years affected by the highest percentage of drought conditions, whether moderate, severe or extreme, were 2003, 2011, 2015 and 2022.

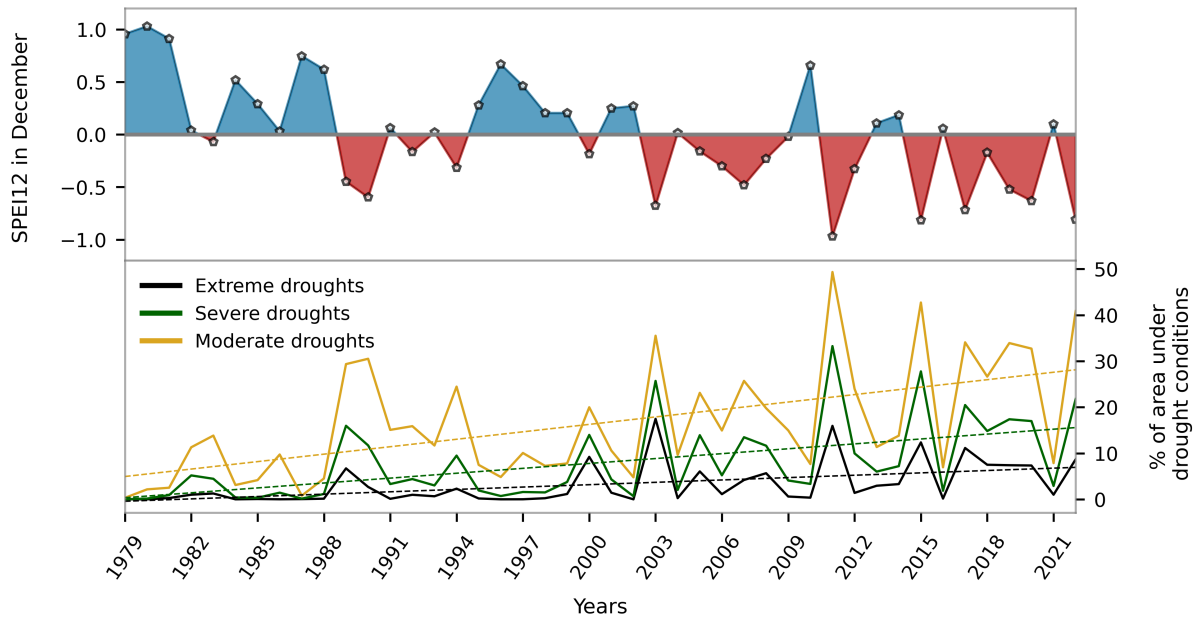


Figure 4.6: Temporal evolution of drought conditions. In the upper panel are displayed the spatial-averaged values of the 12-month SPEI for December over land between 1979 and 2022, and the below panel shows the percentage of area under the occurrence of moderate droughts (yellow curve), severe droughts (green curve) and extreme droughts (black curve), using the definition by Agnew et al., (2000) and considering the December SPEI-12 values. This analysis considers the full region of study. Only land pixels were taken into account. The dashed lines indicate significant linear trends, considering a 0.05 significance level.

4. Results

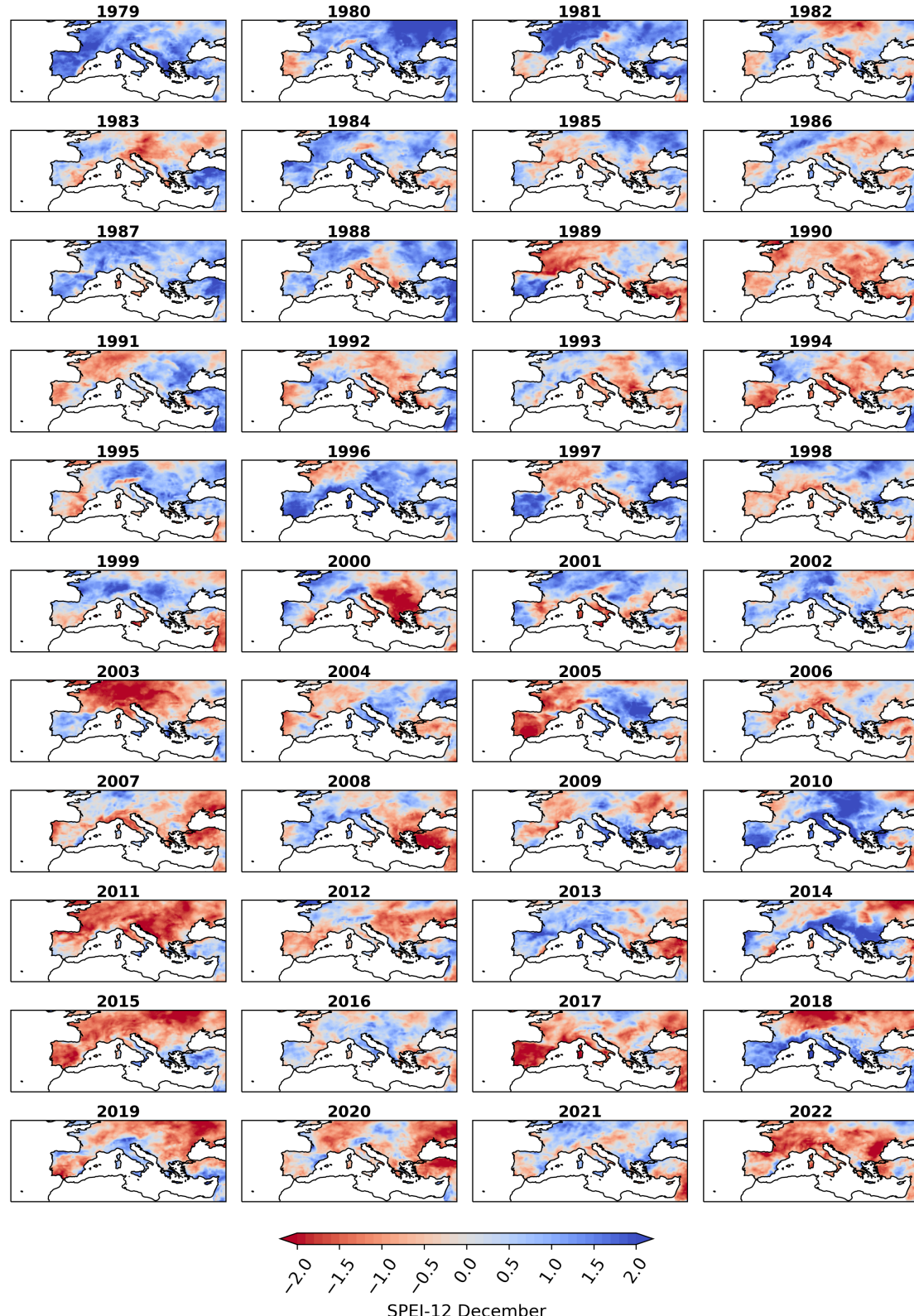


Figure 4.7: Values of the 12-month SPEI in December over the European land area, between 1979 and 2022.

Analysing the spatial distribution of the SPEI-12 values for December (Fig. 4.7), it can be seen that intense drought conditions were prevalent mainly in central Europe in 2003). It can also be emphasized that the year 2005 was affected by intense drought conditions mostly in western Europe, particularly in the Iberian Peninsula. The year 2015 is another example when both strong heatwave conditions (Fig

4. Results

4.5) were accompanied by intense drought conditions that developed over a wide spatial extent of the European continent. The year 2017 was particularly dry in western Europe, which promoted widespread impacts on various resources and was associated with forest fires in Iberia . The region was also affected by severe heatwave conditions (Fig 4.5) during the same period. Lastly, it is important to highlight the year 2022, another example of a very hot (Fig 4.5) and dry year over a considerable part of Europe.

The observed fluctuation in values depicted in both panels of Fig. 4.6 illustrates a pronounced variability in drought levels throughout the study period. As a matter of fact, the temporal changes reflect the spatial extent, as depicted in Fig. 4.7. These changes are not confined solely to temporal changes. The patterns of the SPEI can also exhibit distinct contrasts between closely located regions, as exemplified in years such as 2003, 2005, and 2018.

4.3 Long-term changes in the correlation between temperature and precipitation in the extended summer

The relationship between mean T2m, SST and P during the extended summer season for 1979-2000 and 2001–2022 for all regions of interest is analysed through the computation of bivariate Gaussian probability distribution functions (Fig. 4.8). Additionally, univariate probability distribution functions are depicted to visually demonstrate the temporal evolution of mean temperature and precipitation anomalies individually.

By visually inspecting the univariate probability distribution plots, it can be seen in all cases that both T2m and SST have drastically changed when comparing both periods, exhibiting an abrupt shift towards higher mean anomaly values in the second period. When examining the mean anomaly distribution of accumulated precipitation, this transition exhibits a minor shift, and a contrast between eastern and western regions can be found. In regions 1 and 2, over western Europe, univariate PDFs reveal drier conditions in 2001-2022, while in region 3, in eastern Europe, there is a slight shift in the mean precipitation anomaly distribution in this period, uncovering the presence of wetter conditions.

Upon visually analyzing the bivariate Gaussian distributions, the shape, elongation, and direction of the ellipses provide insights into the apparent correlation between each pair of variables. Elliptical contours aligning along the diagonal from the bottom-right to the top-left suggest the presence of a negative correlation between the two variables. This negative correlation is visibly apparent in the first column of Fig. 4.8 (T2m-P). Conversely, elliptical contours aligning along the diagonal from the bottom-left to the top-right suggest the presence of a positive correlation between the two variables, which is notable for the case of the third column of Fig. 4.8 (T2m-SST). Regarding the second column (SST-P), the contours appear more circular when compared to previous cases, suggesting a less pronounced correlation. To validate the statistical correlation for each case, correlation coefficients were computed and tested for significance (Table 4.1).

4. Results

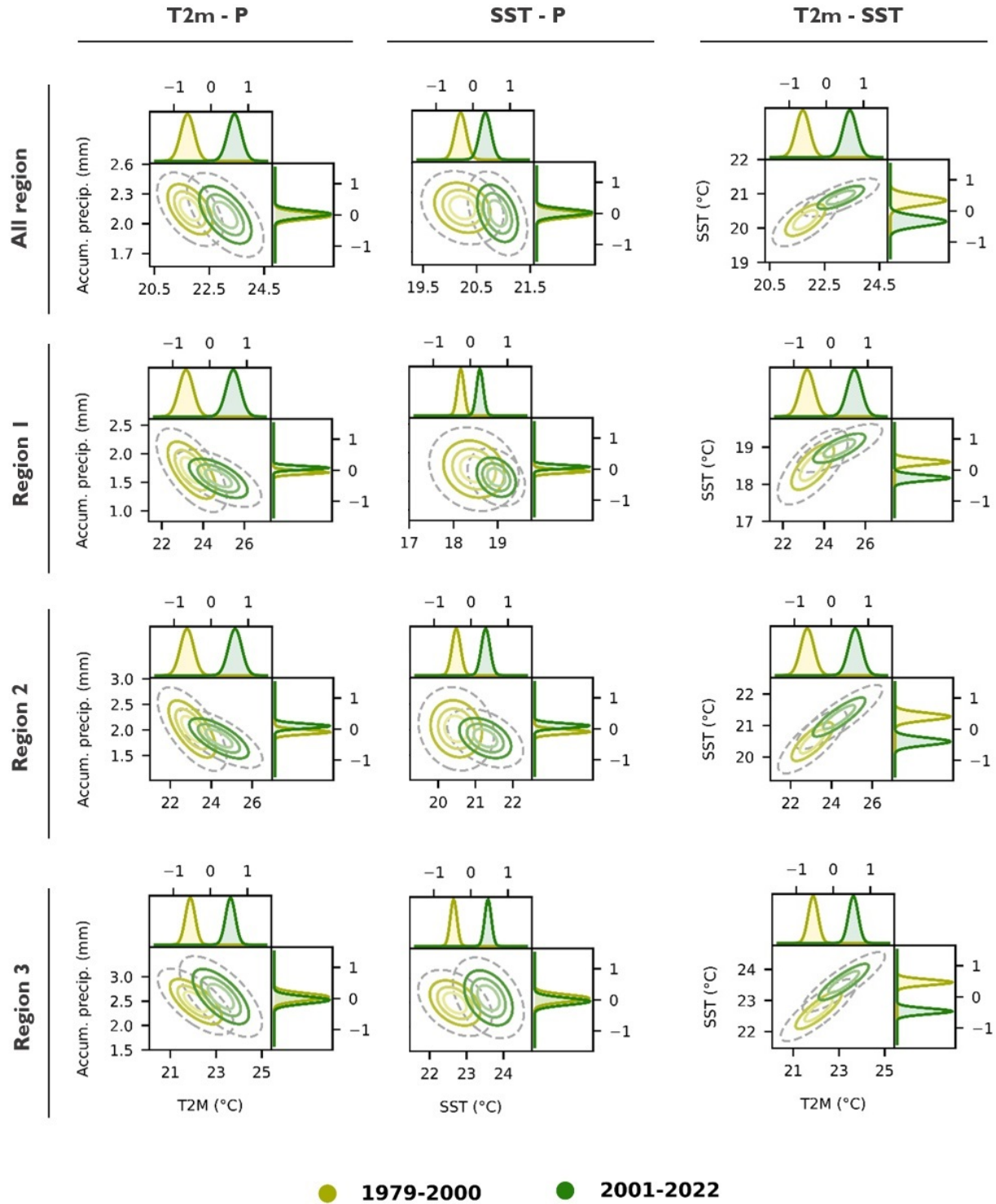


Figure 4.8: Bivariate Gaussian probability distribution functions of extended summer mean temperatures (T2m and SST, $^{\circ}$ C) and accumulated precipitation (mm) (central panel), and the univariate probability distribution functions of the corresponding average anomalies (lateral panels, in the units of the corresponding absolute values), for the period 1979-2000 in yellow, and 2001-2022 in green, over all the regions of interest. The dashed gray ellipses represent the 95% level of the Gaussian probability distributions.

In all regions, correlations between T2m-P show to be negative and significant in both periods (1st column - Fig. 4.8, Table 4.1). The T2m-P correlation intensified in 2001-2022, in comparison with the former period, in the full region and region 2. The correlation between SST-P shows to be negative and

4. Results

Table 4.1: Correlation coefficient values calculated for each pair of values analysed in Fig. 4.8., for the different periods and regions of study. The statistical significance was tested and revealed to be non-significant for all the coefficients in the case of SST - P, and significant for the rest.

		Correlation coefficients		
		T2m - P	SST - P	T2m - SST
Full region	1979-2000	-0.50	-0.21	0.66
	2001-2022	-0.56	-0.37	0.74
Region 1	1979-2000	-0.62	-0.17	0.68
	2001-2022	-0.62	-0.27	0.74
Region 2	1979-2000	-0.66	-0.13	0.78
	2001-2022	-0.70	-0.4	0.86
Region 3	1979-2000	-0.67	-0.39	0.84
	2001-2022	-0.65	-0.37	0.86

very low, but in the second period, the correlation rises considering the full region, region 1 and region 2 (2nd column - Fig. 4.8, Table 4.1). However, in neither of the cases these correlations are statistically significant. Regarding the analysis of T2m-SST, there is a strong and significant positive correlation between these variables in both periods. The correlation coefficients reveal to be higher in the second period for all analysed regions (3rd column - Fig. 4.8, Table 4.1). A pronounced correlation is found between air temperatures and sea temperatures in regions 2 and 3. These correlations are stronger than for the case of region 1 (Atlantic Ocean), suggesting a possible closer association between air temperatures over land and sea temperatures in the Mediterranean Sea.

4.4 Fire activity and its relationship with temperature and precipitation patterns

4.4.1 Temporal analysis and spatial distribution of wildfires

Since the beginning of the century, fire occurrence has varied considerably throughout the years and along the different regions of Europe, as depicted by Fig. 4.9. Given the lack of BA data before 2001, only the period 2001-2022 will be analysed in the following sections.

When analyzing the entire Mediterranean area, 2017 was the most severe year, with a record of more than one million hectares burned throughout the year, followed by 2007, 2012, 2003 and 2005 , which burned from 700.000 hectares to 800.000 hectares (c.f. Appendix, Fig. A3). The spatial distribution of the accumulated burned pixels highlights the Iberian Peninsula as the most affected area in the domain of study between 2001 and 2022 (Fig. 4.10). Portugal, in particular, has experienced a significant incidence of wildfire events throughout the years.

4. Results

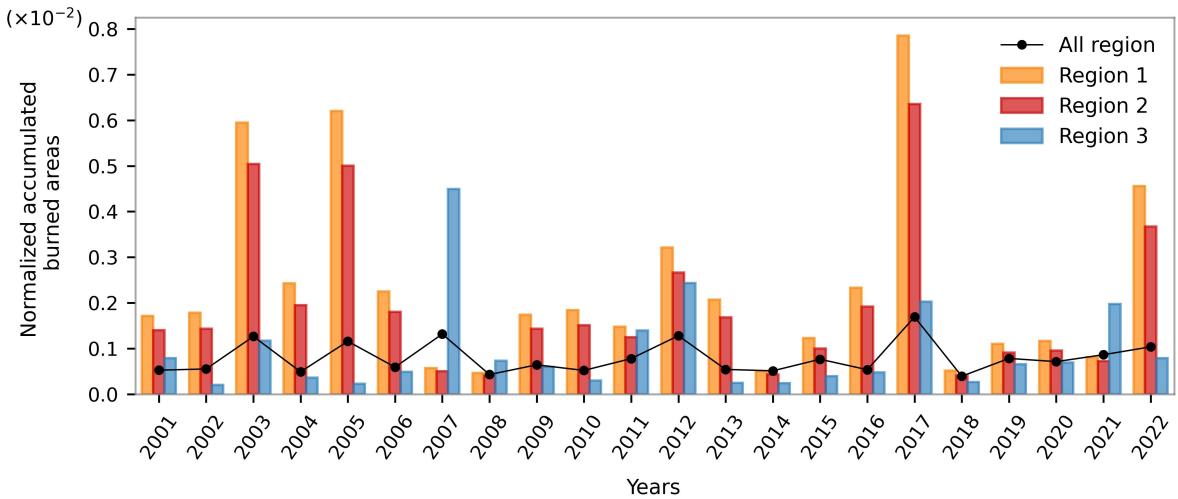


Figure 4.9: Yearly normalized burned areas between 2001 and 2022 for region 1 (orange bars), region 2 (red bars), region 3 (blue bars) and for the overall study region (black curve). Normalized burned areas are obtained by dividing the BAs in hectares by the total land hectares in each of the regions.

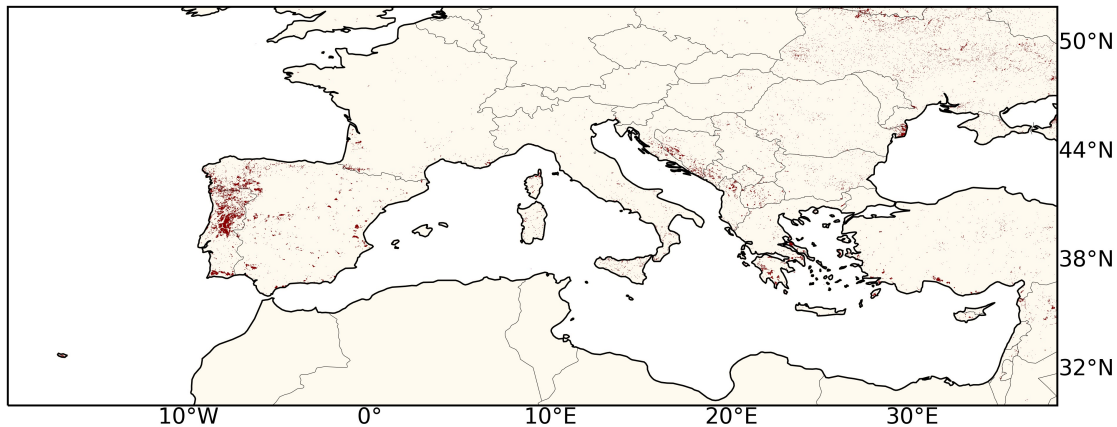


Figure 4.10: Accumulated burned pixels for the period 2001-2022 considering the full land region and masking cropland areas.

Specifically in western Europe, regions 1 (the Atlantic region) and 2 (the Mediterranean region) show similar patterns concerning the extent of normalized BAs, owing to their significant geographical overlap, although region 1 typically exhibits a higher incidence of burning, as demonstrated by its higher values (Fig. 4.9). The years of 2017, 2003, 2005 and 2022 stand out as the most impactful ones in terms of normalized BAs for these regions. In 2017, approximately 600.000 hectares were burned (surpassing 60% of the total BA considering the full region for this year), while in 2003 and 2005, the burned area surpassed 400.000 hectares. In 2022, the yearly burned area was almost 370.000 hectares (c.f. Appendix, Fig. A3). On the other hand, in eastern Europe (region 3), the year 2007 was the most exceptional of all, having burned a total of 530.000 hectares (c.f. Appendix, Fig. A3). Other notable years include 2012, 2017, and 2021. It should be noted that the most affected area is in close proximity to the Adriatic Sea and southern Greece (Fig. 4.10).

4. Results

4.4.2 Seasonal averages of precipitation, air temperature and sea temperature and its association with fire occurrence

In this section, the objective is to analyze the compound occurrence of dry-hot conditions and their association with recorded yearly burned areas, particularly in the most severe years. The analysis is made for pairs T2M-P, SST-P, and T2M-SST, aligning with the structure presented in Fig. 4.8. Yearly accumulated BAs, in hectares, are represented in Fig. 4.11, along with the average values of daily accumulated precipitation and daily maximum temperatures for each year. This approach complements existing studies by incorporating the evaluation of adjacent marine temperatures into the assessment of wildfire occurrence. A seasonal assessment is carried out, covering the interval from May to October, offering a thorough exploration of the seasonal patterns.

These calculations focus particularly on the years marked by the highest incidence of burned areas in the extended summer season, between 2001 and 2022. Considering the whole region, notable examples of severe fire occurrences during the extended summer season included 2003, 2005, 2012, 2017 and 2022 (Fig. 4.12). The summers of 2003, 2005, 2017 and 2022 stood out as notable when considering the extent of BAs in regions 1 and 2 (Fig. 4.12). In the eastern Mediterranean (region 3), the most severe proportion of summer BAs were recorded in 2007, 2012, 2017 and 2021 (Fig. 12). The summer BAs in hectares are shown in Fig. A4 for all years and all regions (c.f. Appendix).

4. Results

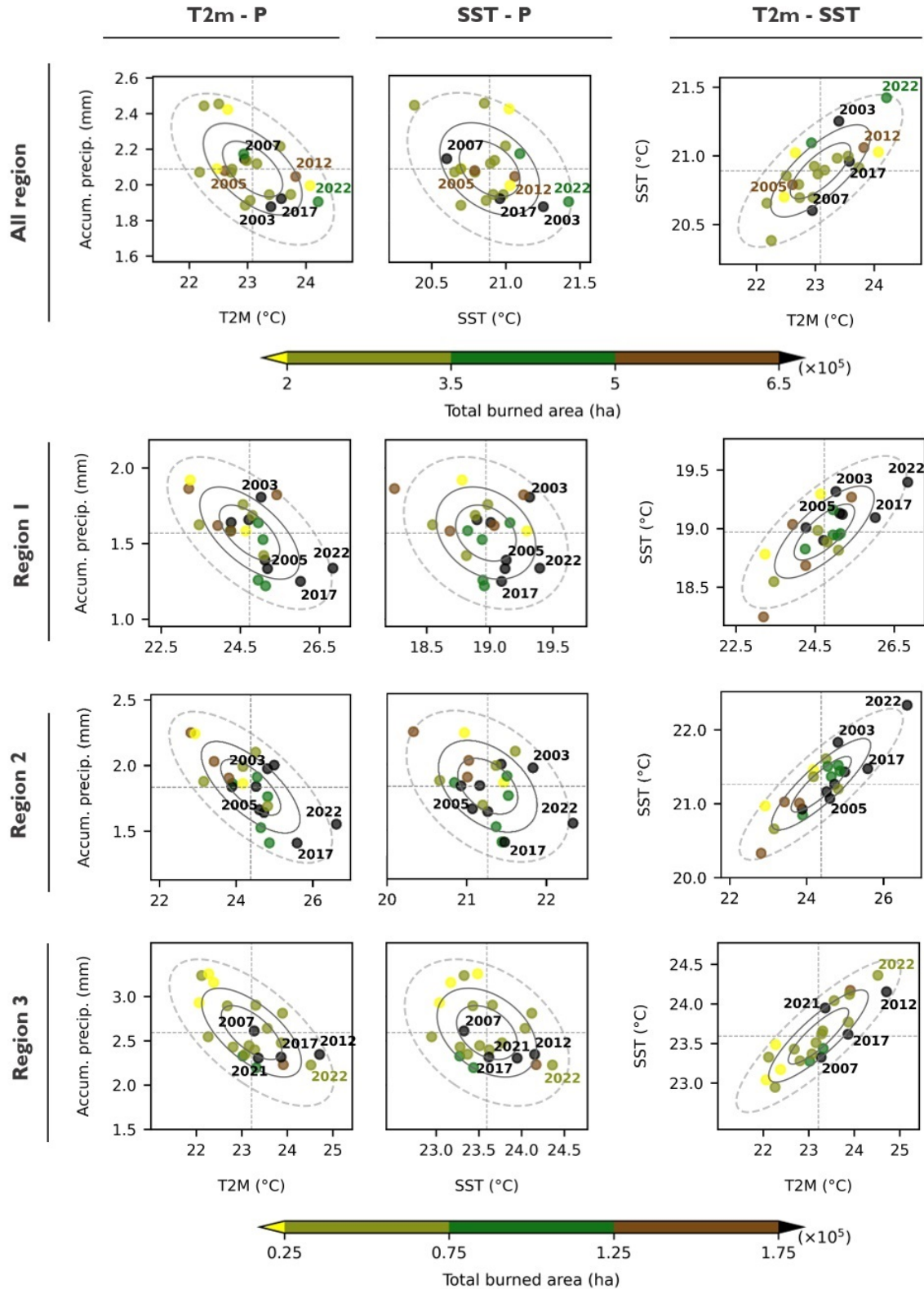


Figure 4.11: Average values of daily accumulated precipitation and daily maximum temperatures (T2m and SST) for each year, calculated for the extended summer (scatter points), and summer accumulated burned area for each year (colors). The bivariate Gaussian probability distributions of all pairs of variables for the period 2001-2022 are represented by the gray ellipses (dashed gray ellipses represent the 95% level). Horizontal and vertical dashed lines correspond, respectively, to precipitation and temperature values averaged over all years of study.

4. Results

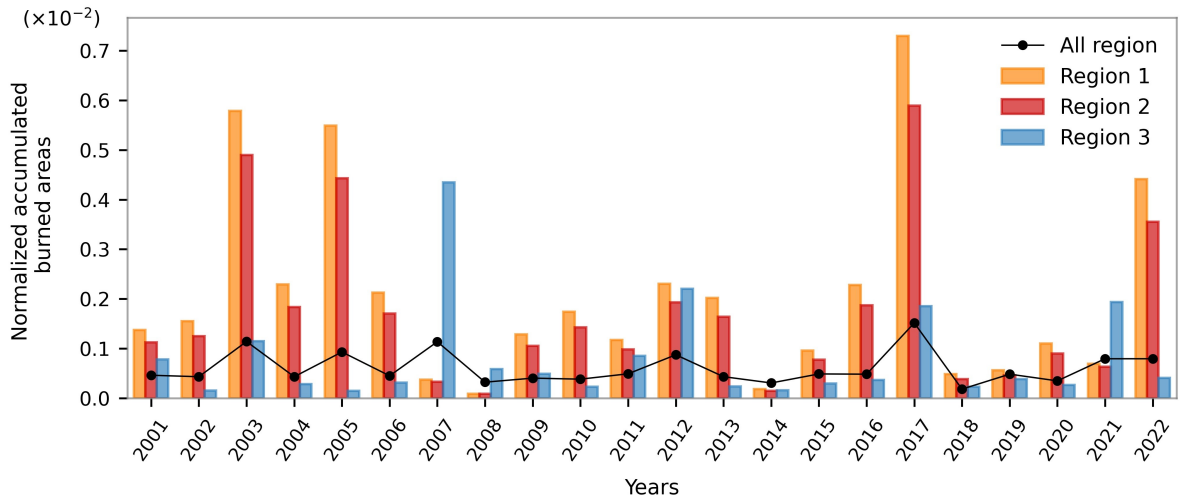


Figure 4.12: As in Fig 4.9, but considering the extended summers.

Considering the whole region, the most notable summers of severe fire occurrences (2003, 2005, 2012, 2017 and 2022), were linked to reduced precipitation and elevated air and sea temperatures, when compared to the average values (Fig. 4.11). The summer of 2003 experienced the driest conditions, while 2022 observed the highest sea and air temperatures since the beginning of the century. Despite its exceptional BA value, the summer of 2007 exhibited relatively less dryness and warmth (in both land and ocean) compared to the average conditions. The summer of 2005, despite having a considerable burned area, was characterized by mean precipitation near the average value and air and sea temperatures below the average.

Shifting the focus to the regional analysis, it can be seen that regions 1 and 2 exhibit analogous patterns, as expected. Some of the most severe years in terms of summer BAs (2003, 2005, 2017, 2022) are situated within the sector of the plots characterized by higher T2m and SST and lower precipitation levels. The summer of 2017, not only had the highest BA value recorded, but it also stood out as the driest and second hottest among all years. The findings depicted in Figure 4.11 also indicate the higher-than-average SST during the prolonged summer of 2017 in both the Atlantic Ocean (region 1) and Mediterranean Sea (region 2). The summer of 2003 was marked by above-average air temperatures in regions 1 and 2. Fig. 4.11 may appear contradictory as it indicates mean precipitation lower than the average for the period. However, this discrepancy is attributed to the very high positive precipitation anomalies in October (c.f. Appendix, Fig. A5), influencing the overall mean results for the entire summer period. The results from Fig. 4.11 illustrate that the SST mean was also markedly elevated for the extended summer of 2003. The summer of 2005 coincided with a very hot and dry period with precipitation anomalies below average values. The summer mean SST surpassed the average in the Atlantic Ocean (region 1) but not in the Mediterranean Sea (region 2). The most recent example of a severely burned summer was in 2022. This period was one of the driest and the warmest of all years of study (Fig. 4.11) and both the Atlantic and Mediterranean regions experienced the highest recorded SSTs.

In region 1, all the significant highlighted years (2003, 2005, 2017 and 2022) exhibit SST values higher than average over the Atlantic Ocean. The region 2 has a similar pattern with region 1 in these years, except for 2005 that manifests lower-than-average SST values in the Mediterranean Sea. Between regions, the SST values contrast, as Mediterranean's tend to be consistently higher than those in the Atlantic ocean.

In the eastern Mediterranean (region 3), the most extensive burned summer, 2007, exhibited T2Ms and precipitation levels relatively close to the average. The close-to-average air temperature values may

4. Results

be attributed to the negative temperature anomalies observed in September and October, counterbalancing the positive anomalies concentrated in May-August (c.f. Appendix, Fig. A6). Substantial positive precipitation anomalies were observed across extensive areas, predominantly in May and October, countering the prevailing high negative anomalies, concentrated mainly in July and August (c.f. Appendix, Fig. A7). The SST's average in the Mediterranean region wasn't markedly elevated during the fire season of 2007 (Fig. 4.11). Conversely, the second most impactful year, 2012, was notably characterized by a very hot and dry summer, with SSTs in the Mediterranean also exceeding the average. The summer of 2017 can also be emphasized by its accumulated burned hectares, associated with very dry and warm conditions and sea temperatures close to the average. The summer of 2021 was the most recent severe case of wildfire incidence in this region, and coincided with dry conditions above the average, mean T2m slightly higher than average and SSTs also above the average. In this region, the years with less extreme burned area extents (2002, 2005, and 2014) correspond to years on average with low SSTs, T2Ms, and precipitation values.

4.5 Heatwave and drought conditions over burned regions on an annual scale

This section aims to specifically analyse heatwave and drought indices over burned pixels on an annual scale. Fig. 4.13 shows the annual atmospheric ICI and SPEI-12 for December, averaged and examined solely over the burned pixels in all study regions. The annual marine ICI is also averaged over the adjacent marine areas in each of these regions categorized into various degrees/thresholds corresponding to different percentiles.

When examining the full region, it is observed that all the years exhibiting an average marine ICI below the 50th percentile also tend to be associated with less dry or less warm (or both) conditions over BAs (compared to the established threshold that delineates the most extreme years), except for 2017. Conversely, some of the years falling above the 50th percentile of marine ICI, mainly 2003, did not exhibit very extreme values for atmospheric ICI and SPEI-12. The years 2007, 2012, 2014, 2015, 2017, 2018, 2020, and 2022 all registered marine ICI values surpassing the 50th percentile while simultaneously recording very high atmospheric ICI and SPEI-12 values, revealing that the conditions over the BAs were considerably hot and arid, and concurrently, the ocean temperatures were also substantially elevated during those years. Although not recording a very high annual marine ICI value, 2017 stood out as the most extreme year in terms of atmospheric ICI and SPEI-12. Meanwhile, 2022 emerged as the most severe year regarding the annual marine ICI.

Considering the partial overlap of land areas between regions 1 and 2, the spatial averaged values of atmospheric ICI and SPEI-12 exhibit similarity. The significant contrast between these regions relates to the average marine ICI values registered over different areas: the Mediterranean Sea (region 2) and the Atlantic Ocean (region 1). In both regions, 2017 stands out as the warmest and driest year across the BAs. The years 2015 and 2022 also experienced very high air temperatures over burned pixels, and the SPEI-12 value remains close to the 20% most extreme cases for 2022 and above for 2015. In all these three cases, temperatures over the Mediterranean Sea were above the 80th percentile threshold. All years registering marine ICI values below the 20th percentile tend to be associated with less dry and warm conditions in comparison to the threshold, except for 2012 for both regions and 2015 for region 1.

In region 3, years for which the average marine ICI surpasses the 80th percentile closely correspond to or exceed the 80th percentile of atmospheric ICI over burned pixels. Notable examples of such extreme

4. Results

years include 2003, 2012, and 2022. The years 2003 and 2022 also revealed to be drier than the threshold. Conversely, years with average marine ICI below the 50th percentile are shown to coincide with less hot and dry conditions over BAs (except for 2011, which revealed to be very dry in this region). In this case, the year 2012 revealed the most extreme atmospheric heatwave conditions and the second most extreme marine heatwave conditions in the surrounding sea.

In all the examined cases, the red line illustrates a negative and significant trend between atmospheric ICI and December SPEI-12 values for burned pixels. This means that years characterized by stronger heatwave conditions tend to also experience drier conditions, and vice-versa.

This long-term assessment of the interplay between marine heatwave, atmospheric heatwave and drought conditions and their association with burned pixels shows that years with considerable marine heatwave conditions (above the 50th percentile of the marine ICI) correspond in nearly 50% of the cases with the occurrence of very strong atmospheric heatwave or dry conditions (or both) over burned regions (above the 80th percentile threshold for atmospheric ICI and SPEI). Conversely, years with lower marine heatwave intensity are mostly associated with less dry and/or warm conditions over burned areas.

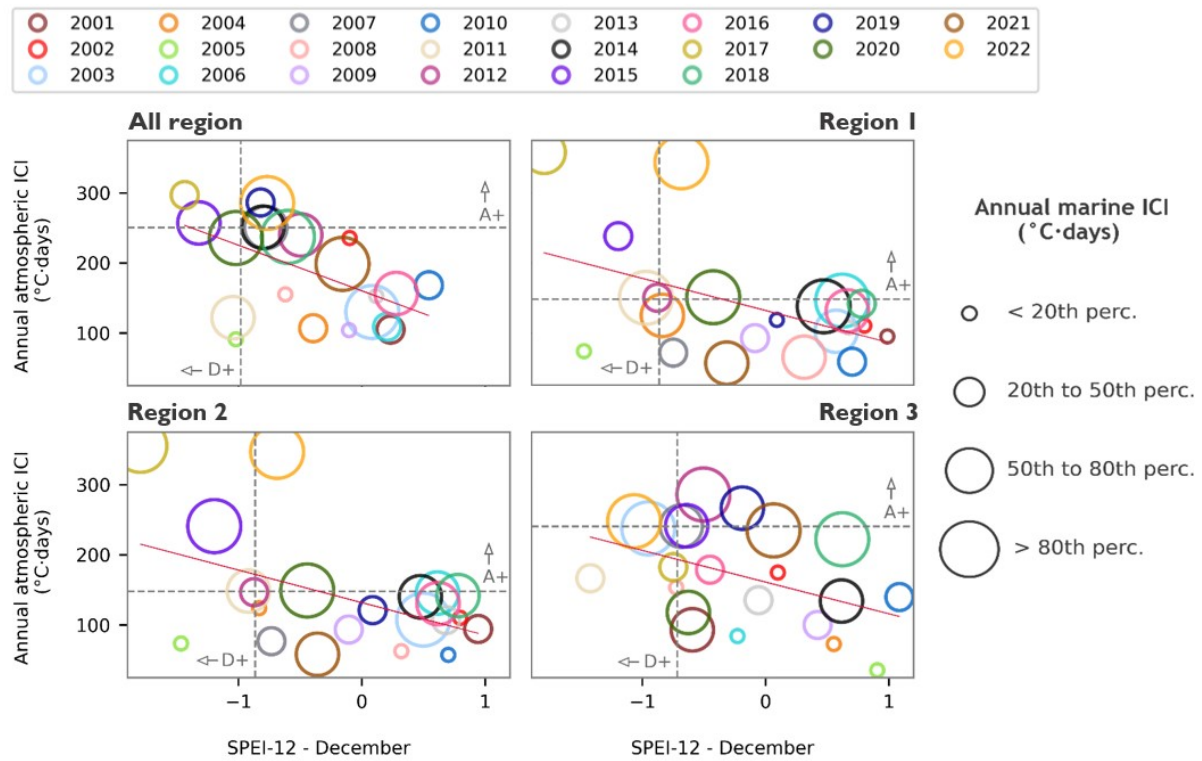


Figure 4.13: Spatial averages of the annual accumulated atmospheric ICI ($^{\circ}\text{C}\cdot\text{days}$) and SPEI-12 for December over burned pixels, regarding each of the study regions. In each region, the annual marine ICI ($^{\circ}\text{C}\cdot\text{days}$) is averaged over the corresponding marine areas and represented through the size of the scatter points, which represent different percentiles. The different scatter colours describe different years from 2001 to 2022. Horizontal and vertical dashed lines separate the 20% most extreme cases regarding the atmospheric ICI (A+) and SPEI-12 values (D+), obtained through the computation of the 80th and 20th percentile, respectively.

4.6 Monthly heatwave and drought conditions over burned regions

This section aims to explore heatwave and drought conditions over BAs on a monthly scale. The distribution of the months affected by the 20% driest and warmest (both in the ocean and the atmosphere)

4. Results

conditions was identified (Fig. 4.14), through the computation of monthly means of atmospheric ICI, and SPEI-3 over burned pixels, and marine ICI in the surrounding seas. This approach provides insights into the occurrence of short-term climatic extreme events in the areas affected by wildfires. Simultaneously, an analysis is conducted to identify months characterized by more or less extensive wildfires, using the 80th percentile of the monthly total burned area. The values corresponding to the thresholds that define the 20% most extreme cases used in this study are presented in Table A2 (c.f. Appendix).

4. Results

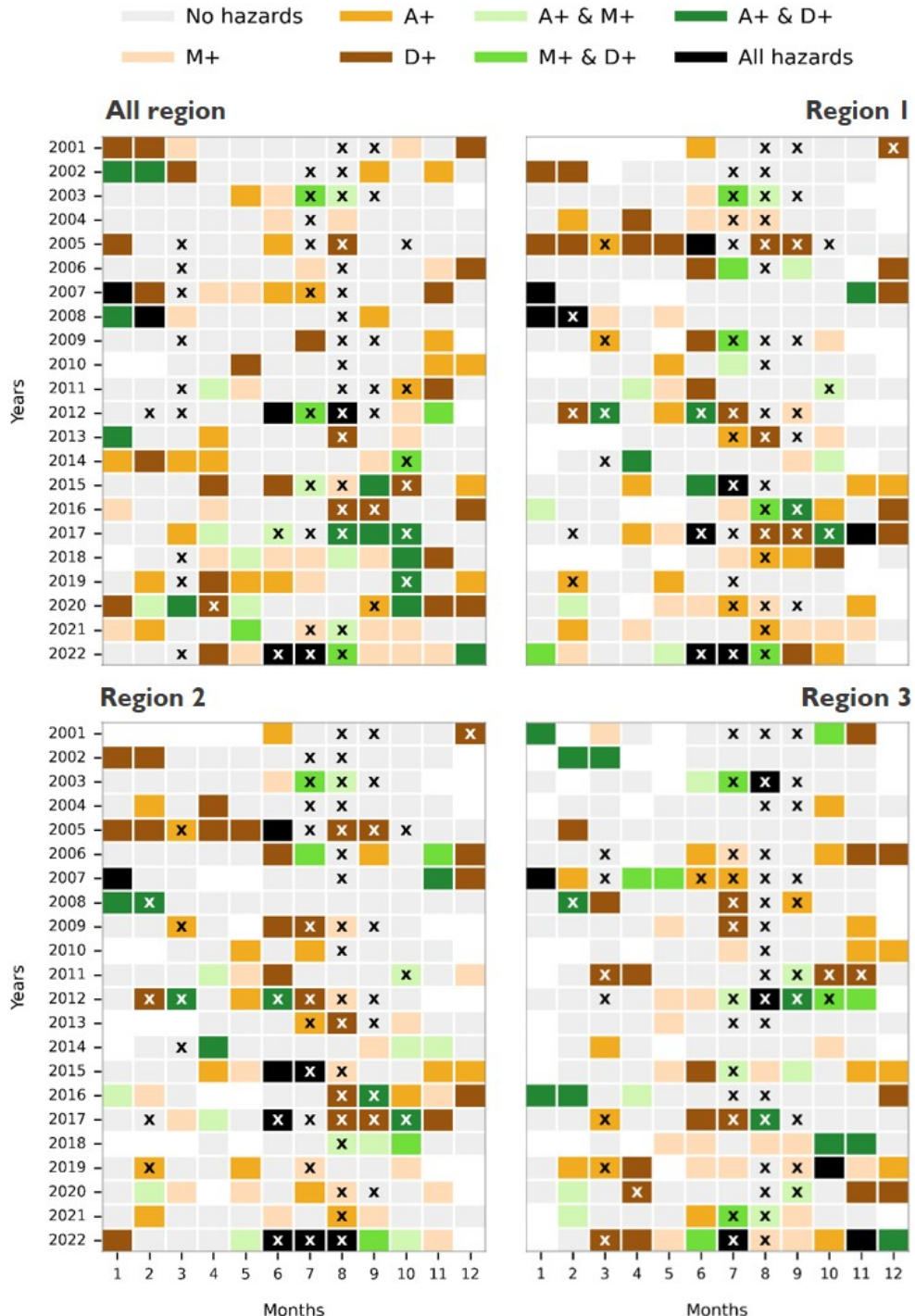


Figure 4.14: Monthly occurrences of single and compound hazards from 2001 to 2022. The 20% warmest and driest months were identified through the computation of the 80th percentile of the monthly-averaged atmospheric and marine ICI and the 20th percentile of the monthly-averaged SPEI-3 (colors), over burned pixels. "A+" and M+" denote a month with atmospheric and marine ICI equal to exceeding the 80th percentile, respectively, and "D+" when the SPEI-3 value equals or falls below the 20th percentile. Months marked with an "X" indicate those where the burned area equals or exceeds the 80th percentile. Months that didn't record any burned pixels are filled in blank.

The month of August consistently records the highest frequency of years with total burned area exceeding the 80th percentile threshold across all analysed regions, followed by July and September. Months characterized by the most extreme climatic conditions are concentrated in more than 50% within the tem-

4. Results

poral window from May to October. March also registers a significant number of years with burned pixels exceeding the 80th percentile, especially when considering the entire region. The occurrence of the driest and warmest months is highlighted during the latter period (2012-2022), when compared to 2001-2011. Concurrently, there is a heightened recurrence of compound hazards in the latter period, while in the first period independent events are more frequent. These observations are coupled with the finding that the incidence of fires associated with non-extreme climatic events decreased in 2012–2022.

The fires which took place in the summer of 2022 need to be highlighted again, as they showed to be particularly extreme in all regions, mainly regarding region 2, where June, July and August revealed to be under the occurrence of all climatic hazards while having recorded extensive burned areas. The summer season of 2022 was the only year which showed the co-occurrence of MHW, AHW, drought and fires for three months (Region 2, June, July, August). Moreover, in this year more than half of the months recorded the occurrence of at least one climatic hazard in all regions. Although 2022 was very extreme, other years also reveal to have been hit by combined extremes. In the Iberian Peninsula, compound occurrences of climatic events leading to severe fire outbreaks were present during the summer of 2003, as well as in May and October of 2017, for example (Fig 4.1). In the eastern area, July and August of 2003 and 2012, as well as the period from July to October of 2012, registered the occurrence of compound hazards associated with extensive wildfires. The results further show the dry conditions that impacted the Iberian Peninsula in 2005, persisting also through the winter, and suggest an association with the occurrence of large fires during the subsequent summer season. Furthermore, in the eastern region, 2007 is characterized by notable dryness preceding the summer season, followed by exceptional atmospheric temperatures during the summer, occurring either concurrently or prior to extensive wildfires. During all the previously mentioned extreme months, there were notable marine heatwave conditions (marine ICI surpassing the 80th percentile) occurring during and prior to these periods.

To succinctly assess the association between climatic events and months of wildfire occurrence and evaluate their coincidence with marine heatwave conditions, Fig. 4.15 showcases the percentage of months associated with the occurrence of the 20% warmest (atmospheric: A+, and marine: M+) and driest conditions (D+), considering both individual and compound occurrences, in each region of study. This analysis is conducted separately for months where the total burned area either exceeded or fell below the 80th percentile threshold. Regarding the left column, which refers to months that did not reach the 80th percentile threshold of accumulated burned area, consistency is shown across all regions of study. The occurrence of these fires is closely associated with occurrences of M+ episodes, constituting approximately 9 to 13.7% of all months. Subsequently, D+ episodes are observed (7.3-10.2%) and following are A+ events (7.3-9.8%), except for region 3, where A+ episodes are more recurrent than D+ events. The remaining combinations of hazards exhibit lower occurrence rates (1-5.1%). Notably, approximately 60% of all months with BAs below the 80th percentile did not experience any of these extreme hazards. Examining months where the total burned area exceeded the 80th percentile threshold (right column of Fig. 14.5), D+ events emerge as highly prevalent across all regions of study, occurring in approximately 11 to 19% of cases. Subsequent rates vary based on individual regions. Overall, these months, marked by more extensive fires, demonstrate a stronger connection with the occurrence of extreme hazards in comparison to months with less extensive fires. Specifically, in regions 1, 2 and 3, over 50% of the months are linked to any type of extreme climatic events. Furthermore, the occurrence of compound hazards is generally more frequent when considering months with a broader extension of BAs, covering more than 25% of all months. The presence of all hazards together (A+, M+ and D+) is associated with 5.7% to 9.4% of the months in these cases. The percentages associated with non-extreme climatic factors correspond to approximately 60% in months characterized by less extensive fires and around 35-50% in

4. Results

months with more extensive fires.

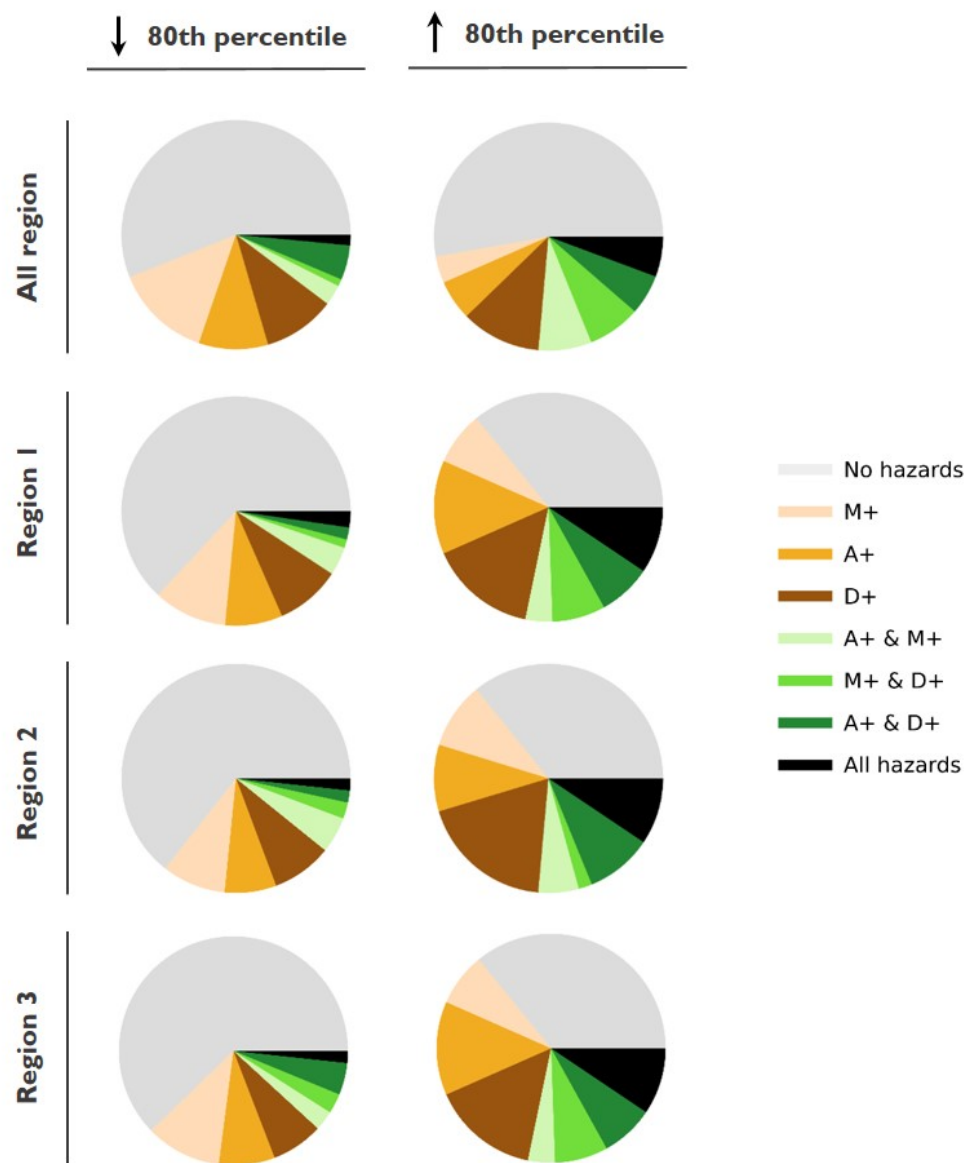


Figure 4.15: Single and compound climatic hazards and its association with wildfires. Percentage of months, shown in Fig. 4.14, that are associated to each of type of hazard or combined hazards, considering only months when any burned area was registered. The categorization is distinguished by the different regions of study and the predefined threshold for burned areas (80th percentile).

4.7 Wildfire incidence under the occurrence of single and compound hazards for 2001-2022

While the concluding segment of the previous section emphasized the proportion of months linked to each category of extreme hazards, the final section of results in this study aims to evaluate the overall association between wildfire occurrence and different types of climatic extremes over the entire study period using a different approach. In this analysis, monthly burned pixels under each type of individual

4. Results

and compound hazards are aggregated and summed, and then normalized by dividing by the total burned area (Fig 4.16). The assessment is carried out for monthly burned areas both under (left panel) and above (right panel) the 80th percentile and provides insights into the prevalence of events across the different regions of study.

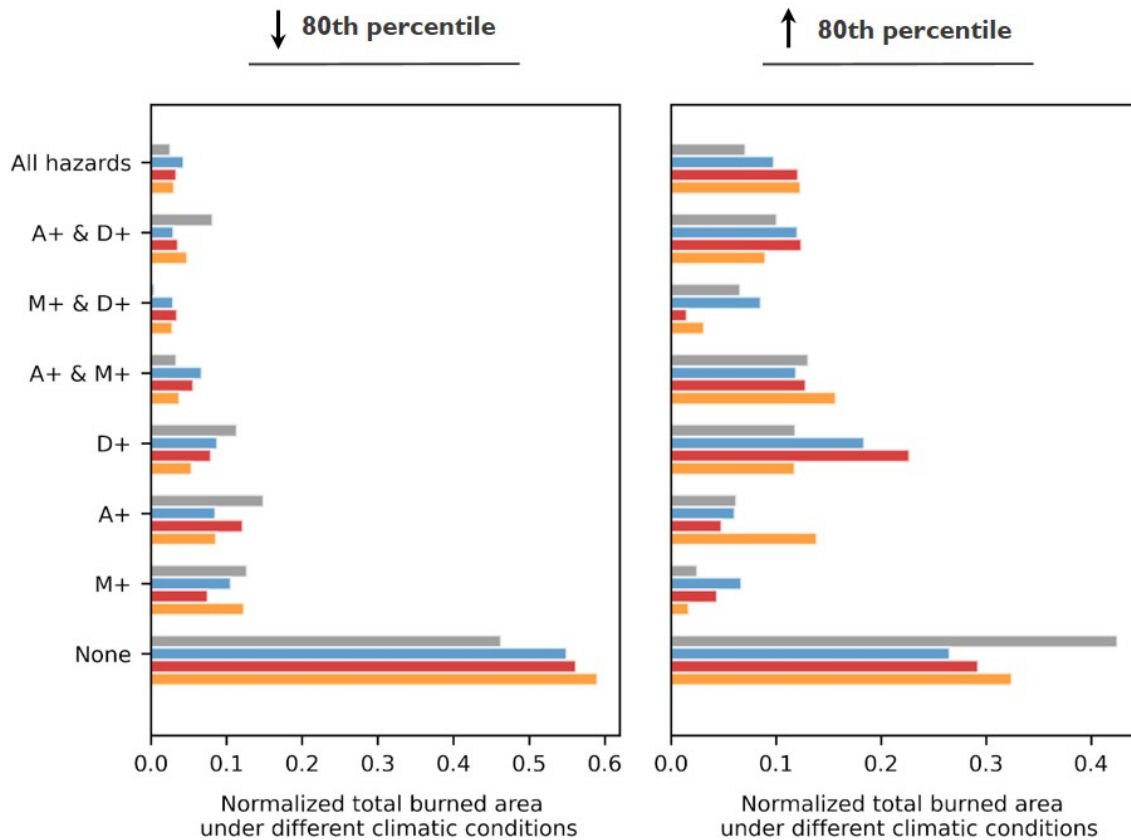


Figure 4.16: Normalized burned areas, from 2001 to 2022, associated to each of type of hazard or combined hazards. The categorization is distinguished by the different regions of study and the predefined threshold for normalized burned areas: months burning less than the 80th percentile threshold (left-side) and months burning above the 80th percentile threshold (right-side). Normalized burned areas are obtained by dividing the BA's in hectares by the total burned pixels in each of the regions.

While a substantial portion of the burned pixels may not exhibit a clear association with the most extreme cases of droughts and heatwaves, as observed in the previous section, the focus here will be solely on burned pixels specifically linked to climatic hazards. For months that burned less than the 80th percentile, consistent with the findings in Figure 4.14, individual hazards (M+, D+, and A+) generally demonstrate higher association with wildfires than compound occurrences across all regions, although at varying degrees. In region 1, M+ events are more prevalent, followed by D+ and A+. In region 2, A+ events show higher prevalence, followed by D+ and M+. In region 3, M+ events are once again the most prevalent, followed by A+ and D+, and then the remaining combinations. In the full region, A+ events show higher prevalence, followed by M+ and D+. The remaining combinations associated with these fires occur less frequently.

In the case of the most extensive fires (above the 80th percentile threshold), the accumulated burned areas exhibit a stronger association with compound occurrences of climatic hazards compared to the previous case, aligning with the results from the previous section. Regarding the full region, region 1

4. Results

and region 2, most of the burned pixels are associated to either A+ & M+ events, individual D+ events, or A+ & D+ events. For region 3, the results show some variation, with the top three rankings being A+ & M+, A+, and all hazards simultaneously.

Overall, strong dry and warm events appear to be coincident with wildfire occurrences at varying levels across all regions. For the most extensive fire occurrences, the marine warmest events, although not being so frequent individually, are often associated with atmospheric strong hot conditions (A+ & M+) or strong dry conditions over land (M+ & D+), or both (all hazards occurring simultaneously).

This analysis reveals that D+ episodes exhibit a potentially stronger association with wildfires in the Iberian Peninsula compared to eastern-southern Europe. In the latter region, A+ and A+ & M+ events coincide with a higher amount of burned area during wildfires in comparison to D+ events. When comparing events in the Atlantic region with the Mediterranean region, the major difference lies in the portion of burned areas associated with M+ & D+ episodes for the most extensive fires, which are more prevalent in region 1. This distinction is further supported by the information presented in Figure 4.14. Conversely, the remaining categories of compound occurrences (A+ & M+, A+ & D+, all hazards) are more commonly observed in region 2.

Chapter 5

Discussion and conclusions

The primary drivers influencing fire ignition and propagation include the presence of fuel (Gouveia et al., 2012), socioeconomic conditions influencing land use/land cover change, fire prevention, firefighting capacity (Moreira F, 2011; Ganteaume et al., 2013), local topography (Carmo et al., 2011), favourable fire weather conditions, and specific conditions preceding or during the fire season, such as droughts or heatwaves (Gouveia et al., 2016; Ruffault et al., 2020; Russo et al., 2017; Turco et al., 2019; Sutanto et al., 2020). As climate change progresses, the escalation of these extreme climatic hazards has become increasingly prevalent. The compounding effects of these hazards may be amplified when they occur simultaneously or in a cascading sequence. This work aims to improve the comprehension of the link between heatwaves and droughts and the occurrence of rural fires in the Mediterranean region throughout the past decades, also considering the evaluation of adjacent marine temperatures.

The identified rising trends in abnormally hot events align with previous studies that have historically analyzed AHWs and MHWs (e.g., Perkins-Kirkpatrick and Lewis 2020; Simon et al. 2022. Given the significant association of anthropogenic activity with this increase (Perkins-Kirkpatrick and Lewis, 2020; Seneviratne et al., 2021; Fischer and Knutti, 2015), there is a pressing need for raising awareness of these phenomena, particularly considering projections indicating a future escalation in their occurrence (Seneviratne et al., 2021; Lhotka et al., 2018; Oliver et al., 2019). The consistency in the temporal variability in the number of heatwaves and their mean duration reinforces the conclusions made by in Aboelkhair et al. (2023), which found a robust correlation between AHWs and MHWs frequency and number of total days for the eastern Mediterranean region, between 1982 and 2021. The aligned patterns of amplification and reduction observed also in other heatwave properties (intensity, cumulative intensity) within both the atmosphere and the ocean highlights the association between atmospheric and marine extreme hot events. The lower variability in MHWs mean intensities and longer MHWs mean durations can be attributed to the heat capacity, persistence, and propagation timescales of oceanic processes, which are much greater than those for the atmosphere (Holbrook et al., 2020).

Some examples of spatial proximity between very intense MHWs and AHWs were also observed over the Mediterranean region, for example, in 2003. The warming in the Mediterranean Sea was attributed to higher rates of air-sea heat flux induced by the intense AHW (Sparnocchia et al., 2006; Olita et al., 2007). This, coupled with subdued winds, resulted in positive SST anomalies. Previous research has also emphasized the role of the high SSTs sustaining and intensifying the AHW (Feudale and Shukla, 2007; García-Herrera et al., 2010). Another example of co-occurring events was found in 2022, when western Europe and the western Mediterranean were notably affected by severe simultaneous AHW and MHW heatwave conditions. Ocean–atmosphere fluxes played a critical role in initiating the abnormally warm SSTs. The presence of an atmospheric blocking system linked to above-climatology surface air

5. Discussion and conclusions

temperature, above-average solar radiation and low surface wind speed (which reduces the effectiveness of turbulent heat fluxes) lead to a notable warming of SSTs (Guinaldo et al., 2023; Simon et al., 2023b).

The usually higher MHW intensity and cumulative intensity (ICI) identified in the Mediterranean Sea when compared to the Atlantic Ocean might be explained by its weaker tidal ranges. In the presence of negative wind anomalies, turbulent heat losses from the ocean and the efficiency of turbulent mixing of surface waters are suppressed, leading to thermal stratification, limiting exchanges with colder subsurface waters (Sen Gupta et al., 2020; Simon et al., 2023a; Guinaldo et al., 2023).

The pronounced positive correlation between air temperatures and sea surface temperatures in the surrounding regions observed in different periods of study and different regions underscores the strong interconnection between atmospheric temperatures over land and sea surface temperatures in the adjacent oceans. When compared to the Atlantic Ocean, sea temperatures over the Mediterranean show to have a stronger correlation with air temperatures in the Iberian Peninsula. The linkages between coastal adjacent MHWs and terrestrial heatwaves over the Mediterranean region have been emphasized by Aboelkhair et al. (2023) and several instances of anomalously high sea surface temperatures during major AHWs have marked this region, such as in 2003 (Sparnocchia et al., 2006; Olita et al., 2007; Feudale and Shukla, 2007; García-Herrera et al., 2010) in 2015 (Ionita et al., 2017) and 2022 (Guinaldo et al., 2023). The linkages between coastal adjacent MHWs and terrestrial heatwaves were previously attempted for other regions, namely in Australia (Pathmeswaran et al., 2022), New Zealand (Salinger et al., 2019, 2020) and on a global scale (Hu, 2021).

The results of this work show a prevalent increase of drought events throughout time, agreeing with the conclusions from previous studies (Vicente-Serrano et al., 2014b; Spinoni et al., 2016; Hoerling et al., 2012), entailing ongoing research due to their critical consequences, especially when associated with heatwave episodes. The negative correlation found between accumulated precipitation and air temperature values, for all regions, is attributed to the role played by land-atmosphere interactions (Miralles et al., 2019; Hao et al., 2022). Elevated temperatures and increased radiative forcing lead to greater evaporation rates, which might result in earlier-season soil moisture deficit and dry conditions. This, in turn, can lead to decreased evapotranspiration and evaporative cooling effects during the summer period. The reduction in latent heat flux and increasing in sensible heat flux leads to the amplification of temperature extremes (Miralles et al., 2019; Hao et al., 2022; Zscheischler and Seneviratne, 2017; Vicente-Serrano et al., 2014b). Although the persistent large-scale circulation anomalies play a crucial role in initiating the frequent co-occurrence of these extreme heatwave and droughts (Tomczyk and Bednorz, 2016; García-Herrera et al., 2010; Faranda et al., 2023), land-atmospheric feedbacks have been proposed as crucial to their evolution (Seneviratne et al., 2010; Sousa et al., 2020; Geirinhas et al., 2021; Liu et al., 2020). This correlation intensified in the full region and region 2, over the most recent period of the analysis, which might be attributed to an increased land-atmosphere feedback in a warmer climate (Seneviratne et al., 2006, 2010; Hao et al., 2022; Zscheischler and Seneviratne, 2017; Vicente-Serrano et al., 2014b).

The non-significant negative correlations between sea surface temperature and precipitation values reflect the potential intricate interactions between these variables. Understanding these interactions still offers ample opportunities for exploration. Earlier studies have explored how SSTs play a crucial role in influencing European climate through interaction with large-scale climatic or oceanic modes of variability and its ability to provide valuable skill for the prediction of drought conditions over Europe (Ionita et al., 2017, 2012; Hertig and Jacobbeit, 2011; Ionita et al., 2015; Sousa et al., 2011). However, the simultaneous occurrence of MHWs and dry events is still a challenge, warranting further investigation.

The potential association found between severe fire occurrences and summer reduced precipitation and/or elevated air temperatures, although showing varying patterns across the analysed sub-regions,

5. Discussion and conclusions

aligns with conclusions drawn in earlier research studies on the same topic (Libonati et al., 2022; Turco et al., 2019; Ermitao et al., 2022; Sutanto et al., 2020; Ruffault et al., 2020; Gouveia et al., 2016; García-Herrera et al., 2010). This association is evident in extreme fire seasons renowned for their devastating societal and environmental impacts (e.g., Sánchez-Benítez et al. 2018; Ramos et al. 2023; Martins et al. 2012). In the majority of these fire seasons, sea surface temperatures were found to be closely associated with the occurrence of other extremes known to significantly impact the occurrence of wildfires both in Western and Eastern Europe.

This work attempts to establish a linkage between marine temperatures and land co-occurring hazards in the fire season. However it must be noted that exceptions exist, especially considering the extensive geographical areas being averaged and the temporal variability that may affect the annual and seasonal assessments. Therefore, in the final sections of this work, a monthly assessment of atmospheric, marine heatwaves and drought conditions over burned pixels were conducted, employing two different methodologies: i) the prevalence of different climatic conditions based on the percentage of months affected; and ii) a quantitative analysis assessing the proportion of burned pixels in each area associated with different climatic conditions. While an event may exhibit a relatively higher prevalence over more months, the overall portion of burned pixels associated with it may be lower. Alternatively, a climatic event may demonstrate a lower percentage of occurrence across months but a higher incidence of burning. The use of these distinct approaches allows for a more comprehensive understanding of the relationship between climatic conditions and wildfire incidence. From the short-term analysis of single and compound extreme climatic conditions over burned pixels, it is important to recognize the significant percentage of months in which wildfires are associated with non-extreme climatic factors. This can be attributed to the utilization of a particularly high threshold applied to heatwaves and droughts, since the analysis solely concentrates on the top 20% historically most extreme cases. Additionally, fire activity can be influenced by a variety of factors beyond extreme fire weather, including vegetation conditions (Ermitao et al., 2022) and human factors affecting ignition and fire spread (Jones et al., 2022). Although this study confines its scope to a time-coincident analysis of extreme climatic events, the occurrence of wildfires can also be closely linked to pre-fire season conditions (Pereira et al., 2005; Gouveia et al., 2016; Ermitao et al., 2022). Gouveia et al. (2016) pointed out the role played by antecedent drought conditions leading up to the simultaneous occurrence of extreme heat conditions in the 2007 exceptional fire season in Greece, highlighting the critical importance of accounting for time-lags between climatic hazards, unravelling the complex synergies among antecedent conditions and concurrent seasonal hazards in forthcoming research on this topic.

While this study has examined the co-occurrence of MHWs and land-based hazards and their possible association with the occurrence of rural fires, there remains a critical need for future analysis to unravel the underlying mechanisms driving these concurrent occurrences, considering both atmospheric and oceanic factors, to confirm and provide a more comprehensive understanding of their interplay. Disclose the coupling mechanisms related to these extreme events and explore the role of atmospheric teleconnections, large-scale circulation patterns, land-atmosphere experiments, and local air-sea interactions emerge as essential in the present context of climate change. In particular, in the context of fire activity, these would offer valuable insights for early-warning alerts, effective risk management and definition of mitigation measures for future events.

This analysis did not explore the understanding of the driving roles or establish causality in the context of this co-occurrence. Future research work could incorporate complex model analysis that considers various possible factors as potential drivers and estimate the causal links connecting marine and land hazards. This could foster progress on the role of SSTs in the development of extreme atmospheric/land conditions. Employing methodologies that effectively address the challenge of the absence of spatial

5. Discussion and conclusions

overlapping between marine and land variables would also be highly beneficial. Additionally, considering different timescales, potential lag effects and time-lagged correlations, aspects not addressed in this analysis, would also be essential for clarifying the relationship between these geographically distinct components of the climate system, as these may not only occur simultaneously but also exhibit temporal dependencies.

Continued examination of potential impacts of these compound episodes on wildfire occurrences is crucial for risk management and preparedness of such a meteorological disaster. The findings of this work might provide a useful reference for addressing these challenges and are not only relevant to the local context but also hold global significance. The challenges posed by compound extreme events extend far beyond this region, as climate change continues to drive an increase in the frequency and severity of extreme events globally while threatening the stability of ecosystems and posing high societal impacts.

Summarizing the principal insights arising from this investigation, it can be concluded that:

- There has been an overall escalation of atmospheric heatwaves and droughts throughout the last decades in Southern Europe, accompanied by the rise of marine heatwaves in the adjacent seas;
- A significant positive correlation was found between 2-meter air and sea surface temperatures, as well as a significant negative correlation between 2-meter air temperature and accumulated precipitation values, considering all the analysed sub-regions;
- Severe fire occurrences are mostly linked to reduced precipitation and/or elevated air temperatures during the summer season. In most of these cases, a close association with sea surface temperatures was observed;
- The concurrent existence of extremely high temperatures and dry conditions may potentially enhance the occurrence of significant wildfires, as months characterized by large fires (above the 80th percentile) are predominantly related to combined extreme climatic conditions. Non-extreme climatic conditions, or individual climatic extreme conditions, are prevalent for months in which burned areas are less extensive (below the 80th percentile);
- Burned areas in the most extreme wildfire months are primarily linked to very dry conditions in the Iberian Peninsula, while in eastern-southern Europe, they are mostly associated with compound warm conditions over land and adjacent oceans;
- The long-term analysis of the interplay between marine and atmospheric heatwaves, with drought conditions over burned areas reveals that years marked by considerable marine heatwaves coincide with intensified atmospheric heatwaves or/and dry conditions in nearly half of the cases. Years with lower marine heatwave intensity are primarily associated with less dry and/or warm conditions over burned areas;
- Short-term assessments of single and compound extreme climatic conditions over burned pixels show that the occurrence of the driest and warmest months is more pronounced in the most recent analyzed period (2012-2022), being also closely associated with fire incidence, which again emphasizes an increased frequency of compound hazards in recent years.
- Marine hot conditions dominate in months with burned areas below the 80th percentile, while intense dry events prevail when burned areas exceed this threshold;

This study underscores the significance of incorporating marine warm conditions when studying regional climate dynamics and compound extreme episodes, given their co-occurrence with other well-known land-occurring extremes during months that align with wildfire events, suggesting potential for further in-depth investigation.

References

- Aboelkhair, H., Mohamed, B., Morsy, M., and Nagy, H. (2023). Co-occurrence of atmospheric and oceanic heatwaves in the eastern mediterranean over the last four decades. *Remote Sensing*, 15(7):1841.
- Abram, N. J., Henley, B. J., Sen Gupta, A., Lippmann, T. J., Clarke, H., Dowdy, A. J., Sharples, J. J., Nolan, R. H., Zhang, T., Wooster, M. J., et al. (2021). Connections of climate change and variability to large and extreme forest fires in southeast australia. *Communications Earth & Environment*, 2(1):8.
- Abramowitz, M. and Stegun, I. A. (1968). *Handbook of mathematical functions with formulas, graphs, and mathematical tables*, volume 55. US Government printing office.
- Amengual, A., Homar, V., Romero, R., Brooks, H. E., Ramis, C., Gordaliza, M., and Alonso, S. (2014). Projections of heat waves with high impact on human health in europe. *Global and Planetary Change*, 119:71–84.
- AppEEARS Team (2023). Application for Extracting and Exploring Analysis Ready Samples (AppEEARS). Accessed Jan, 30, 2023. <https://appears.earthdatacloud.nasa.gov/>.
- Arblaster, J. M. and Alexander, L. V. (2012). The impact of the el niño-southern oscillation on maximum temperature extremes. *Geophysical Research Letters*, 39(20).
- Barriopedro, D., García-Herrera, R., Ordóñez, C., Miralles, D., and Salcedo-Sanz, S. (2023). Heat waves: Physical understanding and scientific challenges. *Reviews of Geophysics*, page e2022RG000780.
- Beguería, S., Vicente-Serrano, S. M., Reig, F., and Latorre, B. (2014). Standardized precipitation evapotranspiration index (spei) revisited: parameter fitting, evapotranspiration models, tools, datasets and drought monitoring. *International journal of climatology*, 34(10):3001–3023.
- Beguería, S. and Vicente-Serrano, S. (2023). *SPEI: Calculation of the Standardized Precipitation-Evapotranspiration Index*.
- Beillouin, D., Schauberger, B., Bastos, A., Ciais, P., and Makowski, D. (2020). Impact of extreme weather conditions on european crop production in 2018. *Philosophical Transactions of the Royal Society B*, 375(1810):20190510.
- Bekar, I. and Tavşanoğlu, Ç. (2017). Modelling the drivers of natural fire activity: the bias created by cropland fires. *International journal of wildland fire*, 26(10):845–851.
- Belhadj-Khedher, C., El-Melki, T., and Mouillet, F. (2020). Saharan hot and dry sirocco winds drive extreme fire events in mediterranean tunisia (north africa). *Atmosphere*, 11(6):590.

-
- Bevacqua, E., De Michele, C., Manning, C., Couasnon, A., Ribeiro, A. F., Ramos, A. M., Vignotto, E., Bastos, A., Blesić, S., Durante, F., et al. (2021). Guidelines for studying diverse types of compound weather and climate events. *Earth's Future*, 9(11):e2021EF002340.
- Brás, T. A., Seixas, J., Carvalhais, N., and Jägermeyr, J. (2021). Severity of drought and heatwave crop losses tripled over the last five decades in europe. *Environmental Research Letters*, 16(6):065012.
- Carmo, M., Moreira, F., Casimiro, P., and Vaz, P. (2011). Land use and topography influences on wildfire occurrence in northern portugal. *Landscape and Urban Planning*, 100(1-2):169–176.
- Cascio, W. E. (2018). Wildland fire smoke and human health. *Science of the total environment*, 624:586–595.
- Ciais, P., Reichstein, M., Viovy, N., Granier, A., Ogée, J., Allard, V., Aubinet, M., Buchmann, N., Bernhofer, C., Carrara, A., et al. (2005). Europe-wide reduction in primary productivity caused by the heat and drought in 2003. *Nature*, 437(7058):529–533.
- Copernicus Climate Change Service (2019). Land cover classification gridded maps from 1992 to present derived from satellite observation. Copernicus Climate Change Service (C3S) Climate Data Store (CDS). Accessed Feb, 25, 2023.
- Copernicus Emergency Management Service - Rapid Mapping (2024). EMSR686 - Flood in Mozambique. Accessed Jan, 16, 2024. <https://rapidmapping.emergency.copernicus.eu/EMSR686/download>.
- De Amorim, W. S., Valduga, I. B., Ribeiro, J. M. P., Williamson, V. G., Krauser, G. E., Magtoto, M. K., de Andrade, J. B. S. O., et al. (2018). The nexus between water, energy, and food in the context of the global risks: An analysis of the interactions between food, water, and energy security. *Environmental Impact Assessment Review*, 72:1–11.
- Defourny, P., Lamarche, C., Bontemps, S., De Maet, T., Van Bogaert, E., Moreau, I., Brockmann, C., Boettcher, M., Kirches, G., Wevers, J., Santoro, M., Ramoino, F., and Arino, O. (2017). *Land Cover Climate Change Initiative - Product User Guide v2. Issue 2.0.* http://maps.elie.ucl.ac.be/CCI/viewer/download/ESACCI-LC-Ph2-PUGv2_2.0.pdf.
- Després, J., Adamovic, M., et al. (2020). Seasonal impacts of climate change on electricity production. *JRC PESETA IV Project–Task 4*.
- EFFIS (2023). European Forest Fire Information System - EFFIS Statistics Estimates. Accessed Oct, 03, 2023. <https://effis.jrc.ec.europa.eu/apps/effis.statistics/estimates>.
- Ermitao, T., Gouveia, C. M., Bastos, A., and Russo, A. C. (2022). Interactions between hot and dry fuel conditions and vegetation dynamics in the 2017 fire season in portugal. *Environmental Research Letters*, 17(9):095009.
- Ermitão, T., Páscoa, P., Trigo, I., Alonso, C., and Gouveia, C. (2023). Mapping the most susceptible regions to fire in portugal. *Fire*, 6(7):254.
- European Space Agency (ESA) Climate Change Initiative (2023). Land Cover Project. Accessed Feb, 15, 2023. <https://climate.esa.int/en/projects/land-cover/>.

-
- Faranda, D., Pascale, S., and Bulut, B. (2023). Persistent anticyclonic conditions and climate change exacerbated the exceptional 2022 european-mediterranean drought. *Environmental Research Letters*.
- Feudale, L. and Shukla, J. (2007). Role of mediterranean sst in enhancing the european heat wave of summer 2003. *Geophysical Research Letters*, 34(3).
- Fink, A. H., Brücher, T., Krüger, A., Leckebusch, G. C., Pinto, J. G., and Ulbrich, U. (2004). The 2003 european summer heatwaves and drought-synoptic diagnosis and impacts. *Weather*, 59(8):209–216.
- Finlay, S. E., Moffat, A., Gazzard, R., Baker, D., and Murray, V. (2012). Health impacts of wildfires. *PLoS currents*, 4.
- Fischer, E. M. and Knutti, R. (2015). Anthropogenic contribution to global occurrence of heavy-precipitation and high-temperature extremes. *Nature climate change*, 5(6):560–564.
- Fischer, E. M., Seneviratne, S. I., Lüthi, D., and Schär, C. (2007a). Contribution of land-atmosphere coupling to recent european summer heat waves. *Geophysical Research Letters*, 34(6).
- Fischer, E. M., Seneviratne, S. I., Vidale, P. L., Lüthi, D., and Schär, C. (2007b). Soil moisture–atmosphere interactions during the 2003 european summer heat wave. *Journal of Climate*, 20(20):5081–5099.
- Ganteaume, A., Barbero, R., Jappiot, M., and Maillé, E. (2021). Understanding future changes to fires in southern europe and their impacts on the wildland-urban interface. *Journal of safety science and resilience*, 2(1):20–29.
- Ganteaume, A., Camia, A., Jappiot, M., San-Miguel-Ayanz, J., Long-Fournel, M., and Lampin, C. (2013). A review of the main driving factors of forest fire ignition over europe. *Environmental management*, 51:651–662.
- García-Herrera, R., Díaz, J., Trigo, R. M., Luterbacher, J., and Fischer, E. M. (2010). A review of the european summer heat wave of 2003. *Critical Reviews in Environmental Science and Technology*, 40(4):267–306.
- Garrabou, J., Coma, R., Bensoussan, N., Bally, M., Chevaldonné, P., Cigliano, M., Díaz, D., Harmelin, J.-G., Gambi, M. C., Kersting, D., et al. (2009). Mass mortality in northwestern mediterranean rocky benthic communities: effects of the 2003 heat wave. *Global change biology*, 15(5):1090–1103.
- Geirinhas, J. L., Russo, A., Libonati, R., Sousa, P. M., Miralles, D. G., and Trigo, R. M. (2021). Recent increasing frequency of compound summer drought and heatwaves in southeast brazil. *Environmental Research Letters*, 16(3):034036.
- Giglio, L., Boschetti, L., Roy, D. P., Humber, M. L., and Justice, C. O. (2018). The collection 6 modis burned area mapping algorithm and product. *Remote sensing of environment*, 217:72–85.
- Giglio, L., Justice, C., Boschetti, L., and Roy, D. (2015). Mcd64a1 modis/terra+aqua burned area monthly l3 global 500m sin grid v006 [data set]. NASA EOSDIS Land Processes Distributed Active Archive Center. Accessed Jan, 20, 2023. <https://doi.org/10.5067/MODIS/MCD64A1.006>.
- Giglio, L., Loboda, T., Roy, D. P., Quayle, B., and Justice, C. O. (2009). An active-fire based burned area mapping algorithm for the modis sensor. *Remote sensing of environment*, 113(2):408–420.

-
- Giorgi, F. (2006). Climate change hot-spots. *Geophysical research letters*, 33(8).
- Giorgi, F. and Lionello, P. (2008). Climate change projections for the mediterranean region. *Global and planetary change*, 63(2-3):90–104.
- Golubeva, E., Kraineva, M., Platov, G., Iakshina, D., and Tarkhanova, M. (2021). Marine heatwaves in siberian arctic seas and adjacent region. *Remote Sensing*, 13(21):4436.
- Gouveia, C., Bastos, A., Trigo, R., and DaCamara, C. (2012). Drought impacts on vegetation in the pre- and post-fire events over iberian peninsula. *Natural Hazards and Earth System Sciences*, 12(10):3123–3137.
- Gouveia, C., Trigo, R. M., Beguería, S., and Vicente-Serrano, S. M. (2017). Drought impacts on vegetation activity in the mediterranean region: An assessment using remote sensing data and multi-scale drought indicators. *Global and Planetary Change*, 151:15–27.
- Gouveia, C. M., Bistinas, I., Liberato, M. L., Bastos, A., Koutsias, N., and Trigo, R. (2016). The outstanding synergy between drought, heatwaves and fuel on the 2007 southern greece exceptional fire season. *Agricultural and Forest Meteorology*, 218:135–145.
- Guinaldo, T., Volodire, A., Waldman, R., Saux Picart, S., and Roquet, H. (2023). Response of the sea surface temperature to heatwaves during the france 2022 meteorological summer. *Ocean Science*, 19(3):629–647.
- Hao, Z., Hao, F., Singh, V. P., and Zhang, X. (2018). Changes in the severity of compound drought and hot extremes over global land areas. *Environmental Research Letters*, 13(12):124022.
- Hao, Z., Hao, F., Xia, Y., Feng, S., Sun, C., Zhang, X., Fu, Y., Hao, Y., Zhang, Y., and Meng, Y. (2022). Compound droughts and hot extremes: Characteristics, drivers, changes, and impacts. *Earth-Science Reviews*, 235:104241.
- Hargreaves, G. H. (1994). Defining and using reference evapotranspiration. *Journal of irrigation and drainage engineering*, 120(6):1132–1139.
- Hersbach, H., Bell, B., Berrisford, P., Biavati, G., Horanyi, A., Munoz Sabater, J., Nicolas, J., Peubey, C., Radu, R., Rozum, I., et al. (2023). Era5 hourly data on single levels from 1940 to present, copernicus climate change servics (c3s) climate data store (cds)[data set].
- Hertig, E. and Jacobbeit, J. (2011). Predictability of mediterranean climate variables from oceanic variability. part ii: Statistical models for monthly precipitation and temperature in the mediterranean area. *Climate Dynamics*, 36:825–843.
- Hobday, A. J., Alexander, L. V., Perkins, S. E., Smale, D. A., Straub, S. C., Oliver, E. C., BenthuySEN, J. A., Burrows, M. T., Donat, M. G., Feng, M., et al. (2016). A hierarchical approach to defining marine heatwaves. *Progress in Oceanography*, 141:227–238.
- Hoerling, M., Eischeid, J., Perlwitz, J., Quan, X., Zhang, T., and Pegion, P. (2012). On the increased frequency of mediterranean drought. *Journal of climate*, 25(6):2146–2161.
- Holbrook, N. J., Scannell, H. A., Sen Gupta, A., BenthuySEN, J. A., Feng, M., Oliver, E. C., Alexander, L. V., Burrows, M. T., Donat, M. G., Hobday, A. J., et al. (2019). A global assessment of marine heatwaves and their drivers. *Nature communications*, 10(1):2624.

-
- Holbrook, N. J., Sen Gupta, A., Oliver, E. C., Hobday, A. J., Benthuysen, J. A., Scannell, H. A., Smale, D. A., and Wernberg, T. (2020). Keeping pace with marine heatwaves. *Nature Reviews Earth & Environment*, 1(9):482–493.
- Hu, L. (2021). A global assessment of coastal marine heatwaves and their relation with coastal urban thermal changes. *Geophysical Research Letters*, 48(9):e2021GL093260.
- Ionita, M., Boroneanț, C., and Chelcea, S. (2015). Seasonal modes of dryness and wetness variability over europe and their connections with large scale atmospheric circulation and global sea surface temperature. *Climate Dynamics*, 45:2803–2829.
- Ionita, M., Lohmann, G., Rimbu, N., Chelcea, S., and Dima, M. (2012). Interannual to decadal summer drought variability over europe and its relationship to global sea surface temperature. *Climate Dynamics*, 38:363–377.
- Ionita, M., Tallaksen, L. M., Kingston, D. G., Stagge, J. H., Laaha, G., Van Lanen, H. A., Scholz, P., Chelcea, S. M., and Haslinger, K. (2017). The european 2015 drought from a climatological perspective. *Hydrology and Earth System Sciences*, 21(3):1397–1419.
- Jones, M. W., Abatzoglou, J. T., Veraverbeke, S., Andela, N., Lasslop, G., Forkel, M., Smith, A. J., Burton, C., Betts, R. A., van der Werf, G. R., et al. (2022). Global and regional trends and drivers of fire under climate change. *Reviews of Geophysics*, 60(3):e2020RG000726.
- Laaha, G., Gauster, T., Tallaksen, L. M., Vidal, J.-P., Stahl, K., Prudhomme, C., Heudorfer, B., Vlnas, R., Ionita, M., Van Lanen, H. A., et al. (2017). The european 2015 drought from a hydrological perspective. *Hydrology and Earth System Sciences*, 21(6):3001–3024.
- Lasslop, G., Coppola, A. I., Voulgarakis, A., Yue, C., and Veraverbeke, S. (2019). Influence of fire on the carbon cycle and climate. *Current Climate Change Reports*, 5:112–123.
- Lee, H., Calvin, K., Dasgupta, D., Krinner, G., Mukherji, A., Thorne, P., Trisos, C., Romero, J., Aldunce, P., Barret, K., et al. (2023). Ipcc, 2023: Climate change 2023: Synthesis report, summary for policymakers. contribution of working groups i, ii and iii to the sixth assessment report of the intergovernmental panel on climate change [core writing team, h. lee and j. romero (eds.)]. ipcc, geneva, switzerland.
- Lhotka, O., Kysely, J., and Farda, A. (2018). Climate change scenarios of heat waves in central europe and their uncertainties. *Theoretical and applied climatology*, 131(3-4):1043–1054.
- Li, M., Yao, Y., Simmonds, I., Luo, D., Zhong, L., and Chen, X. (2020). Collaborative impact of the nao and atmospheric blocking on european heatwaves, with a focus on the hot summer of 2018. *Environmental Research Letters*, 15(11):114003.
- Libonati, R., Geirinhas, J. L., Silva, P. S., Russo, A., Rodrigues, J. A., Belém, L. B., Nogueira, J., Roque, F. O., DaCamara, C. C., Nunes, A. M., et al. (2022). Assessing the role of compound drought and heatwave events on unprecedented 2020 wildfires in the pantanal. *Environmental Research Letters*, 17(1):015005.
- Liu, X., He, B., Guo, L., Huang, L., and Chen, D. (2020). Similarities and differences in the mechanisms causing the european summer heatwaves in 2003, 2010, and 2018. *Earth's Future*, 8(4):e2019EF001386.

-
- Lobell, D. B. and Field, C. B. (2007). Global scale climate–crop yield relationships and the impacts of recent warming. *Environmental research letters*, 2(1):014002.
- Madadgar, S., AghaKouchak, A., Farahmand, A., and Davis, S. J. (2017). Probabilistic estimates of drought impacts on agricultural production. *Geophysical Research Letters*, 44(15):7799–7807.
- Martins, V., Miranda, A., Carvalho, A., Schaap, M., Borrego, C., and Sá, E. (2012). Impact of forest fires on particulate matter and ozone levels during the 2003, 2004 and 2005 fire seasons in portugal. *Science of the Total Environment*, 414:53–62.
- McKee, T. B., Doesken, N. J., Kleist, J., et al. (1993). The relationship of drought frequency and duration to time scales. In *Proceedings of the 8th Conference on Applied Climatology*, volume 17, pages 179–183. California.
- McMichael, A. J. and Lindgren, E. (2011). Climate change: present and future risks to health, and necessary responses. *Journal of internal medicine*, 270(5):401–413.
- Miralles, D. G., Gentine, P., Seneviratne, S. I., and Teuling, A. J. (2019). Land–atmospheric feedbacks during droughts and heatwaves: state of the science and current challenges. *Annals of the New York Academy of Sciences*, 1436(1):19–35.
- Miralles, D. G., Teuling, A. J., Van Heerwaarden, C. C., and Vilà-Guerau de Arellano, J. (2014). Mega-heatwave temperatures due to combined soil desiccation and atmospheric heat accumulation. *Nature geoscience*, 7(5):345–349.
- Moreira F, Viedma O, A. M. C. T. K. N. R. E. B. A. C. P. V. P. X. G. M. F. B. E. (2011). Landscape-wildfire interactions in southern europe: implications for landscape management. *journal of environmental management* 92 (10): 2389-2402.
- Olita, A., Sorgente, R., Natale, S., Gaberšek, S., Ribotti, A., Bonanno, A., and Patti, B. (2007). Effects of the 2003 european heatwave on the central mediterranean sea: surface fluxes and the dynamical response. *Ocean Science*, 3(2):273–289.
- Oliver, E. C., Benthuysen, J. A., Darmaraki, S., Donat, M. G., Hobday, A. J., Holbrook, N. J., Schlegel, R. W., and Sen Gupta, A. (2021). Marine heatwaves. *Annual Review of Marine Science*, 13:313–342.
- Oliver, E. C., Burrows, M. T., Donat, M. G., Sen Gupta, A., Alexander, L. V., Perkins-Kirkpatrick, S. E., Benthuysen, J. A., Hobday, A. J., Holbrook, N. J., Moore, P. J., et al. (2019). Projected marine heatwaves in the 21st century and the potential for ecological impact. *Frontiers in Marine Science*, 6:734.
- Oliver, E. C., Donat, M. G., Burrows, M. T., Moore, P. J., Smale, D. A., Alexander, L. V., Benthuysen, J. A., Feng, M., Sen Gupta, A., Hobday, A. J., et al. (2018). Longer and more frequent marine heatwaves over the past century. *Nature communications*, 9(1):1–12.
- Parente, J., Pereira, M., Amraoui, M., and Fischer, E. M. (2018). Heat waves in portugal: Current regime, changes in future climate and impacts on extreme wildfires. *Science of the total environment*, 631:534–549.
- Páscoa, P., Gouveia, C., Russo, A., Trigo, R., et al. (2017). Drought trends in the iberian peninsula over the last 112 years. *Advances in Meteorology*, 2017.

-
- Pathmeswaran, C., Sen Gupta, A., Perkins-Kirkpatrick, S. E., and Hart, M. A. (2022). Exploring potential links between co-occurring coastal terrestrial and marine heatwaves in australia. *Frontiers in Climate*, 4:37.
- Pausas, J. G. and Ribeiro, E. (2013). The global fire–productivity relationship. *Global Ecology and Biogeography*, 22(6):728–736.
- Pereira, M. G., Trigo, R. M., da Camara, C. C., Pereira, J. M., and Leite, S. M. (2005). Synoptic patterns associated with large summer forest fires in portugal. *Agricultural and Forest Meteorology*, 129(1-2):11–25.
- Pereira, P., Francos, M., Brevik, E. C., Ubeda, X., and Bogunovic, I. (2018). Post-fire soil management. *Current Opinion in Environmental Science & Health*, 5:26–32.
- Perkins, S. E. (2015). A review on the scientific understanding of heatwaves—their measurement, driving mechanisms, and changes at the global scale. *Atmospheric Research*, 164:242–267.
- Perkins, S. E. and Alexander, L. V. (2013). On the measurement of heat waves. *Journal of climate*, 26(13):4500–4517.
- Perkins-Kirkpatrick, S. and Lewis, S. (2020). Increasing trends in regional heatwaves. *Nature communications*, 11(1):3357.
- Plecha, S. M. and Soares, P. M. (2020). Global marine heatwave events using the new cmip6 multi-model ensemble: from shortcomings in present climate to future projections. *Environmental Research Letters*, 15(12):124058.
- Plecha, S. M., Soares, P. M., Silva-Fernandes, S. M., and Cabos, W. (2021). On the uncertainty of future projections of marine heatwave events in the north atlantic ocean. *Climate Dynamics*, 56(7-8):2027–2056.
- Pörtner, H.-O., Roberts, D. C., Tignor, M., Poloczanska, E., Mintenbeck, K., Alegría, A., Craig, M., Langsdorf, S., Löschke, S., Möller, V., et al. (2022). Ippc 2022: Climate change 2022: impacts, adaptation and vulnerability: working group ii contribution to the sixth assessment report of the intergovernmental panel on climate change.
- Rakotoarison, N., Raholijao, N., Razafindramavo, L. M., Rakotomavo, Z. A. P. H., Rakotoarisoa, A., Guillemot, J. S., Randriamialisoa, Z. J., Mafilaza, V., Ramiandrisoa, V. A. M. P., Rajaonarivony, R., et al. (2018). Assessment of risk, vulnerability and adaptation to climate change by the health sector in madagascar. *International Journal of Environmental Research and Public Health*, 15(12):2643.
- Ramos, A. M., Russo, A., DaCamara, C. C., Nunes, S., Sousa, P., Soares, P., Lima, M. M., Hurduc, A., and Trigo, R. M. (2023). The compound event that triggered the destructive fires of october 2017 in portugal. *Iscience*, 26(3).
- Ribeiro, A., Russo, A., Gouveia, C., Páscoa, P., and Zscheischler, J. (2020). Risk of crop-failure due to compound hot and dry extremes in the iberian peninsula. Technical report, Copernicus Meetings.
- Robine, J.-M., Cheung, S. L. K., Le Roy, S., Van Oyen, H., Griffiths, C., Michel, J.-P., and Herrmann, F. R. (2008). Death toll exceeded 70,000 in europe during the summer of 2003. *Comptes rendus biologies*, 331(2):171–178.

-
- Robusto, C. C. (1957). The cosine-haversine formula. *The American Mathematical Monthly*, 64(1):38–40.
- Rodrigues, R. R., Taschetto, A. S., Sen Gupta, A., and Foltz, G. R. (2019). Common cause for severe droughts in south america and marine heatwaves in the south atlantic. *Nature Geoscience*, 12(8):620–626.
- Ruffault, J., Curt, T., Moron, V., Trigo, R. M., Mouillot, F., Koutsias, N., Pimont, F., Martin-StPaul, N., Barbero, R., Dupuy, J.-L., et al. (2020). Increased likelihood of heat-induced large wildfires in the mediterranean basin. *Scientific reports*, 10(1):13790.
- Russo, A., Gouveia, C., Dutra, E., Soares, P., and Trigo, R. M. (2019). The synergy between drought and extremely hot summers in the mediterranean. *Environmental Research Letters*, 14(1):014011.
- Russo, A., Gouveia, C. M., Páscoa, P., DaCamara, C. C., Sousa, P. M., and Trigo, R. M. (2017). Assessing the role of drought events on wildfires in the iberian peninsula. *Agricultural and Forest Meteorology*, 237:50–59.
- Rust, A. J., Hogue, T. S., Saxe, S., and McCray, J. (2018). Post-fire water-quality response in the western united states. *International Journal of Wildland Fire*, 27(3):203–216.
- Ruthrof, K. X., Breshears, D. D., Fontaine, J. B., Froend, R. H., Matusick, G., Kala, J., Miller, B. P., Mitchell, P. J., Wilson, S. K., van Keulen, M., et al. (2018). Subcontinental heat wave triggers terrestrial and marine, multi-taxa responses. *Scientific Reports*, 8(1):13094.
- Salinger, M. J., Diamond, H. J., Behrens, E., Fernandez, D., Fitzharris, B. B., Herold, N., Johnstone, P., Kerckhoff, H., Mullan, A. B., Parker, A. K., et al. (2020). Unparalleled coupled ocean-atmosphere summer heatwaves in the new zealand region: drivers, mechanisms and impacts. *Climatic Change*, 162:485–506.
- Salinger, M. J., Diamond, H. J., Bell, J., Behrens, E., Fitzharris, B. B., Herod, N., McLuskie, M., Parker, A. K., Ratz, H., Renwick, J., et al. (2023). Coupled ocean-atmosphere summer heatwaves in the new zealand region. *Weather and Climate*, 42(1):18–41.
- Salinger, M. J., Renwick, J., Behrens, E., Mullan, A. B., Diamond, H. J., Sirguey, P., Smith, R. O., Trought, M. C., Alexander, L., Cullen, N. J., et al. (2019). The unprecedented coupled ocean-atmosphere summer heatwave in the new zealand region 2017/18: drivers, mechanisms and impacts. *Environmental Research Letters*, 14(4):044023.
- Salvador, C., Vicedo-Cabrera, A. M., Libonati, R., Russo, A., Garcia, B., Belem, L., Gimeno, L., and Nieto, R. (2022). Effects of drought on mortality in macro urban areas of brazil between 2000 and 2019. *GeoHealth*, 6(3):e2021GH000534.
- Samaniego, L., Thober, S., Kumar, R., Wanders, N., Rakovec, O., Pan, M., Zink, M., Sheffield, J., Wood, E. F., and Marx, A. (2018). Anthropogenic warming exacerbates european soil moisture droughts. *Nature Climate Change*, 8(5):421–426.
- Sánchez-Benítez, A., García-Herrera, R., Barriopedro, D., Sousa, P. M., and Trigo, R. M. (2018). June 2017: the earliest european summer mega-heatwave of reanalysis period. *Geophysical Research Letters*, 45(4):1955–1962.

-
- Schiaparelli, S., Castellano, M., Povero, P., Sartoni, G., and Cattaneo-Vietti, R. (2007). A benthic mucilage event in north-western mediterranean sea and its possible relationships with the summer 2003 european heatwave: short term effects on littoral rocky assemblages. *Marine Ecology*, 28(3):341–353.
- Sen Gupta, A., Thomsen, M., Benthuysen, J. A., Hobday, A. J., Oliver, E., Alexander, L. V., Burrows, M. T., Donat, M. G., Feng, M., Holbrook, N. J., et al. (2020). Drivers and impacts of the most extreme marine heatwave events. *Scientific reports*, 10(1):19359.
- Seneviratne, S. I., Corti, T., Davin, E. L., Hirschi, M., Jaeger, E. B., Lehner, I., Orlowsky, B., and Teuling, A. J. (2010). Investigating soil moisture–climate interactions in a changing climate: A review. *Earth-Science Reviews*, 99(3-4):125–161.
- Seneviratne, S. I., Lüthi, D., Litschi, M., and Schär, C. (2006). Land–atmosphere coupling and climate change in europe. *Nature*, 443(7108):205–209.
- Seneviratne, S. I., Zhang, X., Adnan, M., Badi, W., Dereczynski, C., Di Luca, A., Ghosh, S., Iskander, I., Kossin, J., Lewis, S., et al. (2021). Weather and climate extreme events in a changing climate (chapter 11).
- Simon, A., Pires, C., Frölicher, T. L., and Russo, A. (2023a). Long-term warming and interannual variability contributions' to marine heatwaves in the mediterranean. *Weather and Climate Extremes*, 42:100619.
- Simon, A., Plecha, S. M., Russo, A., Teles-Machado, A., Donat, M. G., Auger, P.-A., and Trigo, R. M. (2022). Hot and cold marine extreme events in the mediterranean over the period 1982-2021. *Frontiers in Marine Science*, 9:892201.
- Simon, A., Poppeschi, C., Plecha, S., Charria, G., and Russo, A. (2023b). Coastal and regional marine heatwaves and cold spells in the northeastern atlantic. *Ocean Science*, 19(5):1339–1355.
- Singh, V., Guo, H., and Yu, F. (1993). Parameter estimation for 3-parameter log-logistic distribution (lld3) by pome. *Stochastic Hydrology and Hydraulics*, 7:163–177.
- Sousa, P. M., Barriopedro, D., García-Herrera, R., Ordóñez, C., Soares, P. M., and Trigo, R. M. (2020). Distinct influences of large-scale circulation and regional feedbacks in two exceptional 2019 european heatwaves. *Communications Earth & Environment*, 1(1):48.
- Sousa, P. M., Trigo, R. M., Aizpurua, P., Nieto, R., Gimeno, L., and Garcia-Herrera, R. (2011). Trends and extremes of drought indices throughout the 20th century in the mediterranean. *Natural Hazards and Earth System Sciences*, 11(1):33–51.
- Sparnocchia, S., Schiano, M., Picco, P., Bozzano, R., and Cappelletti, A. (2006). The anomalous warming of summer 2003 in the surface layer of the central ligurian sea (western mediterranean). In *Annales Geophysicae*, volume 24, pages 443–452. Copernicus Publications Göttingen, Germany.
- Spinoni, J., Naumann, G., Vogt, J., and Barbosa, P. (2016). Meteorological droughts in europe: events and impacts-past trends and future projections.
- Spinoni, J., Vogt, J. V., Naumann, G., Barbosa, P., and Dosio, A. (2018). Will drought events become more frequent and severe in europe? *International Journal of Climatology*, 38(4):1718–1736.

-
- Stahl, K., Kohn, I., Blauthut, V., Urquijo, J., De Stefano, L., Acácio, V., Dias, S., Stagge, J. H., Tallaksen, L. M., Kampragou, E., Van Loon, A. F., Barker, L. J., Melsen, L. A., Bifulco, C., Musolino, D., de Carli, A., Massarutto, A., Assimacopoulos, D., and Van Lanen, H. A. J. (2016). Impacts of european drought events: insights from an international database of text-based reports. *Natural Hazards and Earth System Sciences*, 16(3):801–819.
- Sutanto, S. J., Vitolo, C., Di Napoli, C., D'Andrea, M., and Van Lanen, H. A. (2020). Heatwaves, droughts, and fires: Exploring compound and cascading dry hazards at the pan-european scale. *Environment international*, 134:105276.
- Theoharatos, G., Pantavou, K., Mavrakis, A., Spanou, A., Katavoutas, G., Efstatiou, P., Mpekas, P., and Asimakopoulos, D. (2010). Heat waves observed in 2007 in athens, greece: synoptic conditions, bioclimatological assessment, air quality levels and health effects. *Environmental research*, 110(2):152–161.
- Thomas, D., Butry, D., Gilbert, S., Webb, D., Fung, J., et al. (2017). The costs and losses of wildfires. *NIST Special Publication*, 1215(11).
- Tomczyk, A. M. and Bednorz, E. (2016). Heat waves in central europe and their circulation conditions. *International Journal of Climatology*, 36(2):770–782.
- Trigo, R. M., Pereira, J. M., Pereira, M. G., Mota, B., Calado, T. J., Dacamara, C. C., and Santo, F. E. (2006). Atmospheric conditions associated with the exceptional fire season of 2003 in portugal. *International Journal of Climatology: A Journal of the Royal Meteorological Society*, 26(13):1741–1757.
- Tripathy, K. P. and Mishra, A. K. (2023). How unusual is the 2022 european compound drought and heatwave event? *Geophysical Research Letters*, 50(15):e2023GL105453.
- Tuel, A. and Eltahir, E. A. (2020). Why is the mediterranean a climate change hot spot? *Journal of Climate*, 33(14):5829–5843.
- Turco, M., Jerez, S., Augusto, S., Tarín-Carrasco, P., Ratola, N., Jiménez-Guerrero, P., and Trigo, R. M. (2019). Climate drivers of the 2017 devastating fires in portugal. *Scientific reports*, 9(1):13886.
- Turco, M., von Hardenberg, J., AghaKouchak, A., Llasat, M. C., Provenzale, A., and Trigo, R. M. (2017). On the key role of droughts in the dynamics of summer fires in mediterranean europe. *Scientific reports*, 7(1):81.
- Varga, K., Jones, C., Trugman, A., Carvalho, L. M., McLoughlin, N., Seto, D., Thompson, C., and Daum, K. (2022). Megafires in a warming world: What wildfire risk factors led to california's largest recorded wildfire. *Fire*, 5(1):16.
- Vicente-Serrano, S. M., Azorin-Molina, C., Sanchez-Lorenzo, A., Revuelto, J., López-Moreno, J. I., González-Hidalgo, J. C., Moran-Tejeda, E., and Espejo, F. (2014a). Reference evapotranspiration variability and trends in spain, 1961–2011. *Global and planetary change*, 121:26–40.
- Vicente-Serrano, S. M., Beguería, S., and López-Moreno, J. I. (2010). A multiscalar drought index sensitive to global warming: the standardized precipitation evapotranspiration index. *Journal of climate*, 23(7):1696–1718.

- Vicente-Serrano, S. M., Lopez-Moreno, J.-I., Beguería, S., Lorenzo-Lacruz, J., Sanchez-Lorenzo, A., García-Ruiz, J. M., Azorin-Molina, C., Morán-Tejeda, E., Revuelto, J., Trigo, R., et al. (2014b). Evidence of increasing drought severity caused by temperature rise in southern europe. *Environmental Research Letters*, 9(4):044001.
- Vicente-Serrano, S. M., McVicar, T. R., Miralles, D. G., Yang, Y., and Tomas-Burguera, M. (2020). Unraveling the influence of atmospheric evaporative demand on drought and its response to climate change. *Wiley Interdisciplinary Reviews: Climate Change*, 11(2):e632.
- Vogel, J., Paton, E., Aich, V., and Bronstert, A. (2021). Increasing compound warm spells and droughts in the mediterranean basin. *Weather and Climate Extremes*, 32:100312.
- Ward, M. and Ahlquist, J. (2018). *Maximum Likelihood for Social Science: Strategies for Analysis*. Analytical Methods for Social Research. Cambridge University Press.
- World Meteorological Organization (2018). *Guide to climatological practices*. [Accessed 10-2023].
- Wu, Y., Zhao, K., Huang, J., Arend, M., Gross, B., and Moshary, F. (2019). Observation of heat wave effects on the urban air quality and pbl in new york city area. *Atmospheric Environment*, 218:117024.
- Zampieri, M., Ceglar, A., Dentener, F., and Toreti, A. (2017). Wheat yield loss attributable to heat waves, drought and water excess at the global, national and subnational scales. *Environmental Research Letters*, 12(6):064008.
- Zscheischler, J. and Seneviratne, S. I. (2017). Dependence of drivers affects risks associated with compound events. *Science advances*, 3(6):e1700263.
- Zscheischler, J., Westra, S., Van Den Hurk, B. J., Seneviratne, S. I., Ward, P. J., Pitman, A., AghaKouchak, A., Bresch, D. N., Leonard, M., Wahl, T., et al. (2018). Future climate risk from compound events. *Nature Climate Change*, 8(6):469–477.

Appendix

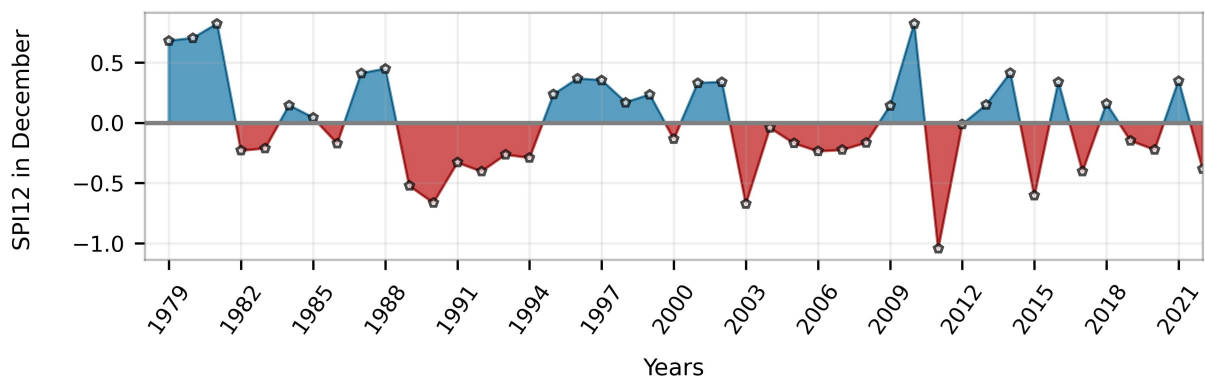


Figure A1: Spatial-averaged values of the 12-month SPI for December over land, between 1979 and 2022. This analysis considers the full region of study.

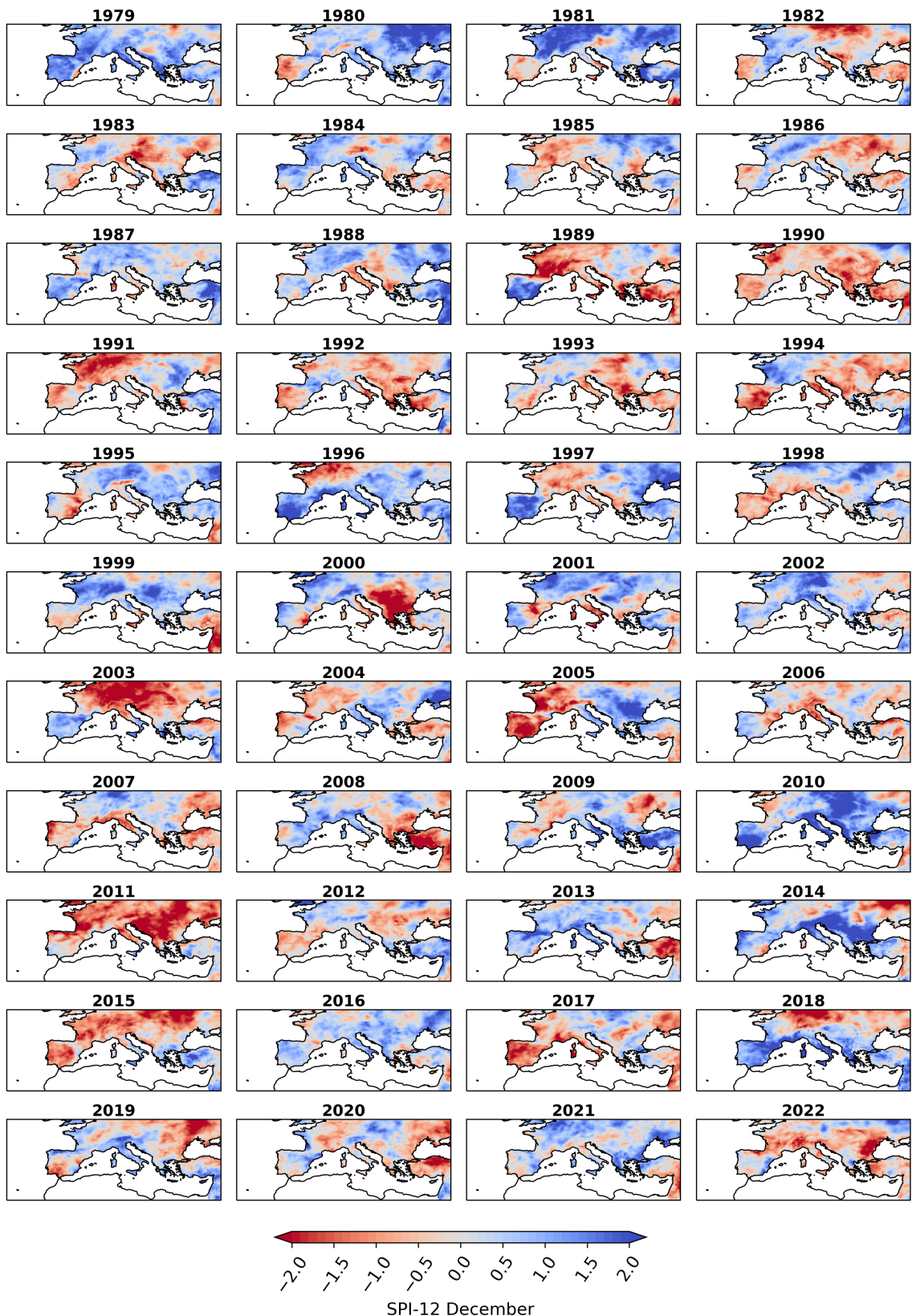


Figure A2: Spatial patterns of the 12-month SPI in December over the European land area, between 1979 and 2022.

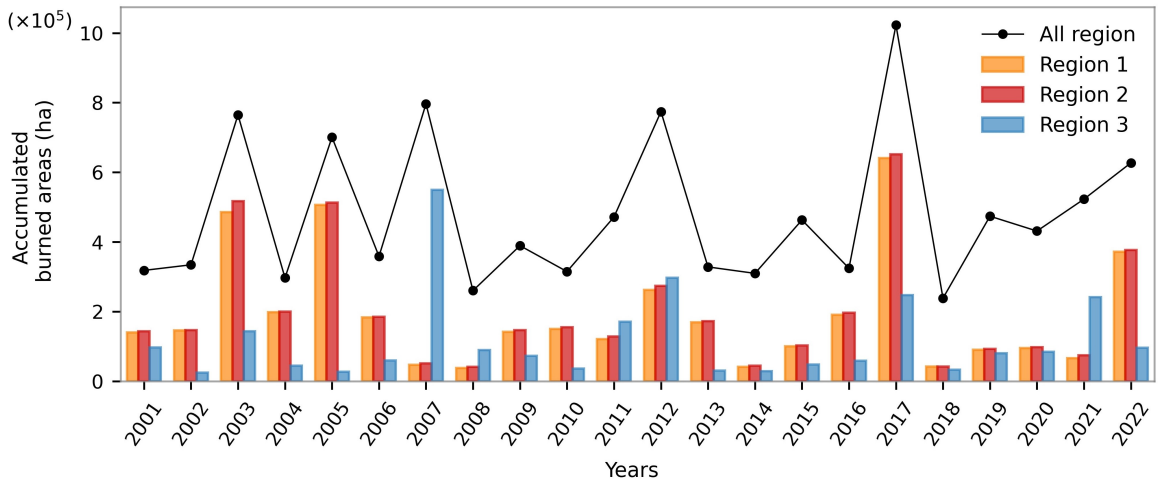


Figure A3: Yearly burned areas between 2001 and 2022, in hectares, for region 1 (orange bars), region 2 (red bars), region 3 (blue bars) and for the overall study region (black curve). Normalized burned areas are obtained by dividing the BAs in hectares by the total land hectares in each of the regions.

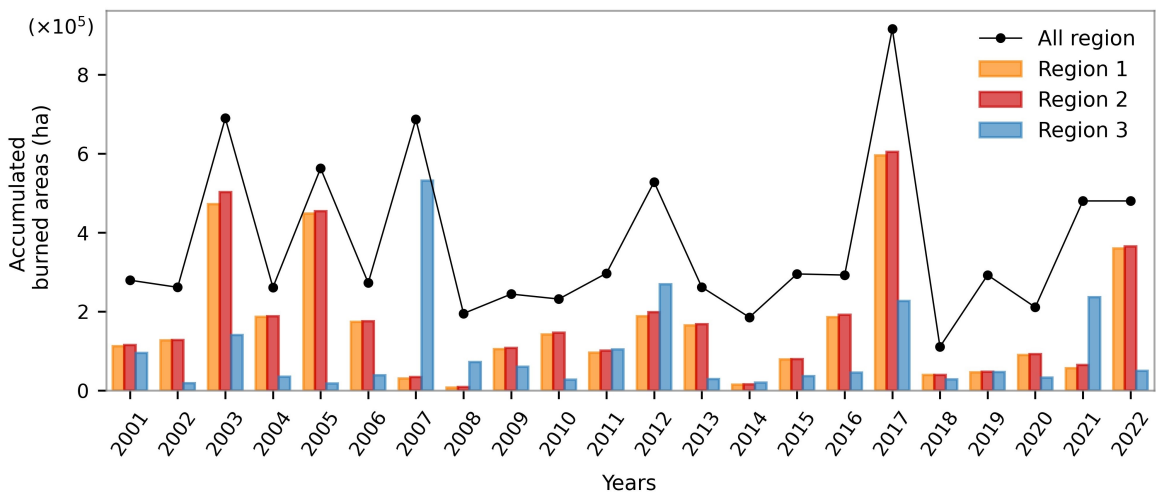


Figure A4: As in Fig A3, but throughout the extended summer seasons.

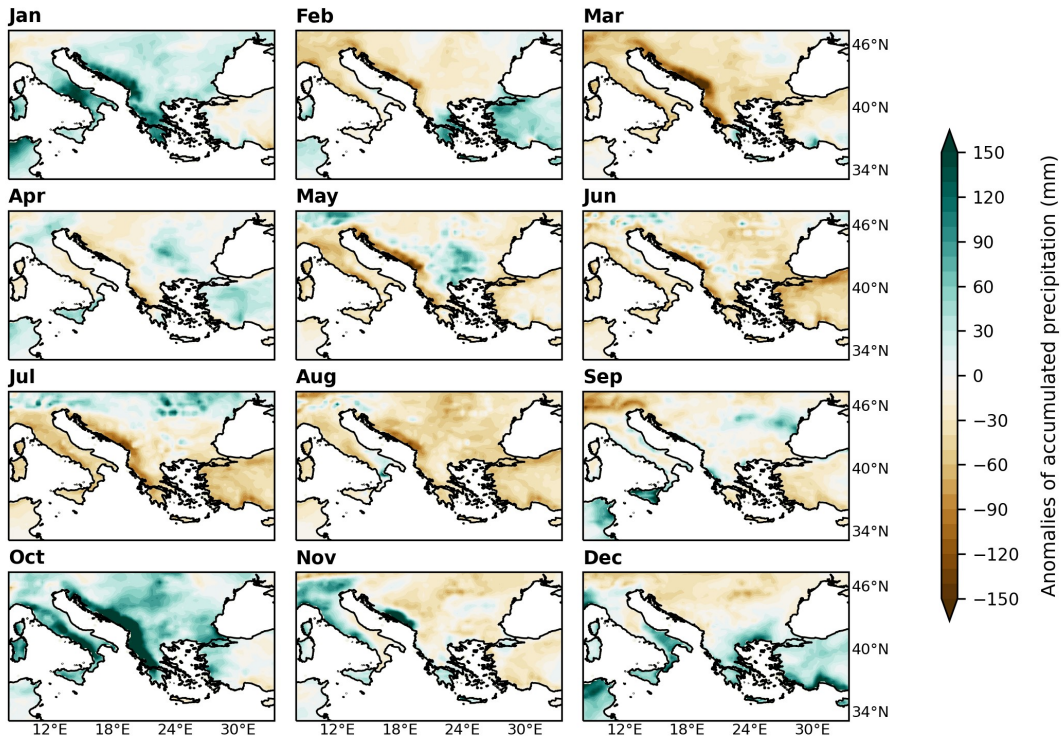


Figure A5: Monthly mean anomalies of accumulated precipitation for every month in 2003. The reference period used was 1979-2022. Daily accumulated precipitation data was retrieved from ERA5 reanalysis dataset (Hersbach et al., 2023)

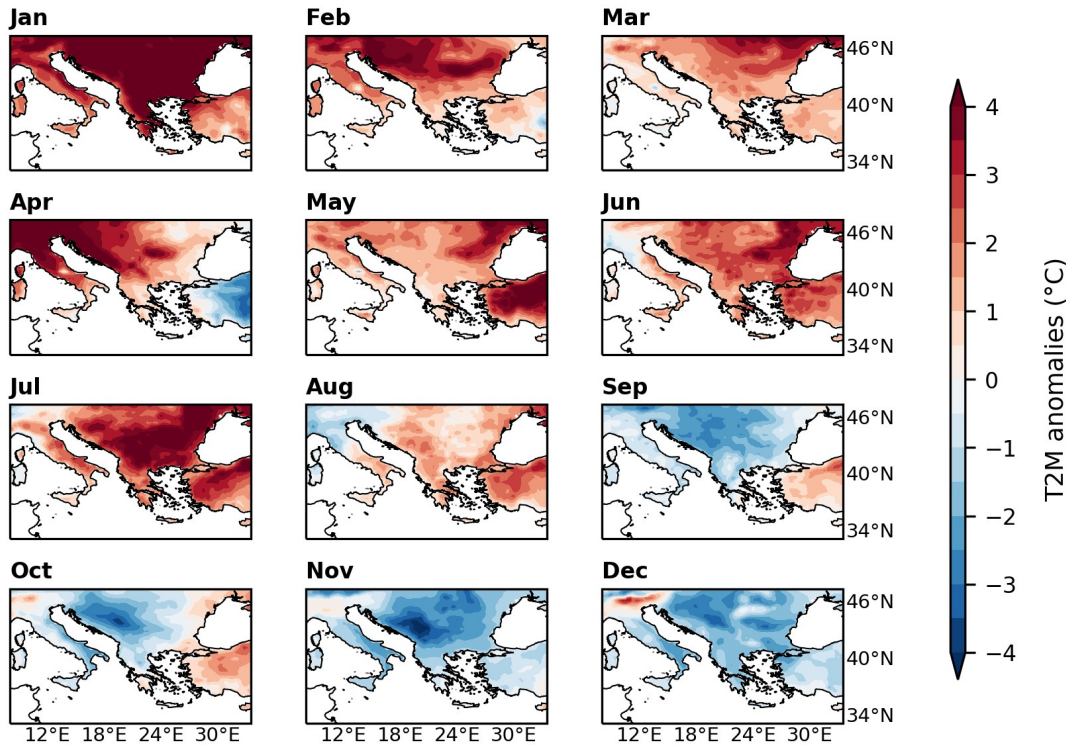


Figure A6: Monthly mean anomalies of maximum T2m for every month in 2007. The reference period used was 1979-2022. T2m data was retrieved from the ERA5 reanalysis dataset (Hersbach et al., 2023)

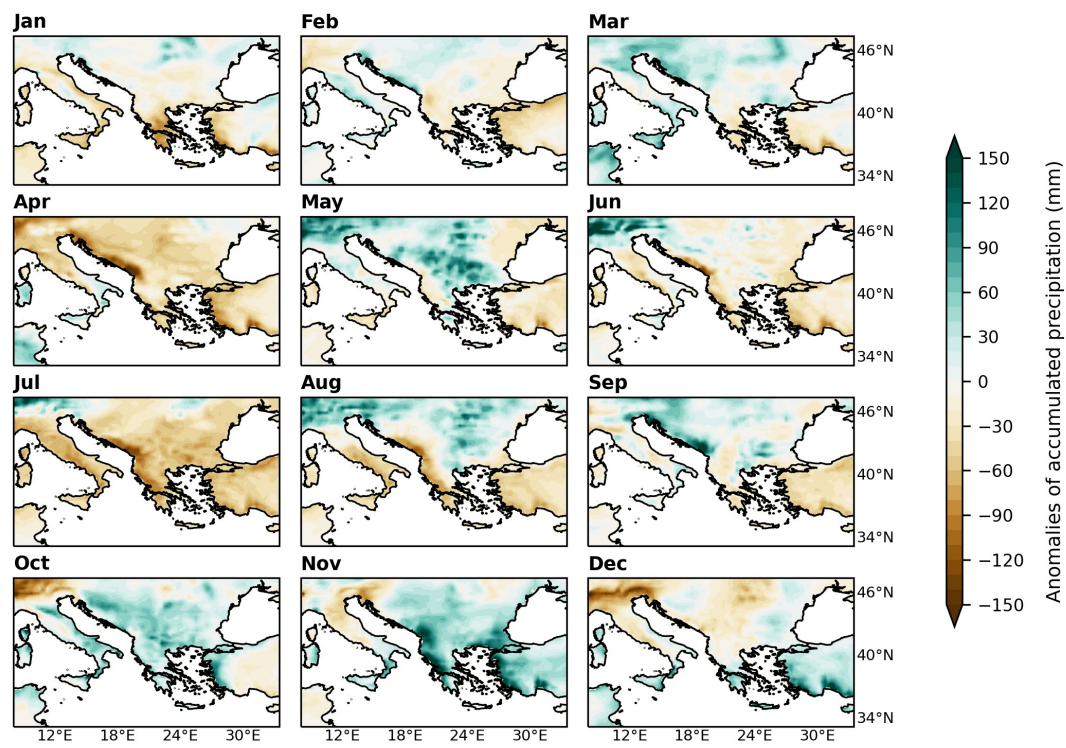


Figure A7: As in Fig A5, but considering accumulated precipitation values.

Table A1: Land cover classes classification from the ESA CCI LC product. The colors represent the 6 primary categories aggregated in this work, based on IPCC land categories used for the change detection (Defourny et al., 2017).

Class	ESA CCI LC number		ESA CCI LC label
	Global	Regional	
Cropland	10		Cropland, rainfed
		11	Cropland, rainfed, herbaceous cover
		12	Cropland, rainfed, tree or shrub cover
	20		Cropland, irrigated or postflooding
	30		Mosaic cropland (>50%) / natural vegetation (tree, shrub, herbaceous cover) (<50%)
Forest	50		Tree cover, broadleaved, evergreen, closed to open (>15%)
	60		Tree cover, broadleaved, deciduous, closed to open (>15%)
		61	Tree cover, broadleaved, deciduous, closed (>40%)
		62	Tree cover, broadleaved, deciduous, open (15-40%)
	70		Tree cover, needleleaved, evergreen, closed to open (>15%)
		71	Tree cover, needleleaved, evergreen, closed (>40%)
		72	Tree cover, needleleaved, evergreen, open (15-40%)
	80		Tree cover, needleleaved, deciduous, closed to open (>15%)
		81	Tree cover, needleleaved, deciduous, closed (>40%)
		82	Tree cover, needleleaved, deciduous, open (15-40%)
	90		Tree cover, mixed leaf type (broadleaved and needleleaved)
	100		Mosaic tree and shrub (>50%) / herbaceous cover (<50%)
	160		Tree cover, flooded, fresh or brakish water
	170		Tree cover, flooded, saline water
Grassland	110		Mosaic herbaceous cover (>50%) / tree and shrub (<50%)
	130		Grassland
Shrubland	120		Shrubland
		121	Evergreen shrubland
		122	Deciduous shrubland
Wetland	180		Shrub or herbaceous cover, flooded, fresh/saline/brakish water
Urban	190		Urban areas
Others	40		Mosaic natural vegetation (tree, shrub, herbaceous cover) (>50%) / cropland (<50%)
	140		Lichens and mosses
	150		Sparse vegetation (tree, shrub, herbaceous cover) (<15%)
		151	Sparse tree (<15%)
		152	Sparse shrub (<15%)
		153	Sparse herbaceous cover (<15%)
	200		Bare areas
	201		Consolidated bare areas
	202		Unconsolidated bare areas
	220		Permanent snow and ice
Water	210		Water bodies

Table A2: Thresholds values to identify the most extreme cases regarding monthly heatwave and dry conditions: the 80th percentile of the monthly ICI is used to define the most severe months for atmospheric and marine hot conditions, and the 20th percentile of the monthly SPEI-3 is utilized to find the driest months of the period.

Thresholds that define the 20% most extreme months			
	Atmospheric ICI ($^{\circ}\text{C}\cdot\text{days}$)	Marine ICI ($^{\circ}\text{C}\cdot\text{days}$)	SPEI
Full region	34.37	8.96	-1.11
Region 1	26.87	7.56	-1.10
Region 2	26.39	12.38	-1.08
Region 3	36.09	13.76	-1.05